Null-Steering in Planar Arrays by Phase Perturbations using Genetic Algorithms

by

Meerja Khalim Amjad

A Thesis Presented to the

FACULTY OF THE COLLEGE OF GRADUATE STUDIES

KING FAHD UNIVERSITY OF PETROLEUM & MINERALS

DHAHRAN, SAUDI ARABIA

In Partial Fulfillment of the
Requirements for the Degree of

MASTER OF SCIENCE

In

ELECTRICAL ENGINEERING

February, 2000

INFORMATION TO USERS

This manuscript has been reproduced from the microfilm master. UMI films the text directly from the original or copy submitted. Thus, some thesis and dissertation copies are in typewriter face, while others may be from any type of computer printer.

The quality of this reproduction is dependent upon the quality of the copy submitted. Broken or indistinct print, colored or poor quality illustrations and photographs, print bleedthrough, substandard margins, and improper alignment can adversely affect reproduction.

In the unlikely event that the author did not send UMI a complete manuscript and there are missing pages, these will be noted. Also, if unauthorized copyright material had to be removed, a note will indicate the deletion.

Oversize materials (e.g., maps, drawings, charts) are reproduced by sectioning the original, beginning at the upper left-hand corner and continuing from left to right in equal sections with small overlaps.

Photographs included in the original manuscript have been reproduced xerographically in this copy. Higher quality 6" x 9" black and white photographic prints are available for any photographs or illustrations appearing in this copy for an additional charge. Contact UMI directly to order.

Bell & Howell Information and Learning
300 North Zeeb Road, Ann Arbor, MI 48106-1346 USA
800-521-0600

Null-Steering in Planar Arrays by Phase Perturbations Using Genetic Algorithms

BY

MEERJA KHALIM AMJAD

A Thesis Presented to the

DEANSHIP OF GRADUATE STUDIES

KING FAHD UNIVERSITY OF PETROLEUM & MINERALS

DHAHRAN, SAUDI ARABIA

In Partial Fulfillment of the
Requirements for the Degree of

MASTER OF SCIENCE

In

ELECTRICAL ENGINEERING

KING FAHD UNIVERSITY OF PETROLEUM & MINERALS

Dhahran, Saudi Arabia

FEBRUARY 2000

KING FAHD UNIVERSITY OF PETROLEUM & MINERALS

DHAHRAN, SAUDI ARABIA

COLLEGE OF GRADUATE STUDIES

This thesis, written by

MEERJA KHALIM AMJAD

under the direction of his Thesis Advisor and approved by his Thesis Committee, has been presented to and accepted by the Dean of the College of Graduate Studies, in partial fulfillment of the requirements for the degree of

MASTER OF SCIENCE IN ELECTRICAL ENGINEERING

Thesis Committee

Mahmoud Dawoud

Dr. Mahmoud M. Dawoud (Chairman)

Dr. Samir Abdul-Jauwad (Member)

Dr. Al-Jamid, Hussain A. (Member)

H. Masoudi 13-2-2000

Masoudi, H. M. Y. (Member)

Dr. Samir Al-Baiyat
(Department Chairman)

Dr. Abdallah M. Al-Shehri
(Dean, College of Graduate Studies)

Date: 20 - 2 - 2000

DEANSHIP OF GRADUATE STUDIES

Dedicated to:

my most loving parents, brothers and sisters

Acknowledgements

This work is an expression of my gratitude to Allah (swt). May Allah bestow peace on his Prophet, Muhammad (pbuh).

My sincere respects to my advisor Dr. Mahmoud M. Dawoud. I am grateful to him for his continuous efforts he puts into his students to guide them through. It was because of him that the work at any point of time never got stressful. His encouragement during the hard times is unforgettable.

I would also wish to thank my committee members Dr. Samir Abdul Jauwad, Dr. Hussain Al-Jamid and Dr. Masoudi H. M. Y. for their valuable suggestions that made the work even better. It was a pleasure to work with them.

My parents, brothers and sisters especially Saleem were a constant source of motivation. It is their love and constant support that let me through the difficult moments. My sincere acknowledgements to my grandparents for their constant duas and Bada Maamaa, Khalusab and Khalabi are too short for words.

Thanks to all my colleagues and friends for their encouragement and support they provided me throughout my graduate studies at KFUPM. They made my stay over here memorable and joyous.

KFUPM has provided me with some of the cherished moment's thanks entirely due to the Research Community. I had the fortune of living in the most boisterous house in NC and hopefully with that experience I can be on my own anywhere.

Finally I would like to thank department chairman Dr. Samir Al-Baiyat for his kind cooperation.

CONTENTS

2 RECTAGULAR MICROSTRIP ARRAYS

3 MUTUAL COUPLING IN MICROSTRIP ANTENNAS

4 CHARACTERISTICS OF THE MICROSTRIP ARRAY

LIST OF TABLES

LIST OF FIGURES

Abstract

Name:	**Meerja Khalim Amjad**
Title:	**Null-Steering in Planar Arrays by Phase Perturbations Using Genetic Algorithms**
Major Field:	**Electrical Engineering**
Date of Degree:	**February, 2000**

Radiation from microstrip planar arrays has been studied in detail. Genetic Algorithms are applied to steer the nulls in the direction of interference for cases of no coupling and with coupling and the results are compared. Phase perturbation is the technique used to steer the nulls. A microstrip array has been analyzed in detail for cases of no coupling and with coupling as an example of the planar array. Coupling effects must be considered for any array as they significantly change the element excitation currents both in amplitude and phases. Results are presented in both 3 dimensional and 2 dimensional plots before and after null steering of the 8×8-element microstrip array with and without coupling. Similar plots for the array factor of the 8×8-element array are presented for comparison. In addition the arrays with different number of elements and different inter-element spacing have been studied. It is concluded that effective interference suppression can be achieved in planar arrays by phase variation.

Master of Science Degree

King Fahd University of Petroleum and Minerals

Dhahran, Saudi Arabia

February 2000

الخلاصة

الاسم : ميزا كليم امجد

العنوان : توجيه الأصفار في المصفوفات السطحية بواسطة تغيير الطور باستخدام الخوارزميات الجينية

التخصص: الهندسة الكهربائية

التاريخ : فبراير ٢٠٠٠

الإشعاع من المصفوفات المسطحة الشريطية الدقيقة قد درست بالتفصيل ولقد استخدمت الخوارزميات الجينية لتوجيه الأصفار في اتجاه التداخل في حالات التزاوج وعدم التزاوج ولقد قورنت هاتين الحالتين . ولقد استخدمت طريقة تغير الطور الطفيف لتوجيه الأصفار. ولقد حللت المصفوفات الشريطية الدقيقة بالتفصيل في حالات التزاوج وعدم التزاوج كمثال للمصفوفات المسطحة . أن اثر التزاوج يجب أن يأخذ بالاعتبار لأي مصفوفات لأنها تغير بمقدار كبير التيارات المحفزة للعناصر في كل من المقادير والأطوار. وعرضت النتائج في أشكال ثلاثية وثنائية الأبعاد قبل وبعد توجيه الأصفار لمصفوفة مسطحة شريطية دقيقة ذات عناصر ٨*٨ في وجود وعدم وجود تزاوج . وعرضت أشكال مشابهة لمعامل المصفوفة ذات عناصر ٨*٨ وذلك للمقارنة . بالإضافة إلى ذلك لقد درست مصفوفات ذات عناصر مختلفة وأيضا ذات مسافات بين العناصر مختلفة . ويمكن أن نستنتج انه بواسطة تغير الطور في المصفوفات المسطحة يمكن أن يقلل التداخل بشكل فعال .

درجة الماجستير في العلوم

جامعة الملك فهد للبترول والمعادن

الظهران ـ المملكة العربية السعودية

فبراير ـ ٢٠٠٠

CHAPTER 1

INTRODUCTION AND LITERATURE REVIEW

An antenna is a metallic device for radiating or receiving radio waves. In addition to this, it is required to optimize or accentuate the radiation in some directions and suppress it in others. Many applications in practice require radiation characteristics that may not be achievable by a single element. An antenna array refers to an antenna system consisting of more than one antenna element arranged such that the desired radiation characteristics are achieved. The total field from the elements of the array is the vector addition of fields radiated by individual elements. Ideally directive pattern of the array requires the fields of the individual elements to add constructively in the desired direction and destructively in the undesired directions. Practical array radiation patterns do have

side lobes in addition to the desired main beam. These side lobes cause interference by receiving unwanted signals coming in their directions. Steering a null in the direction of the side lobe receiving the unwanted signal can mitigate the interference, while keeping the main beam pointing towards the desired signal direction.

While there are many ways to steer the nulls, phase-only perturbation technique is attractive and can be easily realized in practise. Given the physical geometry of the array, a general approach to the problem of steering the nulls is to calculate the required phases of each element by solving a set of equations, equating the array factor of the array to zero in the direction of nulls. However, due to the complexity of the planar array, this method is not suitable. In this case synthesis technique like genetic algorithm, which provides control over the nulls of the antenna pattern, is of great interest for its robustness. Genetic algorithm is computationally simple and always leads to optimal or near optimal solution.

A microstrip array is an array in which the individual elements are microstrip antennas and is also called low profile antenna array. In high-performance aircraft, spacecraft, satellite and missile applications, where size, weight, cost, performance, ease of installation, and aerodynamic profiles are constraints, low profile antenna arrays are required. These arrays have become more and more important in many government and commercial applications, such as mobile radio and wireless communications [1]. However, microstrip antennas do have their own disadvantages. But the advantages

overweigh the disadvantages and in certain situations the use of these arrays become mandatory. The main advantage is that they are conformal.

1.1 Null Steering Techniques

For the past two decades a lot of research has been carried out on the subject of Null Steering, which indicates its importance. In this process, a null is placed at a real space angle where we have interference coming from the unintended sources, which may be noise or interfering signal. This can be done by adjusting the amplitudes/phases of the currents of the elements of the array. Put in simple terms, a null at a given position is obtained by simply equating the array factor to zero for that position and getting the unknown variables which are the amplitudes and phases of currents of individual elements. Another choice of null steering is by varying positions of the individual elements of the array. Depending on the choice of the variable we choose for controlling the pattern of the array, we can classify the null steering into four categories as described in the following sections.

1.1.1 Complex Weight Control Method

Complex weight control technique is a method in which we control the phase and amplitude of the array elements for null steering. The method for pattern synthesis starts

from a given original pattern, with desired main beam and side lobe envelope, corresponding to given element current amplitudes a_{mn} and phases ph_{mn}. Both amplitude and phase of these elements are then varied such that the pattern gets nulls in the desired directions of interference [2]. More information about this technique can be obtained from Ismail [3].

1.1.2 Amplitude Control Method

In this technique only the amplitudes of the individual element currents are varied keeping the phases constant. This is a cheaper choice when compared to the previous complex weight control technique. Also controlling the complex weights to steer the nulls has proven to be slow and ineffective for large radar arrays [4]. Mismar and Ismail used this technique to steer the nulls of 20-element linear and Chebyshev arrays using Minimax approximation [4]. Liao and Chu [5] applied this technique to the planar array.

1.1.3 Phase Control Method

Here the phases of the individual elements are varied keeping the amplitudes of the currents of individual elements constant. This is less costly compared to the complex weight control technique mentioned earlier in this section [4]. In this method the desired

main beam is obtained with the side lobes, having nulls at the required directions of interference, with element excitations, in which only their phase is used to control the direction of nulls. Liao and Chu [6] used a modified genetic algorithm for the phase only null steering of linear arrays. Nurruzzaman [2] gave a good comparison of the three techniques (complex weight control, amplitude only and phase only).

1.1.4 Element Position Perturbation Method

This technique was originally developed at KFUPM by Ismail and Dawoud [3]. In this method controlling the positions of the antenna array elements does the null steering. Also in [7], Dawoud and others applied genetic algorithm and compared the results with the analytic solution for array pattern nulling by element position perturbations. This technique is also applied for phased arrays by Dawoud and Ismail [8] for null steering. Also Magrabi [9] applied this technique for the cancellation of grating lobes in scanned linear antenna arrays.

1.2 Microstrip Antennas and Mutual Coupling

Microstrip antenna arrays have many advantages like lightweight, low volume, low profile planar configurations, which can be made conformal [10]. R. C. Hansen discusses Microstrip antennas in great detail in his very recent book [11]. Also good understanding about microstrip antennas can be gained from [12] and [13].

Alfaouri in his paper [14] describes a study of the relative performance of the far field radiation pattern using different methods from the viewpoint of reducing the side lobes. He discusses the implementation of the fractional change for nonuniform spacing to reduce the side lobe levels. A detailed analysis of patch arrays with corporate feed networks incorporating non-isolating splitters is described in [15]. A small array of microstrip patches is presented in [16]. It has been designed, fabricated and tested by Wojciech Sadowski and others to be used in a GSM 1800 base station antenna. A partial compensation of the free space attenuation along a sector cell is provided.

Daniel et al [17] discuss the flexibility of the printed technology and offer the possibilities of innovative radiating structures well suited to various applications. Academic researchers of the laboratory were focused on the corner fed square patch and the array design of such elements. They investigated both planar and cylindrical

structures. The paper focused on the commercially popular printed antenna elements and their array feeds.

Chen [18] proposed a phased array. Mutual coupling between the elements of the array causes significant change in the behavior of the practical microstrip arrays. Mutual coupling effects in microstrip patch phased linear antenna array were studied by Chen and others [18], results were presented with and without mutual coupling. They concluded that mutual coupling can also be the cause of blind scan angles, which should always be avoided within the scan range of the phased array. In their conclusion they say that the electromagnetic behavior of array elements located at or near one of the edges of the array will differ from the electromagnetic behavior of the elements near the center of the array.

1.3 Analytical Methods and Genetic Algorithms

In the available literature we find both analytic null steering methods as well as genetic algorithm based null steering methods. Schelkunoff [19], in his classic paper presented a method that is conducive to the synthesis of arrays whose patterns posses null in the desired directions. This method requires information about the number of nulls to be placed and their locations. Vu [20] described a method of null steering without using

phase shifters. This is done by forcing the zeros of the array factor to occur in conjugate pairs on the unit circle in the complex plane. The paper also showed that if the number of jammers is much smaller than half the total number of elements in the array, it is possible to optimize the pattern as well as suppress the jammers. Davies and Rizk [21]-[26] proposed a simple method of null steering with the help of phase shifters in the feed network for various applications.

However, later research was more focused towards the Genetic Algorithm based null steering. The reason for this is the complexity involved with analytical modeling for larger arrays for various applications. Genetic Algorithms (GAs) are search techniques based on the mechanism of natural selection and natural genetics. These transform a population of individual objects (Chromosomes), each with an associated fitness value into a new generation of the population using Darwinian principle of reproduction and survival of the fittest and analogs of naturally occurring genetic operations such as *crossover* and *mutation*. The flow chart of the basic modified genetic algorithm is shown in figure 1.1.

John Holland first developed genetic Algorithms in the 1960's [27] and showed how evolutionary process can be applied to solve a wide variety of problems in his pioneering book *Adaptation in Natural and Artificial Systems (1975, 1992)* [28]. The Genetic algorithm starts by generating a population that contains individuals called chromosomes. Each chromosome contains genes and has certain fitness value. The algorithm proceeds to generate a new population, which is a new generation from the old

population by a process of crossover and mutation. In this process the fittest of the chromosomes survive and are able to produce offspring/children. The three main steps in the algorithm which have been the subject of the researchers are

- Selection
- Crossover, and
- Mutation

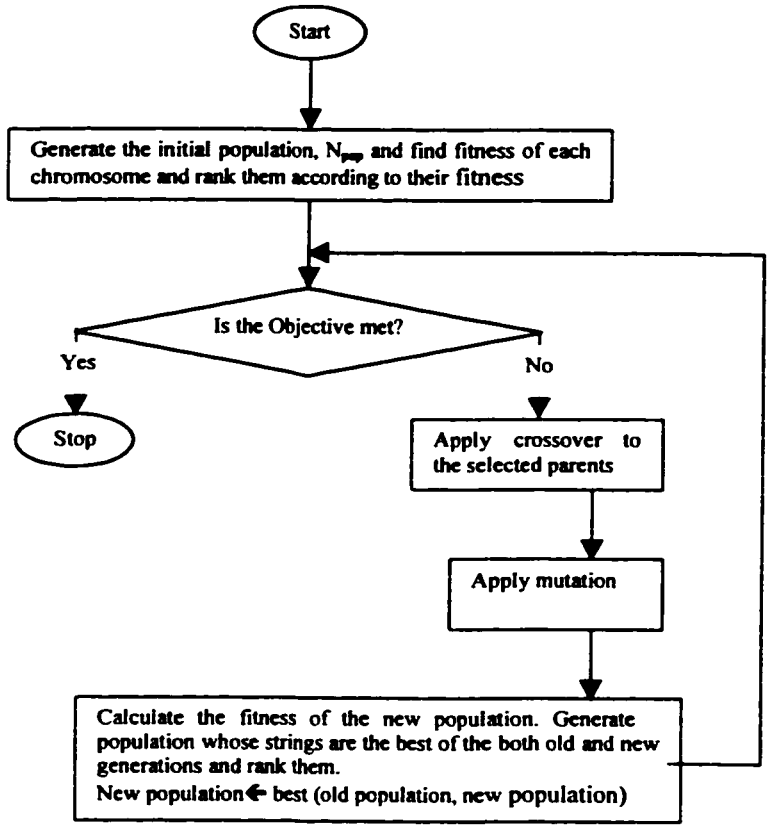

Figure 1.1: Block diagram of a simple modified Genetic Algorithm

Proper implementation of these steps is very important to the performance of the algorithm and is very much dependant on the type of problem. Genetic algorithms are

famous due to their robustness, faster convergence towards optimal solution, easily obtainable null/nulls precisely to the depth required, computer-based solution for calculating the excitation amplitudes/phases of the array elements.

Genetic Algorithms are iterative optimization procedures that start with a randomly selected population of potential solutions, and gradually evolve towards better solutions, through the application of genetic operator's [2]. Daniel and Eric [29] in their review paper addressed genetic algorithm as design tools and problem solvers because of their versatility and ability to optimize in complex multimodal search spaces. Liao and Chu [6] used a modified genetic algorithm for the phase-only null steering of the linear arrays. Another technique is element position perturbation using genetic algorithm was developed at KFUPM by Ismail and Dawoud [3],[7], [8] and [30]. Mismar and Ismail [4] used a linear programming technique using the minimax approximation to steer the nulls. They used only the current amplitudes as the control variables. This allowed the number of controlled nulls to attain the full degree of freedom for the array. Liao and others [5] investigated a technique to steer the nulls for the planar arrays controlling the current amplitudes and using genetic algorithms. While Mitchell and others [31] made the GA take advantage of synthesis in complex plane, is used to find the necessary complex weights for the null steering adaptation of linear array antennas with performance constraints.

Genetic algorithms are not limited to null steering problems. These algorithms are extensively applied to optimization in several other electromagnetic problems. Alona

Boag and others [32] proposed a design procedure based on genetic algorithm driven optimization and applied to the synthesis of wire antennas loaded with lumped components. Randy and others [33] presented how to optimally thin an array using genetic algorithms. The genetic algorithm determines which elements are turned off in a periodic array to yield the lowest maximum relative side lobe level. A modified algorithm was used to solve the parameter identification problem for linear and nonlinear digital filters [34]. Genetic algorithms are also used in many radar applications [35] and [36]. Another important aspect of antenna design is antenna synthesis or antenna pattern synthesis. Synthesis of linear and planar arrays is discussed in [37]-[41]. Dawoud and others studied null steering in adaptive array [42] using genetic algorithms and compared them with the analytically obtained solutions.

Much of the work was concentrated on linear arrays rather than on planar arrays. The work by Nurruzzaman [2] was on null steering of planar arrays but the array factor was separable. No work in the literature was found that treats the array element excitations independent of each other and studies the array factor in the most general form.

1.4 Objectives of the Work

The array factor expressions for the planar rectangular arrays are derived. The aim of this work is to study microstrip planar array radiation characteristics with mutual coupling considerations and steer its nulls to arbitrary directions using phase-only technique by means of genetic algorithms.

Compared to the other techniques, phase-only is less expensive and can be very easily realized in practice. An optimization algorithm like genetic algorithm is the best choice due to the features it offers. The flexibility with which this algorithm adapts itself to solution finding for wide range of problems is the reason why we find so much research in this area.

Microstrip patch antenna has been chosen as the array element to make it conformal and suitable for mobile applications. Mutual coupling effects were also studied to get the resultant current distribution on the elements and study the practical behavior of the antenna. Null steering was incorporated to nullify the interference caused by external sources.

Many array radiation patterns are presented to maintain the generality of applying the technique to any array desired for the application. However microstrip 8×8 element is the array that is used in this work to study its performance with and without mutual

coupling. This was done to get total insight about the behavior of a particular array and the results could be extended to other arrays.

The inter-element spacing was chosen to be dx = dy = 0.5λ and the patch dimensions to be L = 0.5λ and W = 0.01λ where L and W are the length and width of the patch respectively. The patch was assumed to have negligible thickness and current distribution to be sinusoidal along the length of the patch and constant along the width. The results are shown in two-dimensional and three-dimensional plots for the array factor and array pattern.

CHAPTER 2

RECTANGULAR MICROSTRIP ARRAYS

The desired antenna radiation characteristics may be obtained with a single element. However high gain, beam scanning and null steering is possible only when discrete radiators are combined to form arrays. The elements of an array may be identical to or different from one another, and may be spatially distributed to form a linear, planar, or volume array. However practical arrays are built with identical elements, as they are simple to synthesize and tailor the radiation pattern to the requirements. Planar arrays comprise elements distributed on a plane and have many applications. Also planar arrays provide additional variables, which can be used to control and shape the pattern of the array when compared to linear arrays and are more versatile as they can be used to scan

the main beam of the antenna towards any point in space. They are found in applications such as tracking radar, search radar, remote sensing, communications, and many other applications [1].

2.1 Array Factors of Planar Rectangular Arrays

A rectangular planar array is shown in figure 2.1, and assumed to lie in the x-y plane. The element spacing in x and y directions are dx and dy respectively. All the elements are considered to have identical current amplitudes but with progressive phase shifts β_x and β_y in x and y directions respectively.

From the principle of pattern multiplication, the array pattern of the antenna array with identical elements may be factored as the product of the array factor and the element pattern. Array factor is the vector addition of the fields radiated by point sources, which replaced the elements of the array. Once the element is chosen for the array for a particular application, the element far field pattern is multiplied with the array factor to obtain the array pattern. As the element pattern is fixed for a particular element, the array factor is utilized to achieve certain null configuration.

Rectangular arrays in general have odd×odd, odd×even, even×odd and even×even number of elements. Array factor matrix A for each of the following cases is first taken to calculate the array factor and notation of [1] for odd and even element array is followed.

2.1.1 Odd×Odd Element Array

For odd×odd element array we have 2M+1 elements along x-axis in every column and 2N+1 elements along y-axis in each row. The array factor matrix A of the odd×odd element array is given by

$$A_{O\times O}=\begin{bmatrix} a_{-(M+1),-(N+1)} & \cdots & a_{-(M+1),-2} & 2a_{-(M+1),1} & a_{-(M+1),2} & \cdots & a_{-(M+1),(N+1)} \\ \vdots & & & & & & \vdots \\ a_{-2,-(N+1)} & \cdots & a_{-2,-2} & 2a_{-2,1} & a_{-2,2} & \cdots & a_{-2,(N+1)} \\ 2a_{1,-(N+1)} & \cdots & 2a_{1,-2} & 4a_{1,1} & 2a_{1,2} & \cdots & 2a_{1,(N+1)} \\ a_{2,-(N+1)} & \cdots & a_{2,-2} & 2a_{2,1} & a_{2,2} & \cdots & a_{2,(N+1)} \\ \vdots & & & & & & \vdots \\ a_{(M+1),-(N+1)} & \cdots & a_{(M+1),-2} & 2a_{(M+1),1} & a_{(M+1),2} & \cdots & a_{(M+1),(N+1)} \end{bmatrix} \quad (2.1)$$

The weight of the element is given as $a_{m,n}$ where

$$m \in [-(M+1),-M,..,-2,1,2,..,M,(M+1)] \quad (2.2)$$

$$n \in [-(N+1),-N,..,-2,1,2,..,N,(N+1)] \quad (2.3)$$

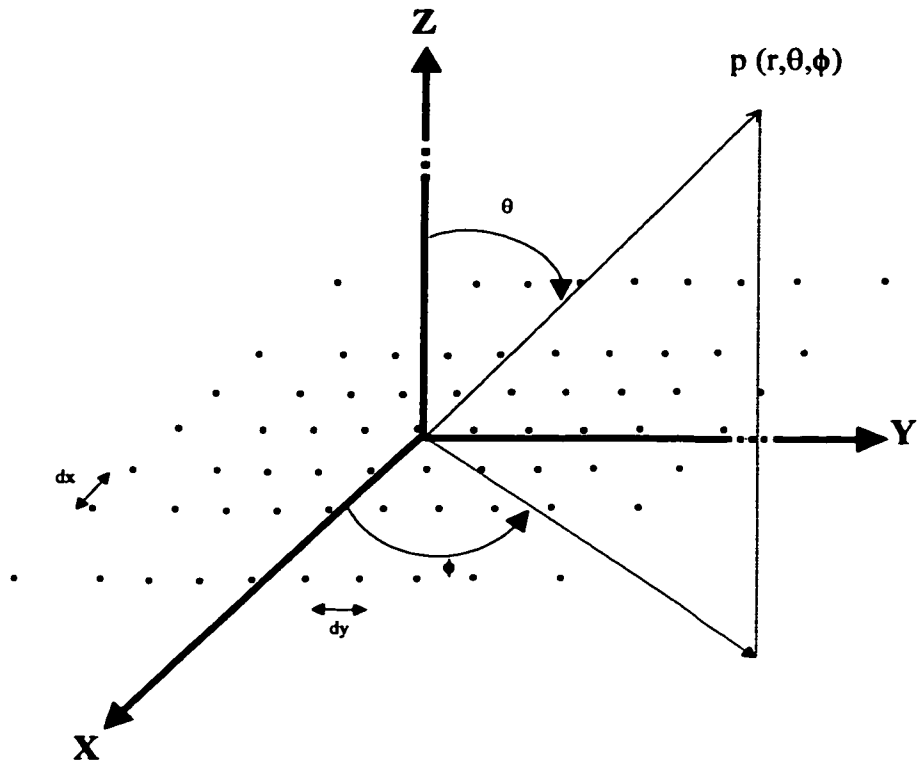

Figure 2.1: The rectangular array

The array factor of the odd x odd element array is given by

$$AF_{O\times O} = 2\left(2a_{1,1} + \sum_{m=-2}^{-(M+1)} a_{m,1}\exp(-j(m+1)\Psi_x) + \sum_{m=2}^{(M+1)} a_{m,1}\exp(-j(m-1)\Psi_x) \right)$$

$$+ \sum_{n=-2}^{-(N+1)} \left(2a_{1,n} + \sum_{m=-2}^{-(M+1)} a_{m,n}\exp(-j(m+1)\Psi_x) + \sum_{m=2}^{(M+1)} a_{m,n}\exp(-j(m-1)\Psi_x) \right) \times p$$

$$+ \sum_{n=2}^{(N+1)} \left(2a_{1,n} + \sum_{m=-2}^{-(M+1)} a_{m,n}\exp(-j(m+1)\Psi_x) + \sum_{m=2}^{(M+1)} a_{m,n}\exp(-j(m-1)\Psi_x) \right) \times q \qquad (2.4)$$

where

$$p = \exp(-j(n+1)\Psi_y) \qquad (2.5)$$

$$q = \exp(-j(n-1)\Psi_y) \qquad (2.6)$$

$$\Psi_x = kd_x\cos\gamma_x + \beta_x \qquad (2.7)$$

$$\Psi_y = kd_y\cos\gamma_y + \beta_y \qquad (2.8)$$

$$\cos\gamma_x = \sin\theta\cos\phi \qquad (2.9)$$

$$\cos\gamma_y = \sin\theta\sin\phi \qquad (2.10)$$

The array factor given by the equation 2.4 can be expressed in the matrix form as follows

$$AF_{O\times O} = X_{O\times O}A_{O\times O}Y_{O\times O} \qquad (2.11)$$

$$X_{O\times O} = \left[\exp(jM\Psi_x)\ \exp(j(M-1)\Psi_x)\ldots 1\ldots\exp(-j(M-1)\Psi_x)\ \exp(-jM\Psi_x)\right] \qquad (2.12)$$

$$Y_{O\times O} = \begin{bmatrix} \exp(jN\Psi_y) \\ \exp(j(N-1)\Psi_y) \\ \vdots \\ 1 \\ \vdots \\ \exp(-j(N-1)\Psi_y) \\ \exp(-jN\Psi_y) \end{bmatrix} \qquad (2.13)$$

For broad side arrays the progressive phase shifts β_x, β_y are both equals to zero. But for phased arrays $\beta_x = \sin\theta_0\cos\phi_0$ and $\beta_y = \sin\theta_0\sin\phi_0$ where (θ_0, ϕ_0) is the direction of the main beam. Equation 2.11 expresses the array factor in matrix form where A_{OxO} is given by equation 2.1.

2.1.2 Odd×Even Element Array

For odd×even element array we have 2M+1 elements along x-axis in every column and 2N elements along y-axis in each row. The array factor matrix A_{OxE} of the odd×even element array and its array factor expressions are given as follows.

$$A_{O\times E} = \begin{bmatrix} a_{-(M+1),-N} & \cdots & a_{-(M+1),-1} & a_{-(M+1),1} & \cdots & a_{-(M+1),N} \\ \vdots & & & & & \vdots \\ a_{-2,-N} & \cdots & a_{-2,-1} & a_{-2,1} & \cdots & a_{-2,N} \\ 2a_{1,-N} & \cdots & 2a_{1,-1} & 2a_{1,1} & \cdots & 2a_{1,N} \\ a_{2,-N} & \cdots & a_{2,-1} & a_{2,1} & \cdots & a_{2,N} \\ \vdots & & & & & \vdots \\ a_{(M+1),-N} & \cdots & a_{(M+1),-1} & a_{(M+1),1} & \cdots & a_{(M+1),N} \end{bmatrix} \tag{2.14}$$

$$AF_{O\times E} = \sum_{n=-1}^{-N}\left[2a_{1,n} + \sum_{m=-2}^{-(M+1)} a_{m,n}\exp(-j(m+1)\Psi_x) + \sum_{m=2}^{(M+1)} a_{m,n}\exp(-j(m-1)\Psi_x)\right]\times\exp\left(-j\left(\frac{2n+1}{2}\right)\Psi_y\right)$$

$$+\sum_{n=1}^{N}\left[2a_{1,n} + \sum_{m=-2}^{-(M+1)} a_{m,n}\exp(-j(m+1)\Psi_x) + \sum_{m=2}^{(M+1)} a_{m,n}\exp(-j(m-1)\Psi_x)\right]\times\exp\left(-j\left(\frac{2n-1}{2}\right)\Psi_y\right) \quad (2.15)$$

Where ψ_x, ψ_y are given by the equations 2.7 and 2.8. The array factor in the matrix form is given by the following equations

$$AF_{O\times E} = X_{O\times E}A_{O\times E}Y_{O\times E} \quad (2.16)$$

$$X_{O\times E} = [\exp(jM\Psi_x)\ldots 1\ldots\exp(-jM\Psi_x] \quad (2.17)$$

$$Y_{O\times E} = \begin{bmatrix} \exp\left(j\left(\frac{2N-1}{2}\right)\Psi_y\right) \\ \vdots \\ 1 \\ \vdots \\ \exp\left(-j\left(\frac{2N-1}{2}\right)\Psi_y\right) \end{bmatrix} \quad (2.18)$$

2.1.3 Even×Odd Element Array

The equations from 2.19 to 2.25 give similar expressions for even × odd element array. For this array in general there are 2M elements along x-axis in every column and 2N+1 elements along y-axis in each row.

The weights of the elements of the array are denoted by $a_{m,n}$ where

$$m \in [-M,\ldots,-2,-1,1,2,\ldots,M] \tag{2.19}$$

$$n \in [-(N+1),\ldots,-2,1,2,\ldots,(N+1)] \tag{2.20}$$

The excitation matrix A_{ExO} of the array is given as

$$A_{E\times O} = \begin{bmatrix} a_{-M,-(N+1)} & \cdots & a_{-M,-2} & 2a_{-M,1} & a_{-M,2} & \cdots & a_{-M,(N+1)} \\ \vdots & & & & & & \vdots \\ a_{-1,-(N+1)} & \cdots & a_{-1,-2} & 2a_{-1,1} & a_{-1,2} & \cdots & a_{-1,(N+1)} \\ \\ a_{1,-(N+1)} & \cdots & a_{1,-2} & 2a_{1,1} & a_{1,2} & \cdots & a_{1,(N+1)} \\ \vdots & & & & & & \vdots \\ a_{M,-(N+1)} & \cdots & a_{M,-2} & 2a_{M,1} & a_{M,2} & \cdots & a_{M,(N+1)} \end{bmatrix} \tag{2.21}$$

$$AF_{E\times O} = 2\left[\sum_{m=-1}^{-M} a_{m,1}\exp\left(-j\left(\frac{2m+1}{2}\right)\Psi_x\right) + \sum_{m=1}^{M} a_{m,1}\exp\left(-j\left(\frac{2m-1}{2}\right)\Psi_x\right) + \right]$$

$$\sum_{n=-2}^{-(N+1)}\left[\sum_{m=-1}^{-M} a_{m,n}\exp\left(-j\left(\frac{2m+1}{2}\right)\Psi_x\right) + \right.$$

$$\left.\sum_{m=1}^{M} a_{m,n}\exp\left(-j\left(\frac{2m-1}{2}\right)\Psi_x\right)\right]\times\exp(-j(n+1)\Psi_y)$$

$$+\sum_{n=2}^{(N+1)}\left[\sum_{m=-1}^{-M} a_{m,n}\exp\left(-j\left(\frac{2m+1}{2}\right)\Psi_x\right)+\right.$$

$$\left.\sum_{m=1}^{M} a_{m,n}\exp\left(-j\left(\frac{2m-1}{2}\right)\Psi_x\right)\right]\times\exp(-j(n-1)\Psi_y) \tag{2.22}$$

$$AF_{E\times O} = X_{E\times O}A_{E\times O}Y_{E\times O} \tag{2.23}$$

$$X_{E\times O} = \left[\exp\left(j\left(\frac{2M-1}{2}\right)\Psi_x\right),\ldots,1,\ldots,\exp\left(-j\left(\frac{2M-1}{2}\right)\Psi_x\right)\right] \tag{2.24}$$

and

$$Y_{E\times O} = \begin{bmatrix}\exp(jN\Psi_y)\\ \vdots \\ 1 \\ \vdots \\ \exp(-jN\Psi_y)\end{bmatrix} \tag{2.25}$$

Where ψ_x, ψ_y are given by the equations 2.7 and 2.8.

2.1.4 Even×Even Element Array

The expressions for the array factor for the even×even element array are given in this section. For even×even element array there are 2M elements along x-axis in every column and 2N elements along y-axis in each row. The array factor matrix A_{ExE} for this array is given by

$$A_{E\times E}=\begin{bmatrix} a_{-M,-N} & \cdots & a_{-M,-1} & a_{-M,1} & \cdots & a_{-M,N} \\ \vdots & & & & & \vdots \\ a_{-1,-N} & \cdots & a_{-1,-1} & a_{-1,1} & \cdots & a_{-1,N} \\ & & & & & \\ a_{1,-N} & \cdots & a_{1,-1} & a_{1,1} & \cdots & a_{1,N} \\ \vdots & & & & & \vdots \\ a_{M,-N} & \cdots & a_{M,-1} & a_{M,1} & \cdots & a_{M,N} \end{bmatrix} \tag{2.26}$$

$$AF_{E\times E}=\sum_{n=-1}^{-N}\left[\sum_{m=-1}^{-M}a_{m,n}\exp\left(-j\left(\frac{2m+1}{2}\right)\Psi_x\right)+\sum_{m=1}^{M}a_{m,n}\exp\left(-j\left(\frac{2m-1}{2}\right)\Psi_x\right)\right]\times\exp\left(-j\left(\frac{2n+1}{2}\right)\Psi_y\right)$$

$$+\sum_{n=1}^{N}\left[\sum_{m=-1}^{-M}a_{m,n}\exp\left(-j\left(\frac{2m+1}{2}\right)\Psi_x\right)+\sum_{m=1}^{M}a_{m,n}\exp\left(-j\left(\frac{2m-1}{2}\right)\Psi_x\right)\right]\times\exp\left(-j\left(\frac{2n-1}{2}\right)\Psi_y\right) \tag{2.27}$$

$$\Rightarrow AF_{E\times E}=X_{E\times E}A_{E\times E}Y_{E\times E} \tag{2.28}$$

where

$$X_{E\times E}=\left[\exp\left(j\left(\frac{2M-1}{2}\right)\Psi_x\right),\ldots,1,\ldots,\exp\left(-j\left(\frac{2M-1}{2}\right)\Psi_x\right)\right] \tag{2.29}$$

$$Y_{E\times E} = \begin{bmatrix} \exp\left(j\left(\frac{2N-1}{2}\right)\Psi_y\right) \\ \vdots \\ 1 \\ \vdots \\ \exp\left(-j\left(\frac{2N-1}{2}\right)\Psi_y\right) \end{bmatrix} \tag{2.30}$$

2.2 Microstrip Antenna

The choice of microstrip antenna as the element of the planar array results in a low profile array, which has many advantages. Deschamps first proposed the concept of microstrip radiators as early as 1953 [10]. However, these arrays were not fabricated as better theoretical models and photo-etch techniques for copper or gold-clad dielectric substrates with a wide range of dielectric constants were not developed. The first practical microstrip antenna was built in the year 1970 by Howell and Munson [10]. Microstrip antennas have the following advantages:

- Light weight, low profile planar configurations which can be made conformal.
- Low fabrication cost; readily amenable to mass production.
- Can be made thin; hence, they do not perturb the aerodynamics of host aerospace vehicles.
- The antennas may be easily mounted on missiles, rockets and satellite without major alterations.

- The antennas have low scattering cross section.
- Linear, circular (left hand or right hand) polarizations are possible with simple changes in feed position.
- Dual frequency antennas easily made.
- Microstrip antennas are compatible with modular designs (Solid state devices such as oscillators, amplifiers, variable attenuators, switches, modulators, mixers, phase shifters etc. can be added directly to the antenna substrate board).
- Feed lines and matching networks are fabricated simultaneously with the antenna structure.

2.2.1 Radiation from a Microstrip Antenna

Often microstrip antennas are also referred to as *patch* antennas [1]. Radiation from microstrip antennas can be understood by considering the simple case of a rectangular patch spaced a small fraction of a wavelength above a ground plane, as shown in figure 2.2(a). Assuming no variations of the electric field along the width and the thickness of the microstrip structure, the electric field configuration of the radiator can be expressed as shown in figure 2.2(b). The field varies along the patch length, which is about half a wavelength ($\lambda/2$). Radiation may be ascribed mostly to the fringing fields at the open-circuited edges of the patch. The fields at the end can be resolved into normal and tangential components with respect to the ground plane. The normal components are 180^0

out of phase because the patch line is λ/2 long; therefore the far field produced by them cancel in the broadside direction [10]. The tangential components (those parallel to the ground plane) are in phase, and the resulting fields combine to give maximum radiated field normal to the surface of the structure; i.e., broadside direction. Therefore, the patch may be represented by two slots λ/2 apart as shown in figure 2.2(c) excited in phase and radiating in the half space above the ground plane.

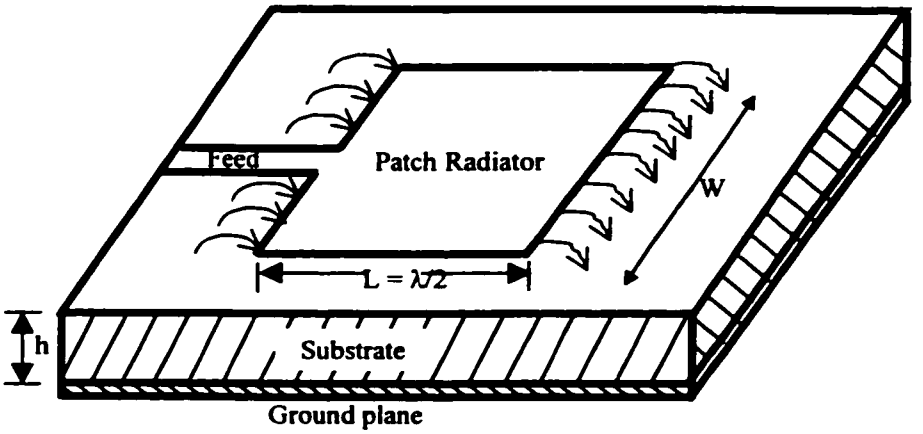

Figure 2.2(a): Rectangular Microstrip Antenna

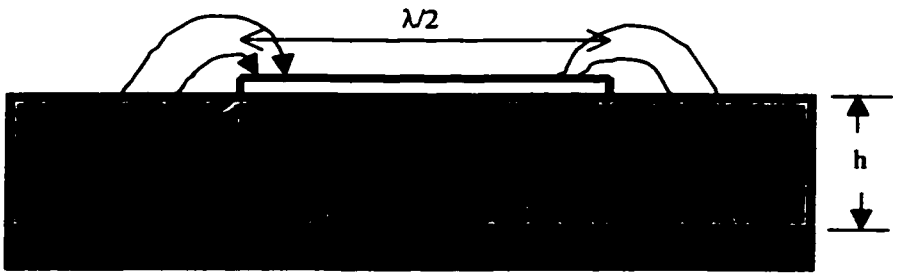

Figure 2.2(b): Side view of the Microstrip Antenna

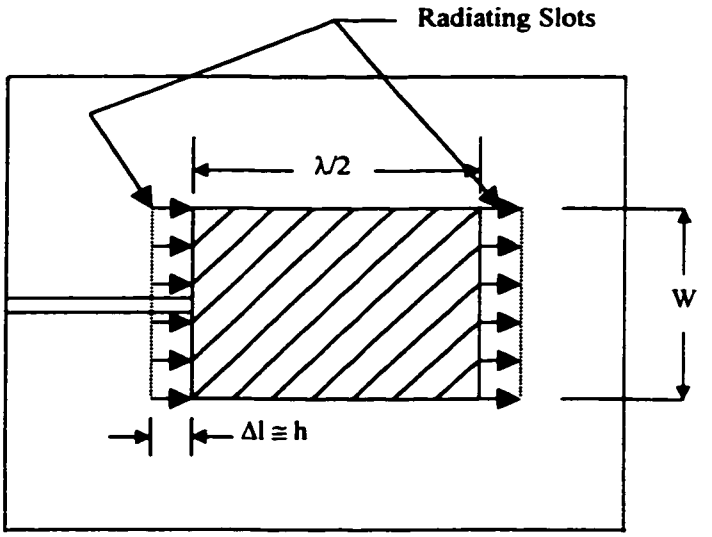

Figure 2.2(c): Top view of the Microstrip Antenna

2.2.2 Far Fields of the Microstrip Antenna

The radiated field of the Microstrip antenna is calculated based on the following assumptions.

1. Width of the antenna is very small compared to its length, i.e., W<<L and therefore there is no field variation along the width of the antenna; the field variation is only along the length of the antenna.
2. Sinusoidal current distribution along the length of the microstrip antenna; current is constant along the width of the microstrip antenna.
3. The thickness of the microstrip antenna is negligible.
4. The height h above the ground plane where the microstrip is located (above the substrate) is considered very small compared to the wavelength of operation; therefore image of the fields can be taken with respect to the surface of the substrate.

To find the fields radiated by the microstrip antenna, with the known current distribution the vector potential **A** is calculated first and from it the fields **E** and **H** by differentiation. Following the assumptions and the orientation of the microstrip antenna with respect to the axes given in figure 2.3 the current density is given by

$$J(x',y') = J(x') = \begin{cases} \bar{a}_x \frac{I_0}{W} \sin\left(k\left(\frac{L}{2} - x'\right)\right) & 0 \le x' \le L/2 \\ \bar{a}_x \frac{I_0}{W} \sin\left(k\left(\frac{L}{2} + x'\right)\right) & -L/2 \le x' \le 0 \end{cases} \tag{2.31}$$

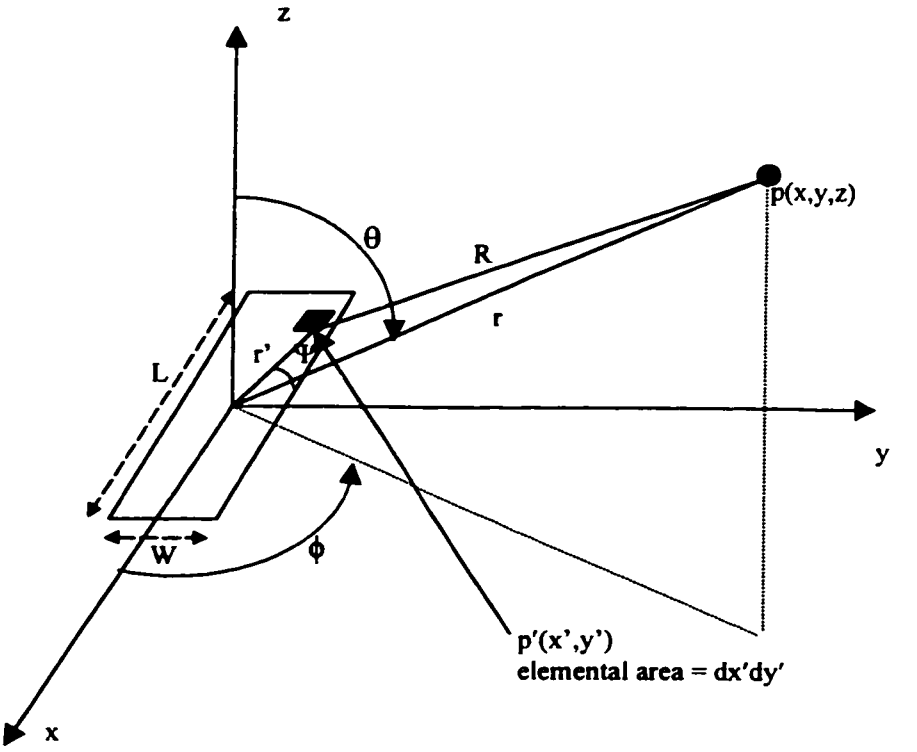

Figure 2.3: Microstrip antenna located in xy-plane with origin at the center of microstrip antenna. p(x,y,z) is an arbitrary point in space and p'(x',y') is an arbitrary point on the microstrip

Where J(x',y') is the current density at any point on the surface of the microstrip, I_0 is the amplitude of the current and L and W are the dimensions of the microstrip. The vector potential A due to the current source (microstrip antenna) can be calculated as

$$A = \frac{\mu}{4\pi}\iint_s J(x',y')\frac{\exp(-jkR)}{R}ds' \tag{2.32}$$

where

$$k = \frac{2\pi}{\lambda} \quad (\textit{wave number for free space})$$
$$R \approx r - r'\cos\Psi \quad (\textit{for far field phase terms})$$
$$R \approx r \qquad (\textit{for far field amplitude terms})$$

$$A = \frac{\mu}{4\pi}\frac{\exp(-jkr)}{r}\int_{-L/2}^{L/2}\int_{-W/2}^{W/2} J(x',y')\exp(-jkr'\cos\Psi)ds' \tag{2.33}$$

$$r'\cos\Psi = x'\sin\theta\cos\phi + y'\sin\theta\sin\phi$$

$$\Rightarrow \quad A_x = \frac{\mu}{2\pi}\frac{\exp(-jkr)}{r}\int_{-L/2}^{L/2}\frac{J(x')\exp(jkx'\sin\theta\cos\phi)}{k\sin\theta\sin\phi}\sin\left(\frac{kW}{2}\sin\theta\sin\phi\right)dx'$$

from equation (2.31), *subsituting for* $J(x')$

$$A_x = \frac{\mu I_0}{\pi}\cdot\frac{\exp(-jkr)}{r}\cdot\frac{\sin\left(\frac{kW}{2}\sin\theta\sin\phi\right)}{k\sin\theta\sin\phi}\cdot\frac{\left[\cos\left(\frac{kL}{2}\sin\theta\cos\phi\right)-\cos\left(\frac{kL}{2}\right)\right]}{kW\left(1-\sin^2\theta\cos^2\phi\right)} \tag{2.34}$$
$$A_y = A_z = 0$$

changing to spherical coordinates, we have

$$A_\theta = \cos\theta\cos\phi\, A_x$$
$$A_\phi = -\sin\phi\, A_x$$

from Maxwell's equations, we have the following relations to obtain E and H fields

$$E_\theta = -j\omega A_\theta \qquad \& \qquad H_\phi = \frac{E_\theta}{\eta} \tag{2.35}$$

$$E_\phi = -j\omega A_\phi \qquad \& \qquad H_\theta = \frac{E_\phi}{\eta} \tag{2.36}$$

Therefore the far-field electric and magnetic fields are given by the equations listed below

$$E_\theta = -j\eta I_0 \frac{\exp(-jkr)}{\pi r} \frac{\sin\left(\frac{kW}{2}\sin\theta\sin\phi\right)}{kW\tan\theta\tan\phi} \frac{\left[\cos\left(\frac{kL}{2}\sin\theta\cos\phi\right)-\cos\left(\frac{kL}{2}\right)\right]}{\left(1-\sin^2\theta\cos^2\phi\right)} \quad (2.37)$$

$$E_\phi = j\eta I_0 \frac{\exp(-jkr)}{\pi r} \frac{\sin\left(\frac{kW}{2}\sin\theta\sin\phi\right)}{kW\sin\theta} \frac{\left[\cos\left(\frac{kL}{2}\sin\theta\cos\phi\right)-\cos\left(\frac{kL}{2}\right)\right]}{\left(1-\sin^2\theta\cos^2\phi\right)} \quad (2.38)$$

$$H_\theta = -jI_0 \frac{\exp(-jkr)}{\pi r} \frac{\sin\left(\frac{kW}{2}\sin\theta\sin\phi\right)}{kW\sin\theta} \frac{\left[\cos\left(\frac{kL}{2}\sin\theta\cos\phi\right)-\cos\left(\frac{kL}{2}\right)\right]}{\left(1-\sin^2\theta\cos^2\phi\right)} \quad (2.39)$$

$$H_\phi = -jI_0 \frac{\exp(-jkr)}{\pi r} \frac{\sin\left(\frac{kW}{2}\sin\theta\sin\phi\right)}{kW\tan\theta\tan\phi} \frac{\left[\cos\left(\frac{kL}{2}\sin\theta\cos\phi\right)-\cos\left(\frac{kL}{2}\right)\right]}{\left(1-\sin^2\theta\cos^2\phi\right)} \quad (2.40)$$

where

$\eta = \frac{\omega\mu}{k}$ (*for free space*)

therefore, the total Electric and Magnetic fields are given by

$$E = \sqrt{(E_\theta)^2 + (E_\phi)^2} \quad (2.41)$$

$$H = \sqrt{(H_\theta)^2 + (H_\phi)^2} \quad (2.42)$$

The expressions for **E** and **H** fields given by the expressions 2.37 through 2.40 are valid only when θ is not a multiple of π. Also the expressions are not valid when θ is multiple of π/2 and ϕ is a multiple of π. Under these cases the expressions are derived applying the limits. To obtain the expressions for the fields of the microstrip oriented at an angle ϕ_0

with respect to the x-axis the equations 2.37-2.40 are modified in which ϕ is replaced by ϕ' where $\phi' = \phi - \phi_0$.

The far-field element pattern for the microstrip antenna shown in figure 2.3 is plotted. The plots for these patterns are shown in figure 2.4 and 2.5. Equations 2.41 and 2.42 takes indeterminate form under two cases. The two cases are dealt separately in subsections below.

Case I: When θ equals to $2n\pi$ [where n=0,+/-1,+/-2...]

When θ is $2n\pi$, all the expressions 2.37-2.40 will obtain 0/0 form which is undefined. However, the value of those can be obtained by applying the limits as $\theta \rightarrow 2n\pi$.

$$E_\theta \approx -j\eta I_0 \frac{\exp(-jkr)}{2\pi r}\cos\theta\cos\phi\frac{\left[\cos\left(\frac{kL}{2}\sin\theta\cos\phi\right)-\cos\left(\frac{kL}{2}\right)\right]}{\left(1-\sin^2\theta\cos^2\phi\right)} \tag{2.43}$$

substituting $\theta = 0$

$$E_\theta = -j\eta I_0 \frac{\exp(-jkr)}{2\pi r}\cos\phi\left[1-\cos\left(\frac{kL}{2}\right)\right]$$

and similarily

$$E_\phi = j\eta I_0 \frac{\exp(-jkr)}{2\pi r}\sin\phi\left[1-\cos\left(\frac{kL}{2}\right)\right]$$

$$E = j\eta I_0 \frac{\exp(-jkr)}{2\pi r}\left[1-\cos\left(\frac{kL}{2}\right)\right] \tag{2.44}$$

and

$$H = jI_0 \frac{\exp(-jkr)}{2\pi r}\left[1-\cos\left(\frac{kL}{2}\right)\right] \tag{2.45}$$

The above equations are valid for | $\sin^2\theta \cos^2\phi$ | not equal to one. The case in which the expression | $\sin^2\theta \cos^2\phi$ | becomes equal to one is when θ is equal to $(2n+1)\pi/2$ and ϕ equals to $2m\pi$ where m, n $\in$ ...-2,-1,0,1,2,... and the case is discussed in the next section.

Case II: When θ is $(2n+1)\pi/2$ and ϕ is $2m\pi$

Under this case equation 2.43 attains divided by zero form, which has to be evaluated. To do these substitute θ as $(2n+1)\pi/2$ in equation 2.43 and then apply the limits to the expression as $\phi \rightarrow 2m\pi$ to the resultant expression. Then result is

$$\begin{aligned} E_\theta = 0 &\Rightarrow H_\phi = 0 \\ E_\phi = 0 &\Rightarrow H_\theta = 0 \\ E = H &= 0 \end{aligned} \qquad (2.46)$$

Thus the field along the axis of the microstrip is zero. The far-field pattern of the single element is thus Omnidirectional. When used as an element in the planar array, we should expect suppression of radiation along ϕ equal to 0 and 180 degrees for θ equal 90 degrees.

2.3 Array Pattern of the Microstrip Array

The array pattern of an array with any element can be obtained by the principle of pattern multiplication where the element factor is multiplied by the array factor of the

array. However this is only true when there is no mutual coupling between the elements. If there is no coupling between the elements, then

$$\mathbf{E}\ (\text{total}) = [\mathbf{E}\ (\text{single element at reference point})] \times [\text{array factor}] \qquad (2.47)$$

The equation 2.47 assumes that all elements of the array are identical. For a practical array, there will however be mutual coupling between the elements of the array and must be taken into consideration, as it will change the exciting current amplitudes and phases. For finding the mutual coupling between the elements, it is required to calculate the near fields of the elements. This is the subject of the next chapter.

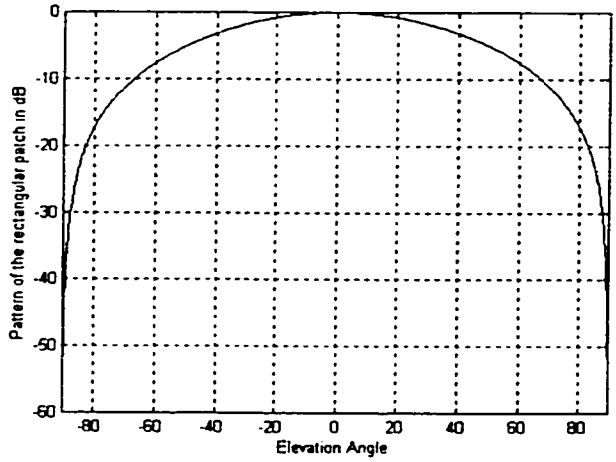

Figure 2.4: Element pattern of the microstrip antenna showing the pattern variation with θ for $\phi = 0^0$

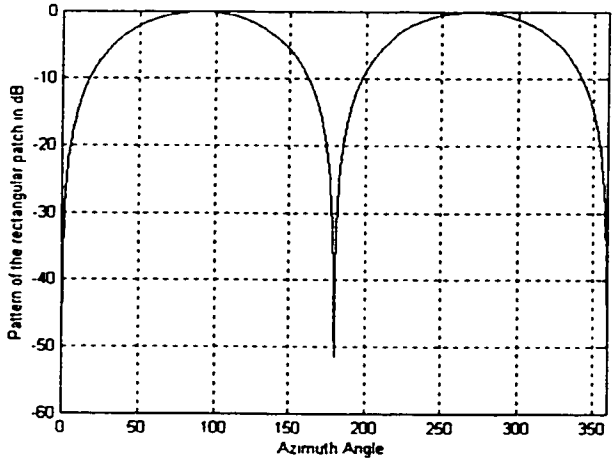

Figure 2.5: Element pattern of the microstrip antenna showing the pattern variation with ϕ for $\theta = 90^0$

CHAPTER 3

MUTUAL COUPLING IN MICROSTRIP ANTENNAS

In this chapter the coupling effects that are present in microstrip array are studied analytically. The expressions are derived based on the assumptions made in section 2.2.2. After obtaining the expressions for the mutual- and self- impedance, the currents in the microstrip elements are obtained. The patterns are then obtained from the resultant currents. However to get the mutual- and self-impedance expressions the near fields due to the microstrip antenna have to be obtained. So first the near fields due to a rectangular microstrip element in its plane are obtained. Then when another element is brought in the vicinity of the existing element, the current in the elements changes in both amplitude and phase. The amount of change depends on the mutual coupling between the elements.

As now the currents are changed, the far-fields due to these elements change from the case when there is no mutual coupling. This is the phenomenon for any number of elements that exist in the vicinity of one another, as is the case of array. Therefore the next logical step is to calculate the self- and mutual-impedance expressions for the two elements and then applying to the array elements. Thus the impedance matrix of the array is obtained from which the currents in the elements are derived. The sections devoted for this chapter follows the same line of approach as is illustrated here.

3.1 Near Fields of the Microstrip Antenna

For the microstrip antenna shown in figure 2.3, the expressions for the near fields can be calculated by using the vector potential equation given by the expression 2.32 for the current density distribution given by the expression 2.31. These expressions are reproduced here for convenience.

$$J(x',y') = J(x') = \begin{cases} \bar{a}_x \dfrac{I_0}{W} \sin\left(k\left(\dfrac{L}{2} - x'\right)\right) & 0 \le x' \le L/2 \\ \bar{a}_x \dfrac{I_0}{W} \sin\left(k\left(\dfrac{L}{2} + x'\right)\right) & -L/2 \le x' \le 0 \end{cases} \tag{3.1}$$

$$A = \frac{\mu}{4\pi} \iint_s J(x',y') \frac{\exp(-jkR)}{R} ds' \tag{3.2}$$

$$R = \sqrt{(x-x')^2 + (y-y')^2 + (z-z')^2} \tag{3.3}$$

But the approximation made for R in the section 2.2.2 is no longer a valid. The integral given by the equation 3.2 has to be evaluated for exact R otherwise the procedure is the same. The complexity lies in evaluating this integral for which only the plane of the microstrip antenna is considered, as we only require the fields in the plane of the microstrip antenna for mutual coupling calculations. And we require fields in cylindrical coordinates (unlike far fields that are found in spherical coordinates) and the formulae required for conversion from rectangular coordinates to the cylindrical coordinates are derived for our geometry and are included in the appendix A. Only A_x component exists as the current variation is only along x-direction.

$$H = \frac{1}{\mu}(\nabla \times A) \qquad \text{(from Maxwells Equations)} \tag{3.4a}$$

$$\Rightarrow \qquad H_\theta = \frac{1}{\mu}\frac{\partial A_x}{\partial \rho} \tag{3.4b}$$

$$\& \quad H_\rho = -\frac{1}{\mu}\frac{\partial A_x}{\rho \partial \theta} \qquad (\because \quad A_y \,\&\, A_z \text{ are both zero}) \tag{3.4c}$$

H_ρ is zero when θ equals to $+/-90^0$

$$\therefore \; H_\theta = \frac{1}{4\pi}\int_{-L/2}^{L/2}\int_{-W/2}^{W/2} \frac{\partial}{\partial \rho}\left(J(x',y')\frac{e^{-jkR}}{R}\right)dx'dy' \tag{3.5}$$

$as \;\; x = x;\; y = \rho\sin\theta;\; z = \rho\cos\theta \;\; and \; \theta = \pi/2;$

$$\Rightarrow \;\; y = \rho \;\; and \;\; \frac{\partial}{\partial y} = \frac{\partial}{\partial \rho}$$

now consider

$$\frac{1}{4\pi}\int_{-L/2}^{L/2}\frac{\partial}{\partial\rho}\left(J(x',y')\frac{e^{-jkR}}{R}\right)dx' \tag{3.6}$$

$$=\frac{1}{4\pi}\int_{-L/2}^{L/2}\frac{\partial}{\partial y}\left(J(x',y')\frac{e^{-jkR}}{R}\right)dx' \tag{3.7}$$

$$=\frac{I_0}{4\pi W}\left[\int_{-L/2}^{0}\frac{\partial}{\partial y}\left[\sin\left(k\left(\frac{L}{2}+x'\right)\right)\frac{e^{-jkR}}{R}\right]dx'+\int_{0}^{L/2}\frac{\partial}{\partial y}\left[\sin\left(k\left(\frac{L}{2}-x'\right)\right)\frac{e^{-jkR}}{R}\right]dx'\right]$$

$$=\frac{I_0}{8\pi jW}\left[e^{j\frac{kL}{2}}\int_{-L/2}^{0}\frac{\partial}{\partial y}\left[\frac{e^{-jk(R-x')}}{R}\right]dx'-e^{-j\frac{kL}{2}}\int_{-L/2}^{0}\frac{\partial}{\partial y}\left[\frac{e^{-jk(R+x')}}{R}\right]dx'\right.$$
$$\left.+e^{j\frac{kL}{2}}\int_{0}^{L/2}\frac{\partial}{\partial y}\left[\frac{e^{-jk(R+x')}}{R}\right]dx'-e^{-j\frac{kL}{2}}\int_{0}^{L/2}\frac{\partial}{\partial y}\left[\frac{e^{-jk(R-x')}}{R}\right]dx'\right] \tag{3.8}$$

consider

$$e^{j\frac{kL}{2}}\int_{-L/2}^{0}\frac{\partial}{\partial y}\left[\frac{e^{-jk(R-x')}}{R}\right]dx'=e^{j\frac{kL}{2}}\int_{-L/2}^{0}\left\{\frac{1}{R}\frac{\partial}{\partial y}\left(e^{-jk(R-x')}\right)+e^{-jk(R-x')}\frac{\partial}{\partial y}\left(\frac{1}{R}\right)\right\}dx'$$
$$=(y-y')e^{j\frac{kL}{2}}\int_{-L/2}^{0}\left[-\frac{jk}{R^2}e^{-jk(R-x')}-\frac{1}{R^3}e^{-jk(R-x')}\right]dx' \tag{3.9}$$

now consider

$$d\left(\frac{e^{-jk(R-x')}}{R(R-x'+x)}\right)=e^{-jk(R-x')}\left[\frac{dR^{-1}}{(R-x'+x)}+\frac{d(R-x'+x)^{-1}}{R}-jk\frac{d(R-x')}{R(R-x'+x)}\right]$$
$$=e^{-jk(R-x')}\left[\frac{jk}{R^2}+\frac{1}{R^3}\right]dx' \tag{3.10}$$

therefore

$$e^{j\frac{kL}{2}}\int_{-L/2}^{0}\frac{\partial}{\partial y}\left[\frac{e^{-jk(R-x')}}{R}\right]dx'=(y-y')e^{j\frac{kL}{2}}\left[\frac{e^{-jk(R_1+L/2)}}{R_1(R_1+L/2+x)}-\frac{e^{-jkR_2}}{R_2(R_2+x)}\right]$$
$$=\frac{e^{j\frac{kL}{2}}}{(y-y')}\left[\left(1-\frac{L/2+x}{R_1}\right)e^{-jk(R_1+L/2)}-\left(1-\frac{x}{R_2}\right)e^{-jkR_2}\right]$$

$$-e^{-j\frac{kL}{2}}\int_{-L/2}^{0}\frac{\partial}{\partial y}\left[\frac{e^{-jk(R+x')}}{R}\right]dx'=\frac{e^{-j\frac{kL}{2}}}{(y-y')}\left[\left(1+\frac{L/2+x}{R_1}\right)e^{-jk(R_1-L/2)}-\left(1+\frac{x}{R_2}\right)e^{-jkR_2}\right]$$

$$e^{j\frac{kL}{2}}\int_{0}^{L/2}\frac{\partial}{\partial y}\left[\frac{e^{-jk(R+x')}}{R}\right]dx'=\frac{e^{j\frac{kL}{2}}}{(y-y')}\left[\left(1-\frac{L/2-x}{R_3}\right)e^{-jk(R_3+L/2)}-\left(1+\frac{x}{R_2}\right)e^{-jkR_2}\right]$$

$$-e^{-j\frac{kL}{2}}\int_0^{L/2}\frac{\partial}{\partial y}\left[\frac{e^{-jk(R-x')}}{R}\right]dx' = \frac{e^{-j\frac{kL}{2}}}{(y-y')}\left[\left(1+\frac{L/2-x}{R_3}\right)e^{-jk(R_3-L/2)}-\left(1-\frac{x}{R_2}\right)e^{-jkR_2}\right]$$

where,

$$R_1 = \sqrt{(x+L/2)^2+(y-y')^2}$$

$$R_2 = \sqrt{x^2+(y-y')^2}$$

$$R_3 = \sqrt{(x-L/2)^2+(y-y')^2}$$

$$\therefore \frac{1}{4\pi}\int_{-L/2}^{L/2}\frac{\partial}{\partial y}\left(J(x',y')\frac{e^{-jkR}}{R}\right)dx' = \frac{I_0}{4\pi jW}\frac{1}{(y-y')}\left[e^{-jkR_1}+e^{-jkR_3}-2\cos\left(\frac{kL}{2}\right)e^{-jkR_2}\right]$$

$$H_\theta = \frac{I_0}{4\pi jW}\int_{-W/2}^{W/2}\frac{1}{(y-y')}\left[e^{-jkR_1}+e^{-jkR_3}-2\cos\left(\frac{kL}{2}\right)e^{-jkR_2}\right]dy' \qquad (3.11)$$

to evaluate equation 3.11, *consider the following*

$$\int_{-W/2}^{W/2}\frac{e^{-jkR_1}}{(y-y')}dy'$$

$$(y-y')^2 = R_1^2-(x+L/2)^2 = R_2^2-x^2 = R_3^2-(x-L/2)^2$$

$$\frac{dy'}{(y-y')} = -\frac{R_1dR_1}{(y-y')^2} = -\frac{R_1dR_1}{\left(R_1^2-(x+L/2)^2\right)}$$

$$= \int_{U_1}^{L_1}\frac{R_1e^{-jkR_1}}{R_1^2-(x+L/2)^2}dR_1 = \frac{1}{2}\int_{U_1}^{L_1}\frac{e^{-jkR_1}dR_1}{R_1+(x+L/2)}+\frac{1}{2}\int_{U_1}^{L_1}\frac{e^{-jkR_1}dR_1}{R_1-(x+L/2)}$$

(making use of the formulae given in tables book [43])

$$= \frac{1}{2}e^{jk(x+L/2)}\left[Ei(-jk(L_1+x+L/2)-Ei(-jk(U_1+x+L/2)\right]+$$

$$+\frac{1}{2}e^{-jk(x+L/2)}\left[Ei(-jk(L_1-x-L/2)-Ei(-jk(U_1-x-L/2)\right]$$

with a similar approach, the integral for H_θ can be evaluated and is given by the equation 3.12

$$H_\theta = \frac{I_0}{8\pi jW}\left\{\begin{array}{l} e^{jk(x+L/2)}\left[Ei[-jk(L_1+x+L/2)]-Ei[-jk(U_1+x+L/2)]\right] \\ +e^{-jk(x+L/2)}\left[Ei[-jk(L_1-x-L/2)]-Ei[-jk(U_1-x-L/2)]\right] \\ +e^{jk(x-L/2)}\left[Ei[-jk(L_3+x-L/2)]-Ei[-jk(U_3+x-L/2)]\right] \\ +e^{-jk(x-L/2)}\left[Ei[-jk(L_3-x+L/2)]-Ei[-jk(U_3-x+L/2)]\right] \\ -2\cos\left(\frac{kL}{2}\right)e^{jkx}\left[Ei[-jk(L_2+x)]-Ei[-jk(U_2+x)]\right] \\ -2\cos\left(\frac{kL}{2}\right)e^{-jkx}\left[Ei[-jk(L_2-x)]-Ei[-jk(U_2-x)]\right] \end{array}\right\} \tag{3.12}$$

$$E = \frac{1}{j\omega\varepsilon}(\nabla \times H) \tag{3.13}$$

as $A_y = A_z = 0$; A_θ *and* A_ρ *are both zero*

$$E = E_x = \frac{1}{j\omega\varepsilon}\left(-\frac{1}{\rho}\frac{\partial(\rho H_\theta)}{\partial\rho}\right) \tag{3.14}$$

$$E_x = -\frac{1}{j\omega\varepsilon y}\frac{\partial(yH_\theta)}{\partial y} \qquad (as\ \rho = y)$$

$$\Rightarrow E_x = \left\{\begin{array}{l} \frac{\eta}{4\pi}\frac{I_0}{W}\frac{1}{k}\left[\begin{array}{l} \frac{(y+W/2)}{L_1{}^2-(x+L/2)^2}e^{-jkL_1}-\frac{(y-W/2)}{U_1{}^2-(x+L/2)^2}e^{-jkU_1} \\ +\frac{(y+W/2)}{L_3{}^2-(x-L/2)^2}e^{-jkL_3}-\frac{(y-W/2)}{U_3{}^2-(x-L/2)^2}e^{-jkU_3} \\ -2\cos\left(\frac{kL}{2}\right)\left(\frac{(y+W/2)}{L_2{}^2-x^2}e^{-jkL_2}-\frac{(y-W/2)}{U_2{}^2-x^2}e^{-jkU_2}\right) \end{array}\right] \\ +\frac{j\eta}{ky}H_\theta \end{array}\right\} \tag{3.15}$$

where

$$U_1 = \sqrt{(x+L/2)^2+(y-W/2)^2} \quad ; \quad L_1 = \sqrt{(x+L/2)^2+(y+W/2)^2}$$
$$U_2 = \sqrt{x^2+(y-W/2)^2} \quad ; \quad L_2 = \sqrt{x^2+(y+W/2)^2}$$
$$U_3 = \sqrt{(x-L/2)^2+(y-W/2)^2} \quad ; \quad L_3 = \sqrt{(x-L/2)^2+(y+W/2)^2}$$

E_x is used for mutual coupling calculations and is given by equation 3.15.

3.2 Self- and Mutual- Impedances of the two Microstrip Elements

The expressions for the input impedance of a microstrip element and the mutual impedance due to other microstrip elements are derived in this section. For isolated elements, self-impedance referred to the input terminals is the input impedance and is also called the driving impedance. However when a number of elements exist in vicinity of each other, then the driving impedance of an element is the sum of self-impedance due to itself and the mutual impedance due to the other existing elements multiplied by the ratio of the current amplitude of that particular element to its current amplitude.

i.e.,

$$Z_d = \frac{V_1}{I_1} = Z_{11} + \sum_m Z_{1m} \frac{I_m}{I_1}$$

3.2.1 Mutual Impedance

Due to mutual impedance, the performance not only depends on its own current distribution but also on the current distribution of the neighboring elements. The antenna designer, therefore, must take into account the mutual effects between elements. Therefore the driving point impedance will depend on the self-impedance and the mutual impedance between the driven element and the other obstacles or elements.

referring to figure 3.1, the mutual impedance as referred to the input terminals is given by

$$Z_{21i} = \frac{V_{21i}}{I_{1i}} = -\frac{1}{I_{1i}I_{2i}} \int_{-l_2/2}^{l_2/2} E_{x21}(x) I_2(x) dx \tag{3.16}$$

the relation between the impedances when referred to the input terminals and and the current maximum is given by

$$Z_{21m} = Z_{21i} \times \frac{I_{1i}}{I_{1m}} \frac{I_{2i}}{I_{2m}}$$

for identical patches

$$Z_{21m} = -\frac{\eta}{4\pi} \frac{1}{W} \frac{1}{k} \int_{-L/2}^{L/2} \left\{ \sin\left(k\left(\frac{L}{2} - |x| \right) \right) p(x) \right\} dx - \frac{j\eta}{Wky''} \int_{-L/2}^{L/2} \left\{ \sin\left(k\left(\frac{L}{2} - |x| \right) \right) q(x) \right\} dx \tag{3.17}$$

where

$$p(x) = \frac{(y''+W/2)}{L_1^2 - (x''+L/2)^2} e^{-jkL_1} - \frac{(y''-W/2)}{U_1^2 - (x''+L/2)^2} e^{-jkU_1} + \frac{(y''+W/2)}{L_3^2 - (x''-L/2)^2} e^{-jkL_3} - \frac{(y''-W/2)}{U_3^2 - (x''-L/2)^2} e^{-jkU_3} - 2\cos\left(\frac{kl}{2}\right) \left[\frac{(y''+W/2)}{L_2^2 - x''^2} e^{-jkL_2} - \frac{(y''-W/2)}{U_2^2 - x''^2} e^{-jkU_2} \right] \tag{3.18}$$

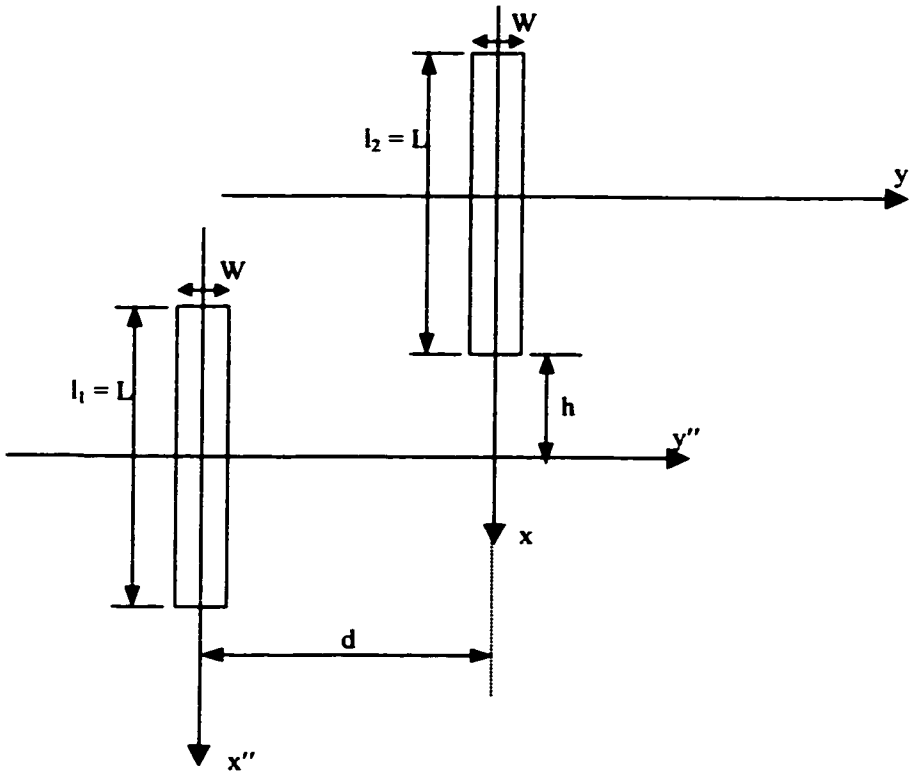

Figure 3.1: Microstrip antenna positioning for mutual coupling

and,

$$q(x)=\frac{1}{8\pi j}\left\{\begin{array}{l} e^{jk(x-h)}\left[Ei\left[-jk(L_1+x-h)\right]-Ei\left[-jk(U_1+x-h)\right]\right] \\ +e^{-jk(x-h)}\left[Ei\left[-jk(L_1-x+h)\right]-Ei\left[-jk(U_1-x+h)\right]\right] \\ +e^{jk(x-h-L)}\left[Ei\left[-jk(L_3+x-h-L)\right]-Ei\left[-jk(U_3+x-h-L)\right]\right] \\ +e^{-jk(x-h-L)}\left[Ei\left[-jk(L_3-x+h+L)\right]-Ei\left[-jk(U_3-x+h+L)\right]\right] \\ -2\cos\left(\frac{kL}{2}\right)e^{jk(x-h-L/2)}\left[\begin{array}{l} Ei\left[-jk(L_2+x-h-L/2)\right] \\ -Ei\left[-jk(U_2+x-h-L/2)\right] \end{array}\right] \\ -2\cos\left(\frac{kL}{2}\right)e^{-jk(x-h-L/2)}\left[\begin{array}{l} Ei\left[-jk(L_2-x+h+L/2)\right] \\ -Ei\left[-jk(U_2-x+h+L/2)\right] \end{array}\right] \end{array}\right\} \tag{3.19}$$

in equations 3.18 & 3.19,

U_1, L_1, U_2, L_2 & U_3, L_3 are given by the expressions given below

$$U_1=\sqrt{(x''+L/2)^2+(y''-W/2)^2} \quad ; \quad L_1=\sqrt{(x''+L/2)^2+(y''+W/2)^2}$$
$$U_2=\sqrt{x''^2+(y''-W/2)^2} \quad ; \quad L_2=\sqrt{x''^2+(y''+W/2)^2}$$
$$U_3=\sqrt{(x''-L/2)^2+(y''-W/2)^2} \quad ; \quad L_3=\sqrt{(x''-L/2)^2+(y''+W/2)^2}$$

from figure 3.1

$$x''=x-h-L/2 \quad ; \quad y''=y+d$$

substituting $y=0$ *and* $\eta=120\pi$

$$Z_{21m}=-\frac{30}{Wk(d+W/2)}I_1+\frac{30}{Wk(d-W/2)}I_2-\frac{15}{Wkd}I_3 \tag{3.20}$$

where,

$$I_1=\int_{-L/2}^{L/2}\sin\left[k\left(\frac{L}{2}-|x|\right)\right]\times\left[e^{-jkL_1}+e^{-jkL_3}-2\cos\left(\frac{kL}{2}\right)e^{-jkL_2}\right]dx$$

$$I_2=\int_{-L/2}^{L/2}\sin\left[k\left(\frac{L}{2}-|x|\right)\right]\times\left[e^{-jkU_1}+e^{-jkU_3}-2\cos\left(\frac{kL}{2}\right)e^{-jkU_2}\right]dx$$

$$I_3 = \int_{-L/2}^{L/2} \sin\left[k\left(\frac{L}{2} - |x|\right)\right] \times S(x)\,dx$$

where

$$S(x) = \left\{ \begin{array}{ll} & e^{jk(x-h)}\left[Ei[-jk(L_1 + x - h)] - Ei[-jk(U_1 + x - h)]\right] \\ + & e^{-jk(x-h)}\left[Ei[-jk(L_1 - x + h)] - Ei[-jk(U_1 - x + h)]\right] \\ + & e^{jk(x-h-L)}\left[Ei[-jk(L_3 + x - h - L)] - Ei[-jk(U_3 + x - h - L)]\right] \\ + & e^{-jk(x-h-L)}\left[Ei[-jk(L_3 - x + h + L)] - Ei[-jk(U_3 - x + h + L)]\right] \\ - & 2\cos\left(\frac{kL}{2}\right)e^{jk(x-h-L/2)}\left[\begin{array}{c} Ei[-jk(L_2 + x - h - L/2)] \\ -Ei[-jk(U_2 + x - h - L/2)] \end{array}\right] \\ - & 2\cos\left(\frac{kL}{2}\right)e^{-jk(x-h-L/2)}\left[\begin{array}{c} Ei[-jk(L_2 - x + h + L/2)] \\ -Ei[-jk(U_2 - x + h + L/2)] \end{array}\right] \end{array} \right\}$$

The variation of mutual coupling as a function of d/λ, for side-by-side arrangement is shown in the figure 3.2 and its variation as a function of s/λ for collinear arrangement is shown in figure 3.3, where s = h – L/2. These results were simulated for a microstrip of length L = 0.5λ and width W = 0.01λ.

3.2.2 Self Impedance

The self-impedance of an antenna is a very important parameter, and it is also used to determine the efficiency of the antenna. The real part of this impedance is called the radiation resistance and is responsible for the radiation of power from the antenna (assuming the antenna is loss less). The reactance part is responsible for the imaginary power and is dominant in the near-field region and is negligible in far-field region.

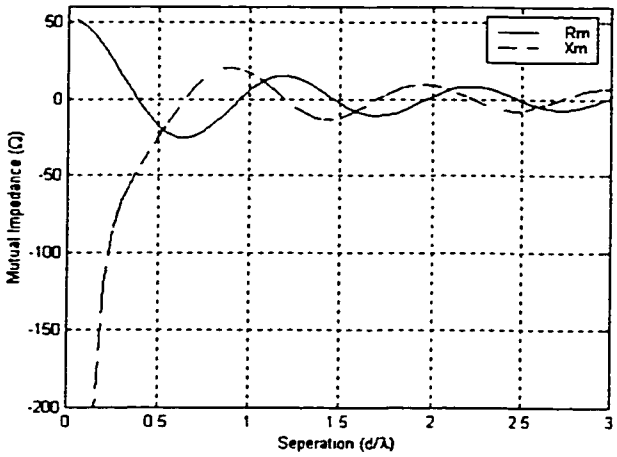

Figure 3.2: Variation of mutual coupling between the two elements arranged side-by-side as a function of separation between the elements expressed in wavelength (h = -L/2)

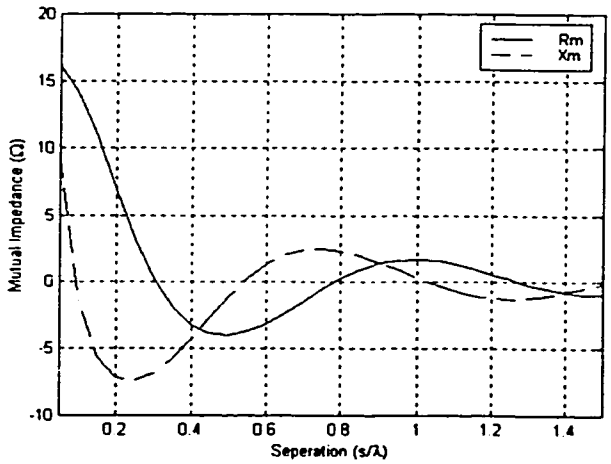

Figure 3.3: Variation of mutual coupling between the two elements arranged collinearly as a function of separation between the elements expressed in wavelength (s = h-L/2)

The expression for self-impedance Z_{11} is derived as follows

the self impedance referred to the input terminals is given by

$$Z_{11_r} = \frac{V_{11_r}}{I_{1_r}} = -\frac{1}{I_{1_r}^{\,2}} \int_{-l_1/2}^{l_1/2} E_{x11}(x) I_1(x)\, dx \tag{3.21}$$

referring to the current maximum, we get

$$Z_{11m} = Z_{11_r} \times \frac{I_{1_r}^{\,2}}{I_{1m}^{\,2}}$$

for patch dimensions : length = L and width = W

$$\therefore Z_{11m} = -\frac{1}{I_m^{\,2}} \int_{-L/2}^{L/2} E_{x11} I_1(x) dx \Big|_{y \to W/2} \tag{3.22}$$

where,

$$E_{x11}(x) = 30\frac{I_0}{W}\frac{1}{k(y+W/2)}\left\{e^{-jkL_1} + e^{-jkL_3} - 2\cos\left(\frac{kL}{2}\right)e^{-jkL_2}\right\}$$

$$-30\frac{I_0}{W}\frac{1}{k(y-W/2)}\left\{e^{-jkU_1} + e^{-jkU_3} - 2\cos\left(\frac{kL}{2}\right)e^{-jkU_2}\right\}$$

$$+15\frac{I_0}{W}\frac{1}{ky}\left\{\begin{array}{l} e^{jk(x+L/2)}\left[Ei[-jk(L_1+x+L/2)] - Ei[-jk(U_1+x+L/2)]\right] \\ + e^{-jk(x+L/2)}\left[Ei[-jk(L_1-x-L/2)] - Ei[-jk(U_1-x-L/2)]\right] \\ + e^{jk(x-L/2)}\left[Ei[-jk(L_3+x-L/2)] - Ei[-jk(U_3+x-L/2)]\right] \\ + e^{-jk(x-L/2)}\left[Ei[-jk(L_3-x+L/2)] - Ei[-jk(U_3-x+L/2)]\right] \\ - 2\cos\left(\frac{kL}{2}\right)e^{jkx}\left[Ei[-jk(L_2+x)] - Ei[-jk(U_2+x)]\right] \\ - 2\cos\left(\frac{kL}{2}\right)e^{-jkx}\left[Ei[-jk(L_2-x)] - Ei[-jk(U_2-x)]\right] \end{array}\right\} \tag{3.23}$$

where

$$U_1 = \sqrt{(x+L/2)^2 + (y-W/2)^2} \quad ; \quad L_1 = \sqrt{(x+L/2)^2 + (y+W/2)^2}$$

$$U_1 = \sqrt{x^2 + (y-W/2)^2} \quad ; \quad L_1 = \sqrt{x^2 + (y+W/2)^2}$$

$$U_1 = \sqrt{(x-L/2)^2 + (y-W/2)^2} \quad ; \quad L_1 = \sqrt{(x-L/2)^2 + (y+W/2)^2}$$

Equation 3.22 is plotted and is shown in figure 3.4, which plots the self-impedance variation as a function of the length of microstrip antenna for a constant width equal to 0.01λ. The variation is shown as a function of L/λ.

Now the mutual and self impedance was studied in detail for two elements in general where ever they are located, its now time to use these relations to our planar array to study the mutual coupling effects and resultant current distributions due to coupling effects. This is the subject of the next chapter i.e., Chapter 4.

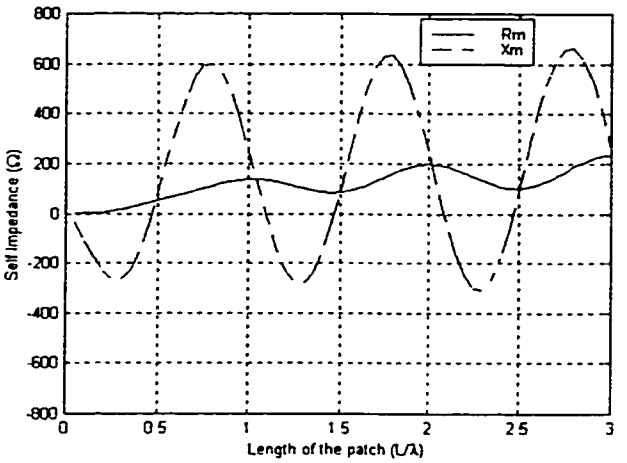

Figure 3.4: Input impedance variation as a function of the patch length (width = 0.01λ)

CHAPTER 4

CHARACTERISTICS OF THE MICROSTRIP ARRAY

In this chapter a practical microstrip array is studied in detail. In microstrip antennas it is very important to consider the mutual coupling between the elements as the coupling changes their exciting current amplitudes and phases. Not only in microstrip array, but also in any practical array, the mutual coupling between radiators significantly alters the array performance [10]. Had there been no mutual coupling, the array pattern of the array can be obtained simply by the multiplication of the array factor and the element pattern. In case of mutual coupling, the element factor must not refer to the pattern of an isolated element, but rather to the pattern of an individual element in the presence of all other elements in the array. This consideration of the other elements can result in a

change in the beam width and other parameters. The strength of mutual coupling is inversely proportional to the separation between the elements and also on their relative orientation.

4.1 Coupling Between Microstrip Elements

Consider a microstrip antenna element with input impedance equal to its self-impedance, Z_{11}. If another microstrip element is brought in its proximity and is parasitic (i.e., unexcited), then the first element induces currents in the second and the reradiated fields from the second effect the current distribution in the first element. If the second element is also excited, then the first element will also be affected by the direct radiation from the second element. This interchange of energy can be represented by mutual impedance Z_{12} or Z_{21}. For linear, reciprocal elements $Z_{12} = Z_{21}$ and if the elements are identical $Z_{11} = Z_{22}$ [10]. For an array, this procedure can be extended to formulate a mutual impedance matrix, mathematically expressed as

$$[V] = [Z][I] \tag{4.1}$$

$$\textit{and} \quad [I] = [Z]^{-1}[V] \tag{4.2}$$

Where, [Z] is the impedance matrix, [V] and [I] are the voltage and current matrices respectively. Each microstrip element is specified by its x and y coordinates and hence by

two numbers m and n (refer figure 4.1); therefore a typical row of matrix equation may by expressed as

$$V_{mn} = \sum_{u} \sum_{v} Z_{mn,uv} I_{uv} \qquad (4.3)$$

where

$Z_{mn,mn}$ are self impedances and

$Z_{mn,uv}$ for mn ≠ uv are mutual impedances

The mutual impedance depends on the spacing between the pair of elements, and their relative orientation, and not upon their position in the array. For self- and mutual-impedance, the expressions derived in the previous chapter can be used in obtaining a mutual impedance matrix in a straightforward manner. Once the impedance matrix is known, the exciting currents can be obtained by taking the matrix inverse and multiplying it with the voltage matrix which is an all ones matrix for uniform array (equation 4.2).

4.2 Z-Matrix Calculation for M×N Array

Following the approach outlined in section 4.1, we proceed to calculate the z-matrix of the M×N-element microstrip array. For the summarized calculations we use

- Inter-element spacing dx = dy = 0.5λ
- Microstrip antenna dimensions, length L = 0.5λ and width W = 0.01λ
- The length of the microstrip is along the x-axis
- Microstrip elements are electrically isolated

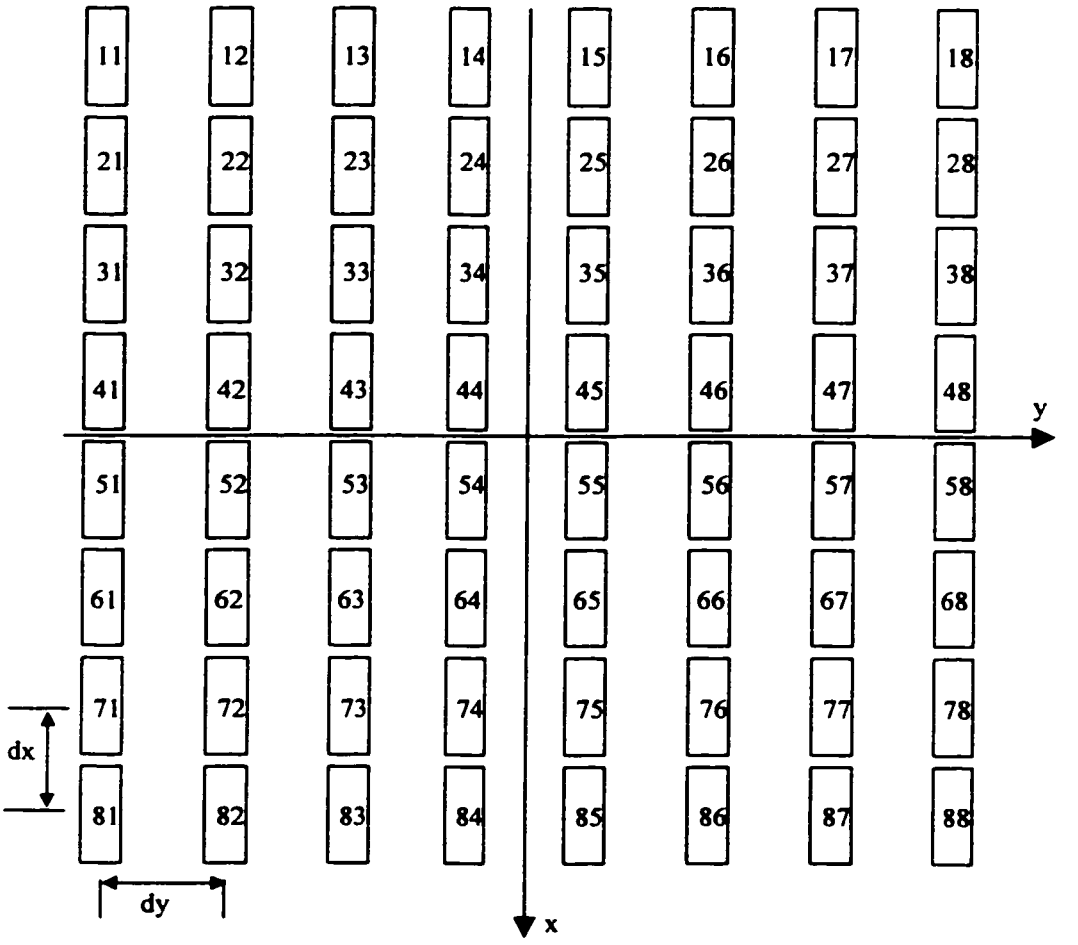

Figure 4.1: The 8×8-element microstrip antenna array; the numbers at the center of microstrip elements represent their coordinates for the axes

For the microstrip array shown in figure 4.1, for each element the self-impedance due to itself and mutual impedance due to the remaining 63 elements has to be calculated. If that is so, the driving point impedance of element mn (refer figure 4.1) can be obtained from the equation 4.4 given below, where M = N = 8.

$$Z_{mnD} = Z_{mn} + \sum_{u=1}^{M} \sum_{v=1}^{N} Z_{mn,uv} \left(\frac{I_{uv}}{I_{11}} \right) \tag{4.4}$$

The self-impedance due to itself and mutual- impedance due to others for element 11 are listed in table 4.1. Similar values can be obtained for the remaining elements and they are not included only for the reason of space.

$Z_{11,11}$ to $Z_{11,28}$	$Z_{11,31}$ to $Z_{11,48}$	$Z_{11,51}$ to $Z_{11,68}$	$Z_{11,71}$ to $Z_{11,88}$
52.8233 +83.5519i	-3.9777 - 1.1086i	-0.9519 - 0.1188i	-0.4186 - 0.0322i
-17.7745 -24.4090i	0.0201 + 1.6766i	-0.6739 + 0.2525i	-0.3639 + 0.0756i
5.7960 +17.0639i	3.7049 - 5.0429i	1.1874 + 0.1103i	0.1555 + 0.2038i
-2.7363 -12.1045i	-6.0961 + 3.0007i	0.4609 - 2.0411i	0.8294 - 0.4656i
1.5738 + 9.2798i	6.2526 - 0.3828i	-2.5124 + 1.4022i	-0.5450 - 0.9143i
-1.0179 - 7.5000i	-5.5048 - 1.2802i	2.9013 + 0.7089i	-1.0039 + 1.2800i
0.7110 + 6.2848i	4.6097 + 2.1576i	-1.9865 - 2.3571i	1.7873 + 0.0160i
-0.5242 - 5.4051i	-3.8122 - 2.5685i	0.6979 + 3.0730i	-1.2112 - 1.4563i
16.4396 +40.0812i	1.7104 + 0.2896i	0.6050 + 0.0625i	0.3085 + 0.0244i
-13.4689 + 0.2551i	0.8519 - 0.5819i	0.4911 - 0.1303i	0.2776 - 0.0477i
9.8538 + 6.3938i	-2.7389 + 0.8263i	-0.4633 - 0.2329i	-0.0239 - 0.1579i
-6.3816 - 7.5811i	2.2678 + 2.4118i	-0.9819 + 1.0554i	-0.5889 + 0.1770i
4.2201 + 7.0671i	0.0486 - 4.1472i	1.6228 + 0.4742i	-0.0454 + 0.7954i
-2.9316 - 6.2802i	-2.0636 + 3.8867i	-0.3325 - 2.0654i	1.1051 - 0.3621i
2.1331 + 5.5488i	3.1818 - 2.8433i	-1.3997 + 2.0450i	-0.7669 - 1.0102i
-1.6132 - 4.9295i	-3.6065 + 1.7420i	2.3925 - 0.9322i	-0.5498 + 1.4647i

Table 4.1: The self- and mutual-impedance values for element 11 of the figure 4.1

4.3 Far Field Radiation Patterns

The array pattern with coupling can be obtained by getting the array factor due to the current distributions obtained after coupling consideration and then multiplying array factor to the element pattern of the microstrip antenna. Then the array pattern AP for an 8×8-element array is given by the equation

$$AP_{8\times 8} = \sum_{n=-4}^{-1}\left[\sum_{m=-4}^{-1} EP\times I_{m,n}\exp\left(-j\left(\left(\frac{2m+1}{2}\right)\Psi_x - ph_{mn}\right)\right)+ \sum_{m=1}^{4} EP\times I_{m,n}\exp\left(-j\left(\left(\frac{2m-1}{2}\right)\Psi_x - ph_{mn}\right)\right)\right]\times\exp\left(-j\left(\frac{2n+1}{2}\right)\Psi_y\right)$$

$$+\sum_{n=1}^{4}\left[\sum_{m=-4}^{-1} EP\times I_{m,n}\exp\left(-j\left(\left(\frac{2m+1}{2}\right)\Psi_x - ph_{mn}\right)\right)+ \sum_{m=1}^{4} EP\times I_{m,n}\exp\left(-j\left(\left(\frac{2m-1}{2}\right)\Psi_x - ph_{mn}\right)\right)\right]\times\exp\left(-j\left(\frac{2n+1}{2}\right)\Psi_y\right) \quad (4.5)$$

where

$$EP = \sqrt{(E_\theta)^2 + (E_\phi)^2} \quad (4.6)$$

$$E_\theta = -j\eta\frac{\exp(-jkr)}{\pi r}\frac{\sin\left(\frac{kW}{2}\sin\theta\sin\phi\right)}{kW\tan\theta\tan\phi}\frac{\left[\cos\left(\frac{kL}{2}\sin\theta\cos\phi\right)-\cos\left(\frac{kL}{2}\right)\right]}{\left(1-\sin^2\theta\cos^2\phi\right)} \quad (4.7)$$

$$E_\phi = j\eta\frac{\exp(-jkr)}{\pi r}\frac{\sin\left(\frac{kW}{2}\sin\theta\sin\phi\right)}{kW\sin\theta}\frac{\left[\cos\left(\frac{kL}{2}\sin\theta\cos\phi\right)-\cos\left(\frac{kL}{2}\right)\right]}{\left(1-\sin^2\theta\cos^2\phi\right)} \quad (4.8)$$

$when\,\theta = 2n\pi$

$$E_\theta = -j\eta\frac{\exp(-jkr)}{2\pi r}\cos\phi\left[1-\cos\left(\frac{kL}{2}\right)\right] \tag{4.9}$$

$$E_\phi = j\eta\frac{\exp(-jkr)}{2\pi r}\sin\phi\left[1-\cos\left(\frac{kL}{2}\right)\right] \tag{4.10}$$

$when\,\theta = (2n+1)\pi/2$

$$E_\theta = E_\phi = 0 \tag{4.11}$$

and

$$\Psi_x = kd_x\cos\gamma_x + \beta_x \tag{4.12}$$

$$\Psi_y = kd_y\cos\gamma_y + \beta_y \tag{4.13}$$

$$\cos\gamma_x = \sin\theta\cos\phi \tag{4.14}$$

$$\cos\gamma_y = \sin\theta\sin\phi \tag{4.15}$$

'I_{mn}' is the excitation current amplitude obtained after coupling

'ph_{mn}' is the excitation current phase obtained after coupling

Using the equation 4.5, the array pattern after coupling $AP_{8\times8}$ can be found. The results of the array patterns before and after null steering of 8× 8-element microstrip array is discussed in detail in chapter 5. The effect of change in the number of elements and its null steering aspects are discussed in chapter 6 with some sample examples. The results of array factor and array pattern change due the change in the inter-element spacing for with and without coupling cases are also included in chapter 5 for 8×8-element array.

CHAPTER 5

RESULTS AND DISCUSSION

The simulated results of 8×8 element planar array are presented in this chapter. These results illustrate the null steering aspects of the array under two cases; one case in which we don't consider the coupling effects that actually exists between the elements of the array and the next case being the results generated with mutual coupling considerations. The nulls are steered using phase variation technique and using genetic algorithms. The algorithms and all other codes are developed in Matlab and are run on Pentium PC's. The results are presented in 3D color plots to view the total far-field pattern and 2D plots to further highlight the null steered results.

In phase perturbation technique, only the phases of the exited currents of the individual elements are varied, keeping the amplitudes constant. The null depths of –60

dB are achieved which is quite effective for all practical considerations. Single and double nulls are steered for 8×8 element microstrip planar array. The array factor results are also presented, which is the pattern due to the point sources along with the array pattern results. As regards the inter-element spacing, we chose dx = dy = 0.5λ (i.e., half wave length) and microstrip dimensions are chosen to be L = 0.5λ and W = 0.01λ. The genetic algorithm parameters used are: Population size = 60; Crossover probability = 0.5; Mutation = 1% of the population.

5.1 3D Representation of the planar array pattern

It was assumed necessary to first illustrate the three-dimensional plot before the result presentation and therefore this section is dedicated to it. Much of the information can be obtained from figure 5.1. The range of angle ϕ is from 0 to 360 and θ is from 0 to 90 degrees. For example moving along the x-axis from origin towards the circumference of the circle, θ obtains values from 0 to 90 degrees and ϕ remains 0 degrees. While moving along the circumference of the circle starting from x-axis and reaching back x-axis, ϕ obtains values from 0 to 360 degrees and θ remains at 90 degrees. The color at any point on the circle corresponds to a particular dB value, which can be obtained from the color

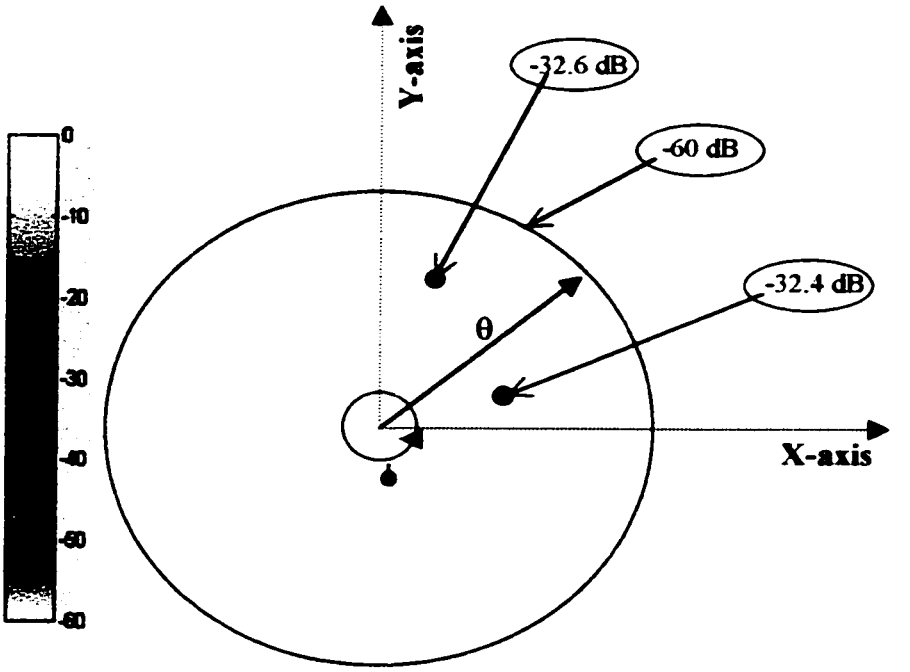

Figure 5.1: Figure illustrating the 3D-pattern setup; XY-plane is the plane of the array. The color bar indicates the coloring scheme followed through out to represent the results

scale indicated. The sample illustrations for red, black and yellow colors are highlighted and they indicate the dB value for which they correspond to.

5.2 The 8×8 Element Array

In this section the 8×8 element array is studied in detail. The results of the array factor, the array pattern with elements of the array being identical microstrips (L = 0.5λ, W = 0.01λ) and array patterns of mutual coupling are presented. The array has 64 elements all spread in xy-plane and the distance between the centers of any two elements is same equal to half wavelength. The microstrip elements lie in xy-plane and their length is along x-axis (figure 4.1) and the far-field equations derived in chapter 2 and mutual coupling equations from chapter 3 are used.

5.2.1 The Array Factor

Array factor of an array is the pattern due to the point sources that are replaced at the center of the elements. This pattern is very useful for the study of an array as it is only the array factor that is used to steer the nulls. The 3D plot of the array factor is shown in figure 5.2 and the figures 5.3 shows the 2D cuts along $\phi = 0$ and $\phi = 90$ degrees. The array is a broad side array in which the radiation is in perpendicular direction to the plane of

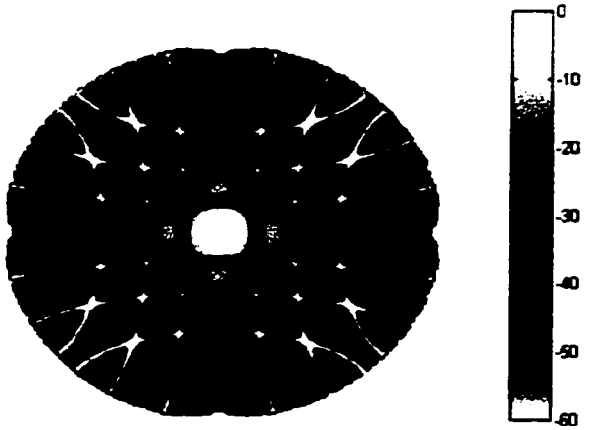

Figure 5.2: The array factor of 8×8 element array

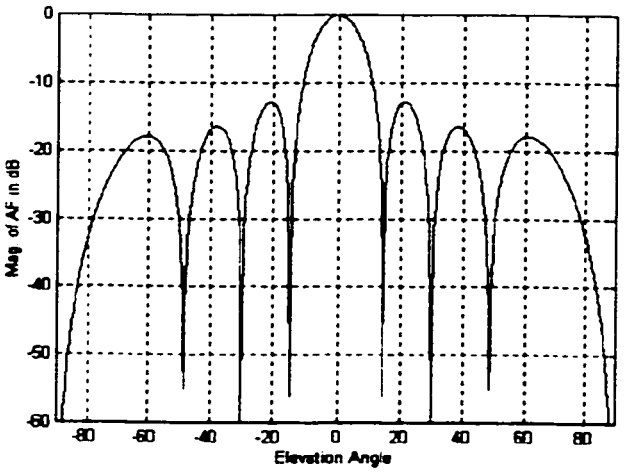

Figure 5.3: 2D plot of the array factor as a function of θ for $\phi = 0$ and 90

the array $\theta = 0$ degrees. The excitation amplitudes of all elements are equal (normalized to unity) and the excitation phases are zero for each. Referring to figure 5.3, there are three side lobes on either side of the main lobe. The side lobe level is -12.8 dB and the half power beam width is 12.8^0.

5.2.2 The Element Pattern

The far field element pattern of the microstrip antenna was discussed in chapter 2. However the 3D plot was not shown there. Figure 5.4 gives the three-dimensional pattern of the microstrip of length $L = 0.5\lambda$, width $W = 0.01\lambda$ and negligible thickness. The element pattern is omnidirectinal with a null along the axis of the microstrip. The radiation from the microstrip is concentrated more towards the direction normal to its axis. The radiation is only above the surface of the microstrip and there is no radiation below the microstrip. Once the element is chosen for an array its pattern is fixed and no pattern synthesis can be done to it. The element pattern shapes the overall array pattern and should be chosen as according to the application. Figure 5.5 is the same result presented in chapter 2 (figure 2.5) but has different microstrip widths results.

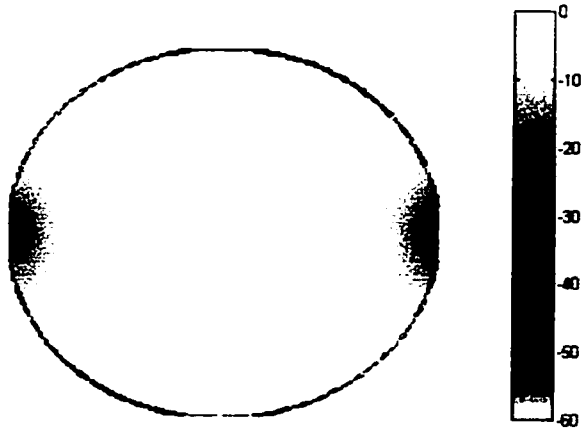

Figure 5.4: Microstrip antenna far-field pattern (L = 0.5λ, W = 0.01λ)

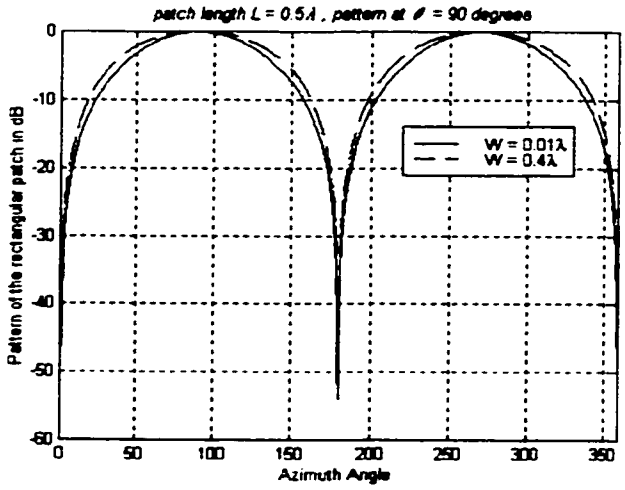

Figure 5.5: Microstrip antenna far-field pattern for different widths

5.2.3 The Array Pattern without Coupling effect

The array pattern without coupling is obtained by the application of pattern multiplication discussed in chapter 2, where the array factor is multiplied by the element pattern. Thus for the omnidirectional pattern of the microstrip, the array pattern of the array is far better than the original array factor. Figures 5.6 and 5.7 displays the 3D and 2D plot of the array pattern and is clear that the side lobes along the x-axis are suppressed when compared to the side lobes along the y-axis. However the number of side lobes is the same as is only dependent on the array geometry and number of elements. The side lobe level in x-direction is –13.65 dB where as the side lobe level in y-direction is –12.8 dB. The half power beam width in x-direction is 12.7^0 where as in y-direction it is 12.8^0. When compared with the array factor values, the side lobe level in x-direction is suppressed by 0.85 dB and is due to the element pattern, which is omnidirectional. However the side lobe level in the y-direction remained the same. Similar comparisons to the half power beam width reveals that there is 0.1^0 decrease in the x-direction and is same in y-direction. The array factor and the array pattern are compared in figures 5.8(a) through 5.8(d). During the multiplication of element pattern with array factor it is assumed through out that the elements are isolated from each other and the assumption is kept through out the results.

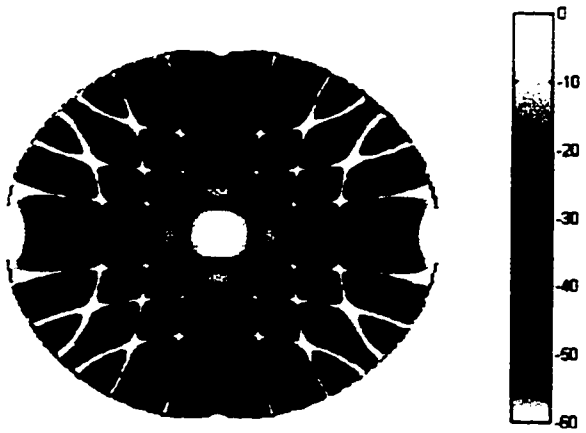

Figure 5.6: The array pattern of 8×8 element array without coupling

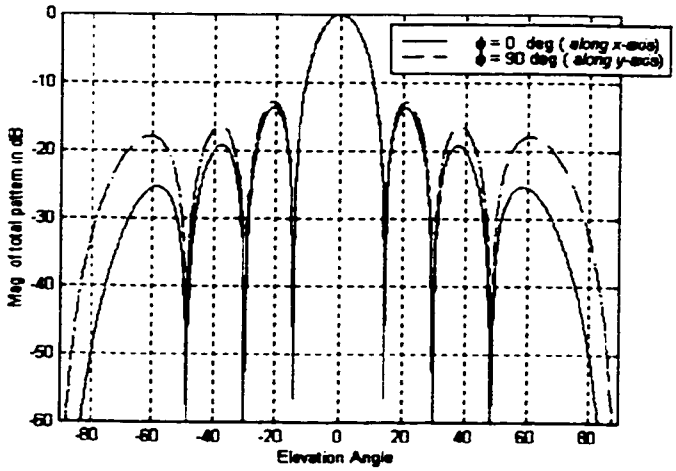

Figure 5.7: Comparison of the array pattern along x-axis and y-axis (Without coupling)

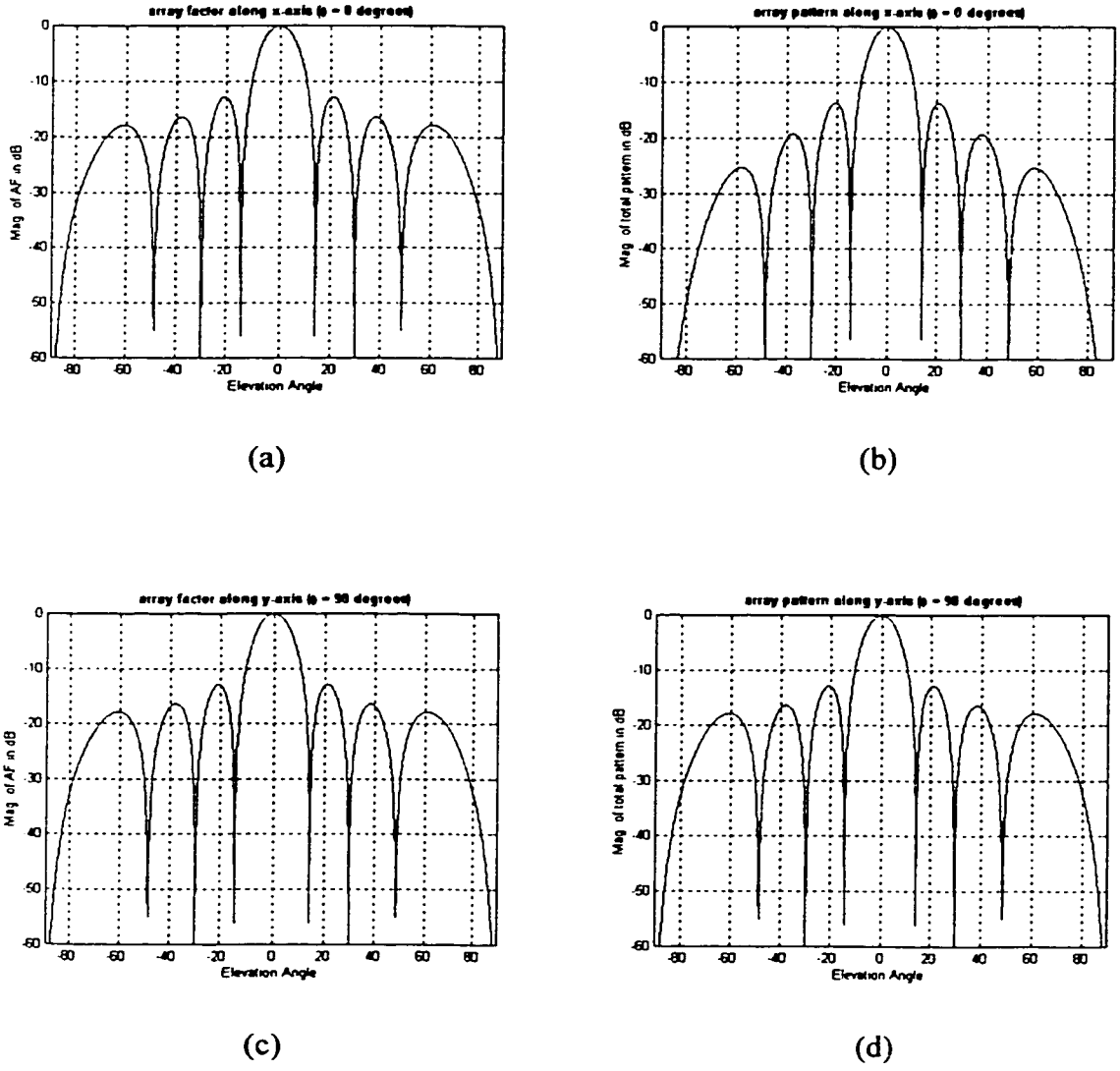

Figure 5.8: Comparison of array factor and array pattern of 8×8 element array

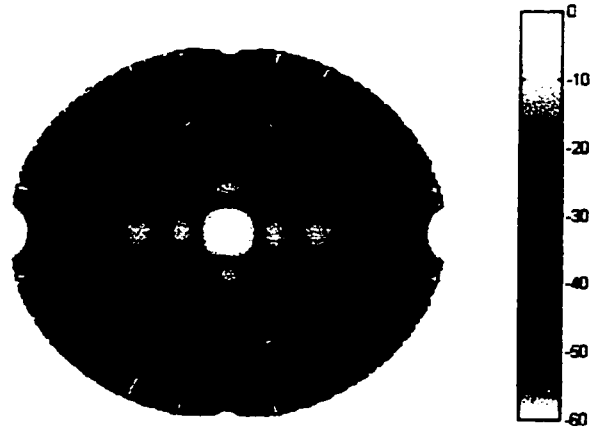

Figure 5.9: The array pattern after coupling considerations

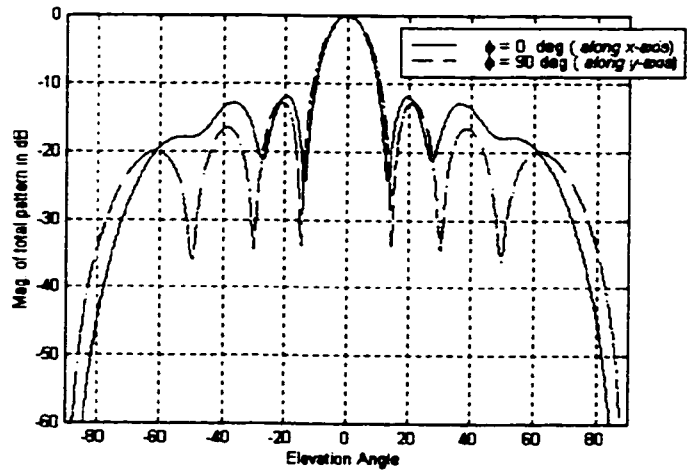

Figure 5.10: The array pattern along x-axis and y-axis (with coupling)

5.2.4 The Array Pattern with Coupling effect

The results of the array pattern with coupling are shown in figures 5.9 and 5.10 in which we observe that there is a more change in the pattern along the x-direction than along the y-direction. There is substantial decrease in the null depth between the side lobes and the side lobe level has increased. The side lobe level has increased to -12 dB and is 1.65 dB more when compared to the array pattern without coupling in x-direction. The side lobe level in y-direction is –12.8 dB, which is same as the side lobe level in the pattern without coupling. The half power beam width along the x-direction of the main beam is 12^0 and along the y-direction is 12.9^0. Comparing the half power beam width results with coupling with that of no coupling indicate that the beam width decreased by 0.7^0 along x-direction and has not changed along y-direction. Figure 5.11 gives the comparison between the pattern with and without coupling along ϕ =0 and figure 5.12 compares the patterns at ϕ = 90 degrees. All the results are tabulated in table 5.1.

8×8-Element Array (dx = dy = 0.5λ)	Along X-axis ($\phi = 0^0$)		Along Y-axis ($\phi = 90^0$)	
	HPBW	SLL	HPBW	SLL
Array factor	12.8^0	-12.8 dB	12.8^0	-12.8 dB
Array pattern without Coupling	12.7^0	-13.65 dB	12.8^0	-12.8 dB
Array pattern with Coupling	12^0	-12 dB	12.8^0	-12.8 dB

Table 5.1: Summary of results of the pattern parameters of the 8×8 array

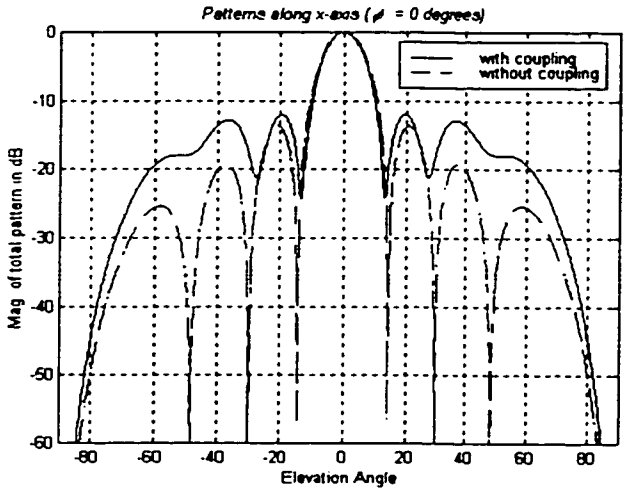

Figure 5.11: Comparison of array patterns (with and without coupling) along x-axis

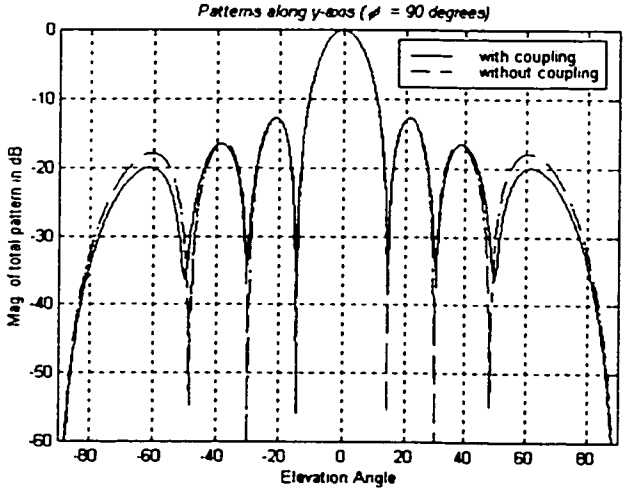

Figure 5.12: Comparison of array patterns (with and without coupling) along y-axis

For no coupling the exciting current amplitudes are all equal, normalized to unity and all the phases are zero. But with coupling, for equal exciting voltages applied to all the elements, the current amplitudes are no longer equal and also the phases. The current amplitude and phases for 8×8-element array were found and are given in the matrix form. The current phases in degrees and amplitudes (un-normalized) of the array after mutual coupling calculations are given by the following matrix expressions.

$$ph(with\ coupling) = \begin{bmatrix} -56.9102 & -56.2757 & -56.1663 & -56.9331 & -56.9331 & -56.1663 & -56.2757 & -56.9102 \\ -93.3052 & -100.1377 & -101.1331 & -99.8057 & -99.8057 & -101.1331 & -100.1377 & -93.3052 \\ -61.1787 & -65.6784 & -53.1030 & -60.2368 & -60.2368 & -53.1030 & -65.6784 & -61.1787 \\ -76.9873 & -81.8273 & -82.9173 & -82.1675 & -82.1675 & -82.9173 & -81.8273 & -76.9873 \\ -76.9873 & -81.8273 & -82.9173 & -82.1675 & -82.1675 & -82.9173 & -81.8273 & -76.9873 \\ -61.1787 & -65.6784 & -53.1030 & -60.2368 & -60.2368 & -53.1030 & -65.6784 & -61.1787 \\ -93.3052 & -100.1377 & -101.1331 & -99.8057 & -99.8057 & -101.1331 & -100.1377 & -93.3052 \\ -56.9102 & -56.2757 & -56.1663 & -56.9331 & -56.9331 & -56.1663 & -56.2757 & -56.9102 \end{bmatrix} \quad (5.1)$$

$$ampl(with\ coupling) = \begin{bmatrix} 0.0095 & 0.0103 & 0.0095 & 0.0098 & 0.0098 & 0.0095 & 0.0103 & 0.0095 \\ 0.0070 & 0.0100 & 0.0095 & 0.0095 & 0.0095 & 0.0095 & 0.0100 & 0.0070 \\ 0.0057 & 0.0045 & 0.0040 & 0.0044 & 0.0044 & 0.0040 & 0.0045 & 0.0057 \\ 0.0071 & 0.0085 & 0.0082 & 0.0082 & 0.0082 & 0.0082 & 0.0085 & 0.0071 \\ 0.0071 & 0.0085 & 0.0082 & 0.0082 & 0.0082 & 0.0082 & 0.0085 & 0.0071 \\ 0.0057 & 0.0045 & 0.0040 & 0.0044 & 0.0044 & 0.0040 & 0.0045 & 0.0057 \\ 0.0070 & 0.0100 & 0.0095 & 0.0095 & 0.0095 & 0.0095 & 0.0100 & 0.0070 \\ 0.0095 & 0.0103 & 0.0095 & 0.0098 & 0.0098 & 0.0095 & 0.0103 & 0.0095 \end{bmatrix} \quad (5.2)$$

5.3 Null Steering of 8×8 Element Array

The array factor and its variation with the element factor and mutual coupling were studied in detail in last section. In this section we effectively steer the single and double

nulls of the 8×8-element microstrip antenna array in both cases of no coupling and coupling and compare the results. Phase variation technique is used to steer the nulls by applying the genetic algorithms. Genetic algorithm parameters used through out the simulation are: Population size = 60; Mutation = 1%; Crossover probability = 0.5.

5.3.1 Single Null Steering

Null at $\theta = 60^0$ and $\phi = 0^0$

Taking a look at figures in section 5.2, we have a peak of one of the side lobe at $\theta = 60^0$ and $\phi = 0^0$. Assuming we have interference signal in that direction and there is a need to have a null in that direction, null steering is done so that null is placed exactly at that particular location. The tolerance of phases that is required to obtain null in that position is essentially greater in an array with coupling effects than in an array of no coupling. The array factor after null steering is shown in figure 5.13 and similar pattern for the microstrip antenna array without coupling and with coupling are shown in figures 5.14 and 5.15. The phases after null steering in a microstrip array without coupling is given by equation 5.3, where the amplitudes for this case are still all equal to unity. The phases and amplitudes of excitation currents of an array with mutual coupling before null steering are given by equations 5.1 and 5.2 and the phases and amplitudes after null steering are given by the equations 5.4 and 5.2.

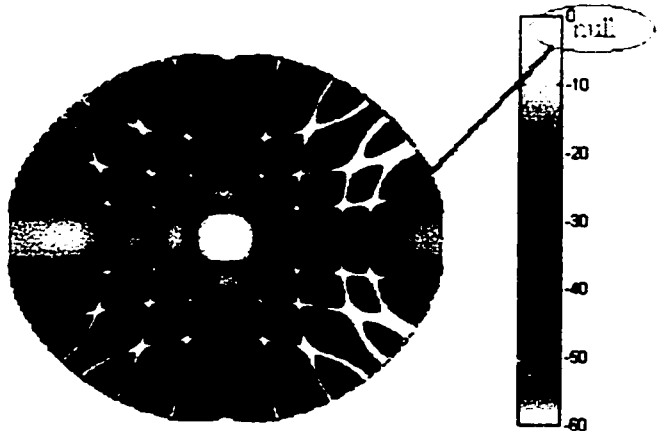

Figure 5.13: Array factor after placing a null on peak of a side lobe at $\theta=60^0$, $\phi=0^0$

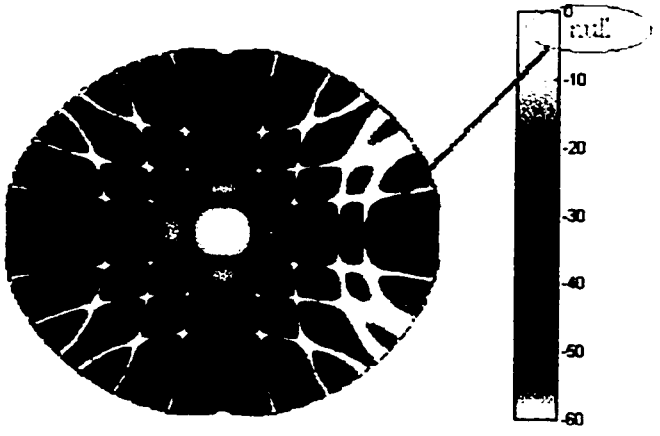

Figure 5.14: Array pattern (no coupling) after placing a null at $\theta=60^0$, $\phi=0^0$

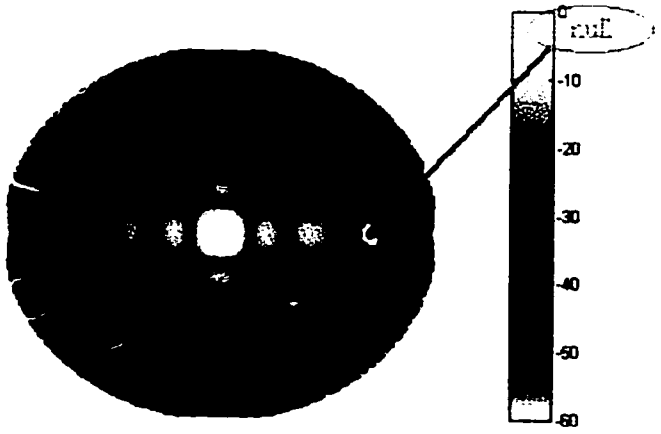

Figure 5.15: Array pattern (with coupling) after placing a null at θ=60,ϕ=0

The tolerance in phase that was required for obtaining the null in this particular location for array without coupling is +/- 12^0. The algorithm has taken 7424 generations to obtain this optimal solution for a population size of 60 and 1% mutation. The crossover probability used was 50% (i.e., 0.5). The pattern thus obtained had half power beam width of 12.65^0 (indicated as BW(P)-meaning half power beam width for perturbed pattern), 0.05^0 less when compared to the original beam width which is 12.7^0 (indicated as BW(O)-meaning half power beam width for original unperturbed pattern) and these details along with others are summarized in table 5.2 for close inspection. The side lobe level rose to –12.6 dB from –13.65 dB.

And for array with coupling the phase tolerance required to obtain the same null was +/- 22^0, which is much higher when compared with the array without coupling. This reason can be explained by looking at the pattern of the array with coupling before null steering, where the nulls between the side lobes have vanished quite considerably. The important point is however we were able to put a null in that location and the pattern thus obtained is not disturbed very much. The genetic algorithm took 1013 generations to obtain the solution. The half power beam width of the perturbed pattern of the array with coupling is 11.75^0 which is less by 0.25^0 when compared to its original unperturbed pattern and 0.9^0 less compared to its counter part without coupling.

$$ph(no\ coupling + NS) = \begin{bmatrix} 11.8722 & 11.9722 & 11.9994 & 11.9345 & 11.9685 & 11.9125 & 11.8479 & 11.9806 \\ -11.9966 & -11.9855 & -11.7931 & -11.9819 & -11.9768 & -11.9780 & -11.8494 & -11.8451 \\ 11.9539 & 11.9580 & 11.9734 & 11.9984 & 11.9783 & 11.9882 & 11.9793 & 11.9359 \\ -11.9725 & -11.9766 & -11.9809 & -11.9854 & -11.9960 & -11.9914 & -11.9873 & -11.9854 \\ 11.9891 & 11.9862 & 11.9435 & 11.9920 & 11.9672 & 11.9450 & 11.9665 & 11.9826 \\ -11.9475 & -11.9632 & -11.9976 & -11.9600 & -11.9090 & -11.9977 & -11.9730 & -11.9914 \\ 11.9002 & 11.8789 & 11.9662 & 11.9473 & 11.8780 & 11.9710 & 11.9391 & 11.9716 \\ -11.9404 & -11.9580 & -11.9768 & -11.8749 & -11.9627 & -11.9740 & -11.9645 & -11.9381 \end{bmatrix} \quad (5.3)$$

$$ph(with\ coupling + NS) = \begin{bmatrix} -78.2240 & -75.5575 & -77.4093 & -78.6161 & -78.2600 & -76.6774 & -77.9516 & -77.0358 \\ -72.6689 & -81.0958 & -79.4739 & -77.9104 & -78.0964 & -79.9867 & -80.0322 & -73.8350 \\ -43.4869 & -44.1757 & -31.1993 & -39.3468 & -38.4082 & -31.2148 & -86.7243 & -82.5636 \\ -77.7088 & -95.5583 & -82.4460 & -82.8395 & -84.1213 & -87.7953 & -91.8744 & -95.8008 \\ -55.7725 & -59.8553 & -61.0202 & -60.6710 & -62.2219 & -61.9998 & -60.5215 & -56.7510 \\ -81.8030 & -87.3231 & -74.1177 & -81.7854 & -81.3463 & -73.7305 & -86.8428 & -83.0348 \\ -73.2920 & -79.3701 & -79.3448 & -78.6638 & -78.0954 & -79.6008 & -78.1438 & -75.1228 \\ -78.8270 & -77.5332 & -77.7546 & -77.9601 & -78.3335 & -76.7620 & -78.1925 & -77.1480 \end{bmatrix} \quad (5.4)$$

Figure 5.16(a) compares the array pattern before and after null steering along the x-axis and an arrow indicates the null location. Figure 5.16(b) is a 2D plot that compares the array pattern with coupling, before and after null steering along y-axis.

Null at $\theta = 38^0$ and $\phi = 0^0$

The results of steering the null at $\theta = 38^0$ and $\phi = 0^0$ are discussed in this section. First consider the array pattern of an array without coupling after null steering. A phase tolerance of +/- 14^0 was required to steer the null at the point under discussion. The genetic algorithm took 838 generations to give the required solution. The half power beam width after null steering remained equal to the value before null steering (equal to12.7^0). However the side lobe level increased to –13 dB from –13.65 dB.

Now coming to the array pattern of array with coupling, a phase tolerance of +/- 28^0 was required. The genetic algorithm took 1223 number of generations to produce the desired result. The half power beam width reduced to 11.85^0 from 12^0 beam width of original unperturbed pattern of the array with coupling. The side lobe level was precisely increased by 2 dB to a value of –10 dB from –12 dB. The three dimensional patterns for the array factor due to point sources after null steering, null steered array pattern of an

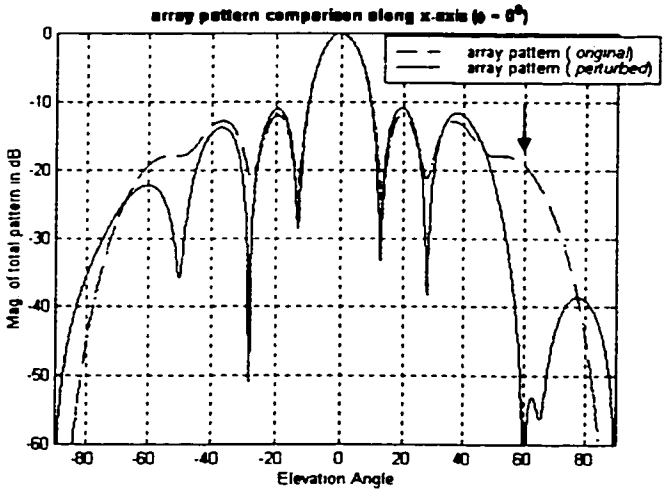

Figure 5.16(a): Comparison of array pattern before and after null steering (with coupling). The null is steered at $\theta = 60^0$, $\phi = 0^0$

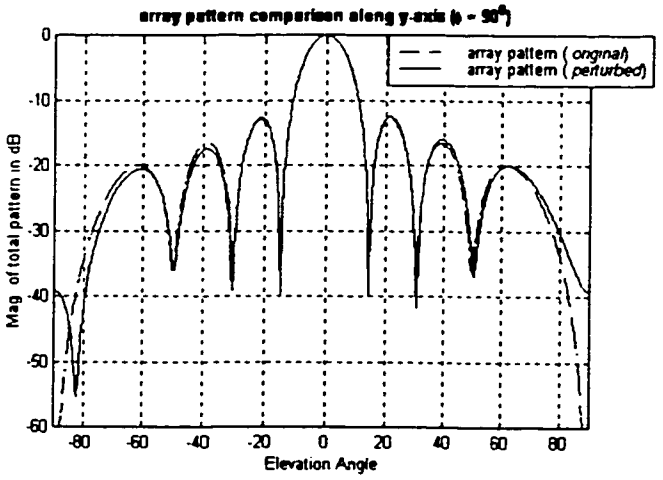

Figure 5.16(b): Comparison of array pattern before and after null steering (with coupling). The null is steered at $\theta = 60^0$, $\phi = 0^0$

array without mutual coupling and null steered array pattern of an array with coupling are shown in figures 5.17, 5.18 and 5.19. The phases of the microstrip antenna without coupling and after null steering are given by equation 5.5 and the phases of array with coupling after null steering is given by equation 5.6. Figures 5.20(a) and 5.20(b) compare the array patterns of microstrip array with coupling before and after null steering along x- and y-axis respectively.

$$ph(no\ coupling + NS) = \begin{bmatrix} 13.7896 & 12.5868 & 13.3428 & 13.7588 & 13.7829 & 13.5334 & 12.6142 & 12.7472 \\ -13.5709 & -13.0863 & -13.7964 & -13.6292 & -12.7550 & -13.5466 & -13.2112 & -13.8027 \\ 12.5179 & 10.9487 & 11.4640 & 8.4219 & 8.9499 & 13.0088 & 10.1374 & 11.8993 \\ 13.7709 & 13.2170 & 13.7081 & 13.8726 & 13.5157 & 13.6844 & 13.3787 & 13.2566 \\ -13.6992 & -13.7976 & -12.6714 & -13.7688 & -13.8528 & -13.6831 & -13.9186 & -13.9153 \\ -8.7935 & -13.9128 & -8.3191 & -8.5104 & -12.8560 & -11.4938 & -12.2241 & -10.4786 \\ 13.4388 & 13.5389 & 13.7146 & 13.4661 & 13.9345 & 12.6985 & 13.5696 & 12.3945 \\ -12.4086 & -13.2568 & -13.6934 & -13.6364 & -13.9351 & -12.0479 & -12.5790 & -13.2378 \end{bmatrix} \quad (5.5)$$

$$ph(with\ coupling + NS) = \begin{bmatrix} -32.9736 & -28.6399 & -29.7381 & -30.9291 & -32.2214 & -29.1883 & -29.2204 & -28.9556 \\ -118.099 & -124.803 & -125.333 & -124.314 & -123.914 & -125.580 & -126.722 & -115.358 \\ -34.6536 & -38.4616 & -25.8927 & -33.8102 & -32.9767 & -25.5767 & -38.7812 & -34.4755 \\ -50.7361 & -53.9856 & -55.1977 & -55.8449 & -54.2486 & -55.6838 & -55.3808 & -50.4048 \\ -103.715 & -109.492 & -109.994 & -110.040 & -110.002 & -110.030 & -109.248 & -103.358 \\ -42.6255 & -44.8818 & -40.2493 & -52.7091 & -38.4469 & -46.5170 & -45.3137 & -41.8156 \\ -65.8508 & -72.8361 & -73.5998 & -72.0165 & -73.3160 & -73.4608 & -72.5196 & -68.6693 \\ -84.7822 & -83.6911 & -82.7662 & -84.3098 & -84.8908 & -84.0214 & -82.4509 & -84.5687 \end{bmatrix} \quad (5.6)$$

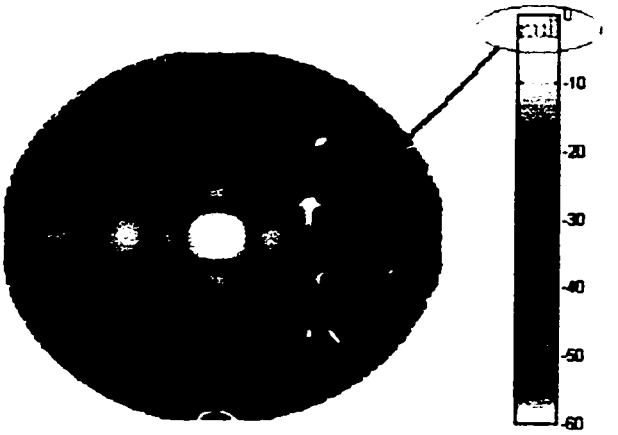

Figure 5.17: Array factor after placing a null on peak of a side lobe at $\theta=38^0$, $\phi=0^0$

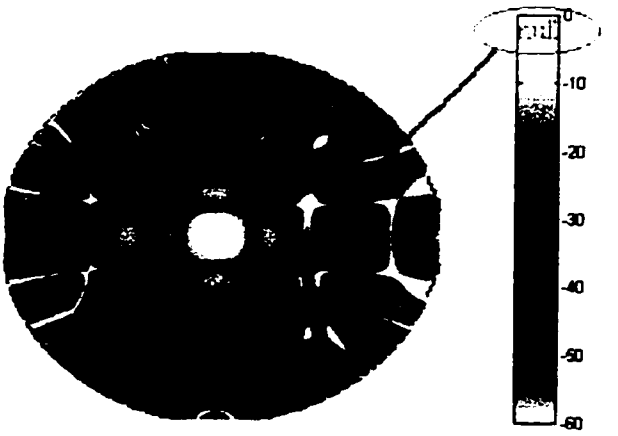

Figure 5.18: Array pattern (no coupling) after placing a null at $\theta=38^0$, $\phi=0^0$

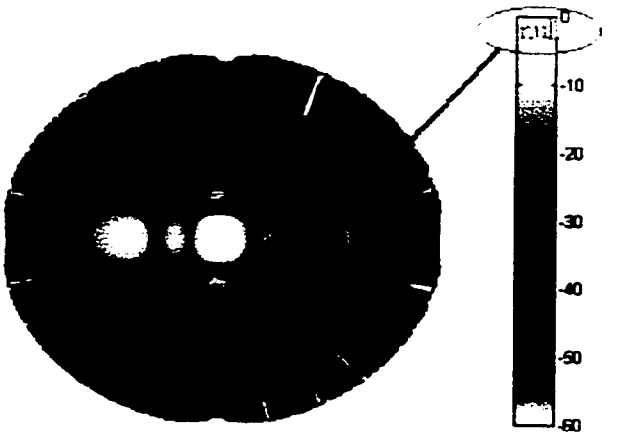

Figure 5.19: Array pattern (with coupling) after placing a null at $\theta=38^0,\phi=0^0$

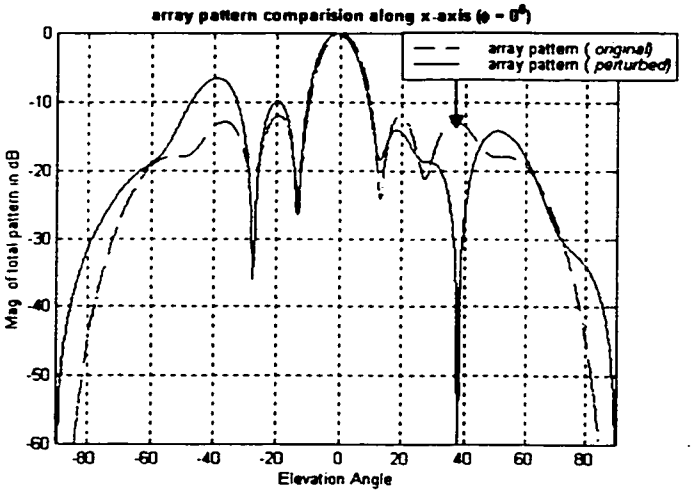

Figure 5.20(a): Comparison of array pattern before and after null steering (with coupling). The null is steered at $\theta = 38^0$, $\phi = 0^0$

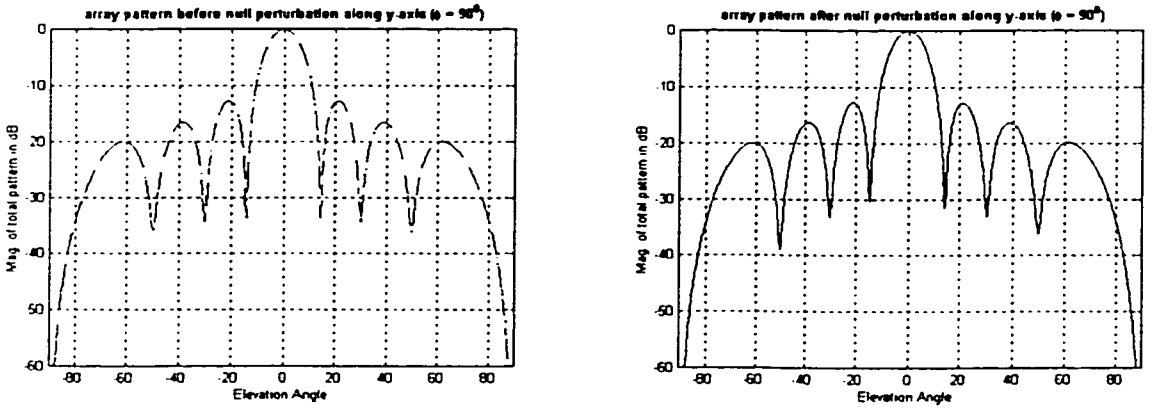

Figure 5.20(b): Comparison of array pattern before and after null steering (with coupling). The null is steered at $\theta = 38^0$, $\phi = 0^0$

	θ	P.T.	Gen.	BW(P)	SLL(P)	BW(O)	SLL(O)
Array Pattern (without coupling)	60	12	7424	12.65	-12.6	12.7	-13.65
	38	14	838	12.7	-13	12.7	-13.65
	θ	**P.T.**	**Gen.**	**BW(P)**	**SLL(P)**	**BW(O)**	**SLL(O)**
Array Pattern (with coupling)	60	22	1013	11.75	-10.8	12	-12
	38	28	1223	11.85	-10	12	-12

Table 5.2: Summary of results of single null steering of the 8×8 array; $\phi=0^0$

5.3.2 Double Null Steering

Microstrip Antenna Array without Coupling

In this section we study the double null steering of 8×8-element microstrip array without considering the mutual coupling between the elements. The two null locations are at $\theta = 60^0$ and 38^0 at $\phi = 0^0$. Figure 5.21 shows the array factor after null steering and figure 5.22 shows the array pattern of the microstrip array without coupling after null steering. The comparison of the array pattern of the microstrip array without coupling before and after null steering is given in figure 5.23 (a) and 5.23(b).

A phase tolerance of +/- 20^0 was used to obtain these nulls for a population size of 60 and crossover probability of 0.5. The mutation of 1% was used and the algorithm took 5933 generations to achieve the desired solution. The half power beam width of the perturbed pattern had remained the same and therefore no effect to the main beam, which is very much desired. The side lobe level also had reduced to –14.2 dB for –13.65 dB, which is 0.55 dB reduction. All the double null results are summarized in table 5.3 for comparison. The phases of the exiting currents after null steering are given by the equation 5.7 for the case of no coupling.

$$ph(no\ coupling) = \begin{bmatrix} 19.6476 & 19.8591 & 19.8741 & 19.9482 & 19.7435 & 19.6884 & 19.9018 & 19.9243 \\ -19.8559 & -19.8627 & -19.8874 & -19.8089 & -19.9037 & -19.9945 & -19.9378 & -19.9895 \\ 18.7939 & 19.9905 & 19.1891 & 19.9597 & 19.9980 & 19.3243 & 19.6740 & 19.9152 \\ -7.0719 & 17.2129 & 4.4914 & 17.4865 & -17.0494 & -18.6330 & 11.2516 & -6.7412 \\ 0.7721 & -13.9701 & 4.3374 & -6.8153 & -19.7820 & -5.9785 & 19.6312 & 17.7502 \\ -19.8903 & -19.9186 & -19.6774 & -19.8736 & -19.8892 & -19.8855 & -19.9922 & -19.1268 \\ 19.8209 & 19.9813 & 19.9894 & 19.8312 & 19.8980 & 19.9863 & 19.9555 & 19.7221 \\ -19.3338 & -19.9972 & -19.8290 & -19.8801 & -19.9851 & -19.9811 & -19.6839 & -19.7921 \end{bmatrix} \quad (5.7)$$

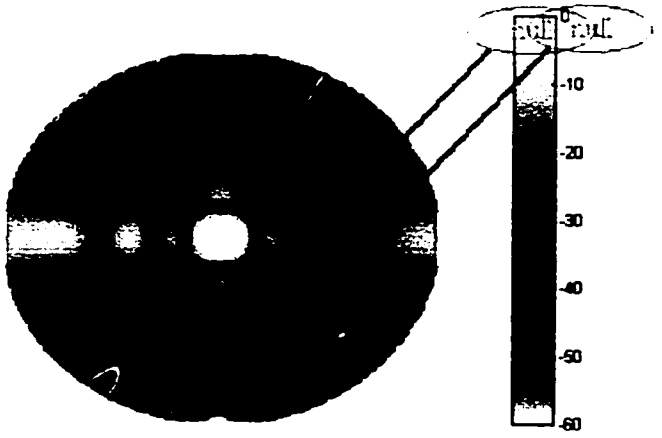

Figure 5.21: Array factor after null steering

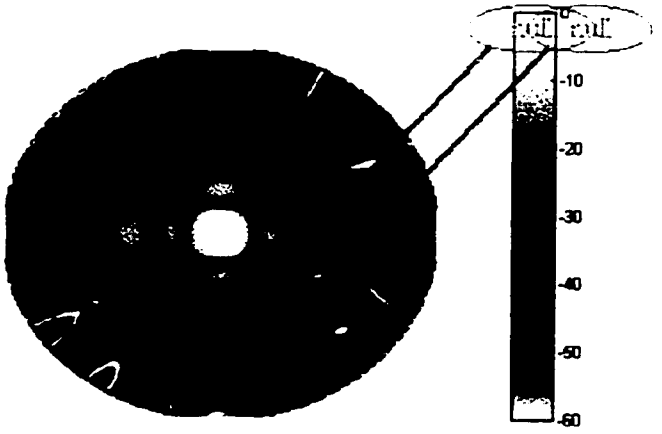

Figure 5.22: Array pattern (without coupling) after null steering

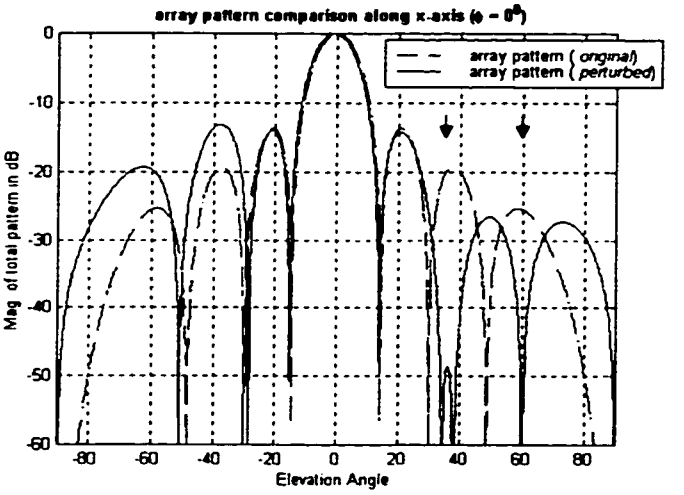

Figure 5.23(a): Pattern comparison before and after null steering along x-axis (without coupling). The two nulls are located at $\theta = 60^0$ and $\theta = 38^0$ where $\phi = 0^0$

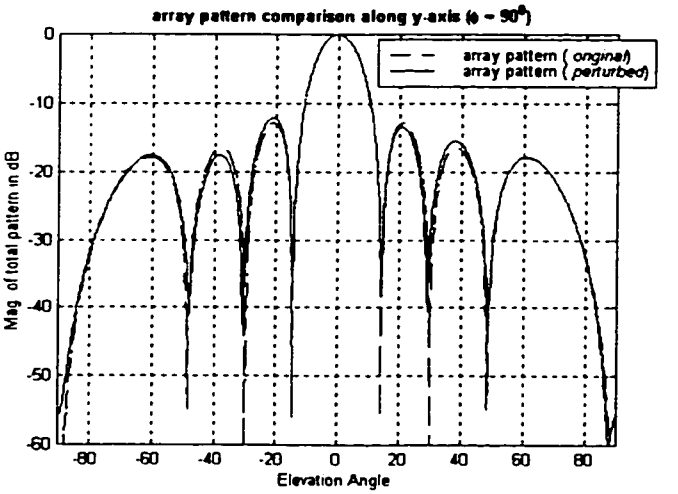

Figure 5.23(b): Pattern comparison before and after null steering along y-axis (without coupling). The two nulls are located at $\theta = 60^0$ and $\theta = 38^0$ where $\phi = 0^0$

Microstrip Antenna Array with Coupling

In this subsection we discuss double null steering result obtained for microstrip array with coupling. The results are presented accordingly. Figure 5.24 shows the 3D pattern of the array with mutual coupling consideration and after double null steering. Figure 5.25 shows the patterns with mutual coupling and compares them as they were obtained before and after null steering. The phases of excitation currents as obtained after null steering is given by the equation 5.8.

$$ph(with\,coupling) = \begin{bmatrix} -18.2556 & -14.7079 & -98.0359 & -15.8844 & -25.3408 & -25.9579 & -95.7160 & -24.0668 \\ -68.9277 & -93.2216 & -101.4966 & -113.6117 & -118.4264 & -90.5040 & -100.2490 & -89.9893 \\ -35.7224 & -63.6254 & -11.4033 & -37.9202 & -18.6575 & -15.7257 & -26.1819 & -29.2480 \\ -46.5354 & -65.5161 & -65.9015 & -56.9953 & -61.6485 & -65.3136 & -61.0437 & -43.7538 \\ -118.9522 & -123.0967 & -41.1397 & -123.7747 & -123.7083 & -124.6096 & -123.5443 & -37.1825 \\ -101.3438 & -107.2219 & -93.9856 & -101.5762 & -102.0036 & -94.7790 & -107.3626 & -100.0029 \\ -52.0038 & -58.7396 & -59.2323 & -58.0674 & -58.1415 & -59.1971 & -58.4278 & -51.3883 \\ -96.8389 & -97.1305 & -97.6891 & -97.5273 & -98.7868 & -98.0164 & -97.1962 & -97.8190 \end{bmatrix} \quad (5.8)$$

Comparing the half power beam width for the patterns obtained before and after null steering for array with coupling, we observe a 0.2^0 difference between them. And as regards the side lobe level, there is a 4.8-dB increase in the side lobe level for the pattern obtained after null steering.

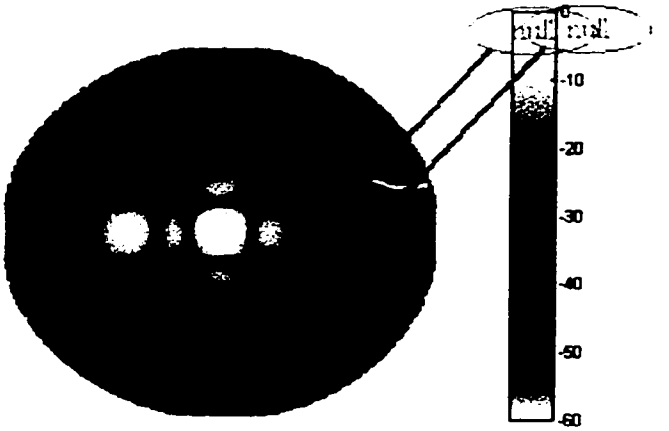

Figure 5.24: Array pattern (with coupling) after null steering

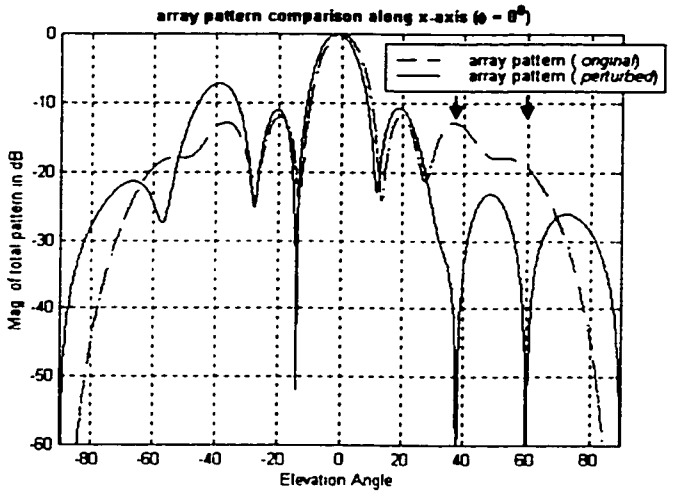

Figure 5.25(a): Pattern comparison before and after null steering along x-axis (with coupling). The two nulls are located at $\theta = 60^0$ and $\theta = 38^0$ where $\phi = 0^0$

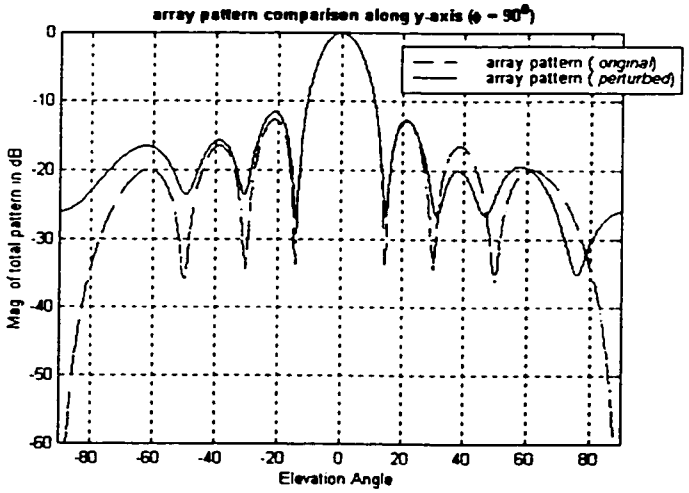

Figure 5.25(b): Pattern comparison before and after null steering along y-axis (with coupling). The two nulls are located at $\theta = 60^0$ and $\theta = 38^0$ where $\phi = 0^0$

Comparison of Patterns obtained after Null Steering for cases of no Coupling and with Coupling

From figures 2.25(a) and 2.25(b), we see difference only in x-direction and very little in y-direction. Comparing the half power beam widths and side lobe levels in x-direction for cases of with coupling and no coupling, the beam width for pattern with coupling is less by 0.9^0 compared to its counter part and side lobe level is 7-dB higher. The summary of the double null steered results are tabulated in table 5.3

Nulls at (θ,ϕ) = (60.0) and (38,0)	P.T.	Gen.	B.W (P)	SLL (P)	B.W (O)	SLL (O)
Array factor	20	5933	12.95^0	-13.3 dB	12.8^0	-12.8 dB
Array pattern (no coupling)	20	5933	12.7^0	-14.2 dB	12.7^0	-13.65 dB
Array pattern (with coupling)	42	3791	11.8^0	-7.2 dB	12^0	-12.0 dB

Table 5.3: Comparison of the results obtained after double null steering to the original patterns (for $\phi = 0^0$)

5.4 Effect of change in the inter element spacing on the array performance

For the microstrip array, the effect of variation of inter element spacing is studied. Mutual coupling effects are inversely proportional to the distance between the elements and as the spacing between the elements is increased, the mutual coupling between the elements decreases. However, as the spacing between the elements is increased, there is increase in the number of side lobes. In this section the effect of variation of the inter element spacing on the array pattern of 8×8 element array is studied. Figures 5.26(a) to 5.26(f) compare the array patterns with and without coupling for inter element spacing of 0.2λ, 0.3λ, 0.4λ, 0.5λ, 0.6λ and 0.7λ.

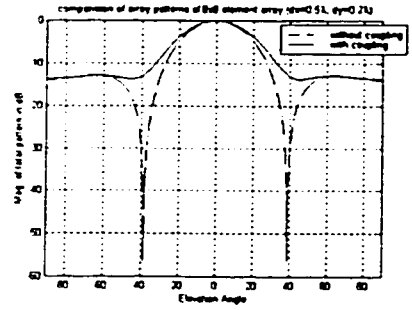

(a)

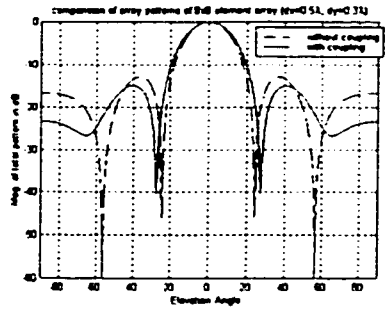

(b)

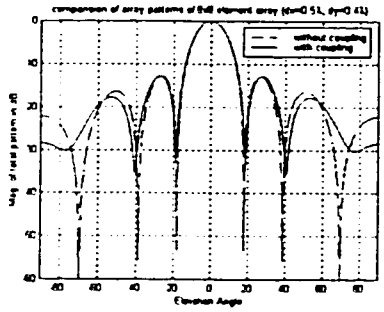

(c)

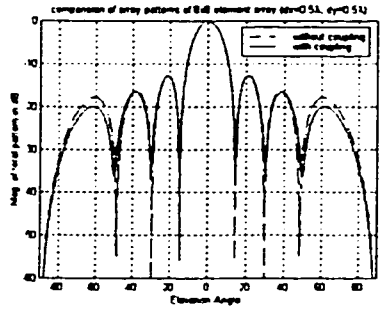

(d)

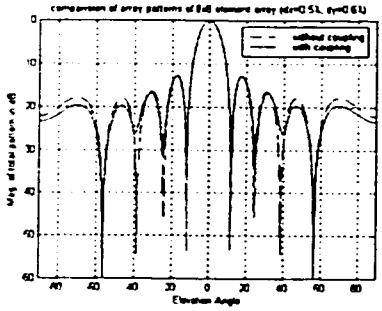

(e)

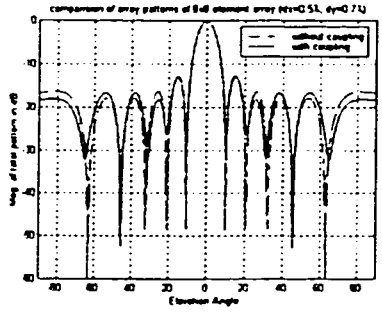

(f)

Figure 5.26: The plots illustrating the effect of the change in the element spacing

CHAPTER 6

EFFECT OF CHANGE OF THE NUMBER OF ELEMENTS ON ARRAY PERFORMANCE

In this chapter a number of arrays other than 8×8 element are studied. The effect of the number of elements on array performance and their null steering aspects is the subject of this chapter. Various arrays are studied and their far field patterns before and after null steering are presented in 2D and 3D plots. Coupling and no-coupling cases are studied separately for each array and the results are compared in 2D plots. The results are then tabulated.

6.1 The 8×4 Element Array

The 3D array factor of the 8×4 element array is shown in figure 6.1. Figures 6.2 and 6.3 displays the 3D array pattern for cases of no coupling and with coupling respectively. Figures 6.4 and 6.5 are the 3D patterns of a microstrip array without coupling after single and double null steering respectively. Similar plots for the case of coupling are given in figures 6.6 and 6.7. Figure 6.8 compares the array pattern of the array without coupling before and after null steering and figure 6.9 compares the array pattern of the array with coupling before and after null steering. The results are tabulated in table 6.1 below.

Null at (θ,ϕ) = (38,0)	P. T.	Pop.	Mute	Gen.	P_cr	BW (p)	SLL (p)	BW (o)	SLL (o)
Array factor	14	60	1%	336	0.5	12.8°	-12.2 dB	12.8°	-12.8 dB
Array pattern (no coupling)	14	60	1%	336	0.5	12.7°	-13.0 dB	12.7°	-13.65 dB
Array pattern (with coupling)	28	60	1%	229	0.5	11.8°	-10.0 dB	11.9°	-12.0 dB
Nulls at (θ,ϕ) = (60,0) and (38,0)	P. T.	Pop.	Mute	Gen.	P_cr	BW (p)	SLL (p)	BW (o)	SLL (o)
Array factor	20	60	1%	4102	0.5	12.8°	-13.4 dB	12.8°	-12.8 dB
Array pattern (no coupling)	20	60	1%	4102	0.5	12.7°	-13.9 dB	12.7°	-13.65 dB
Array pattern (with coupling)	42	60	1%	3775	0.5	11.75°	-10.7 dB	11.9°	-12.0 dB

Table 6.1: comparison of the results of the 8×4 element array ($\phi = 0^0$)

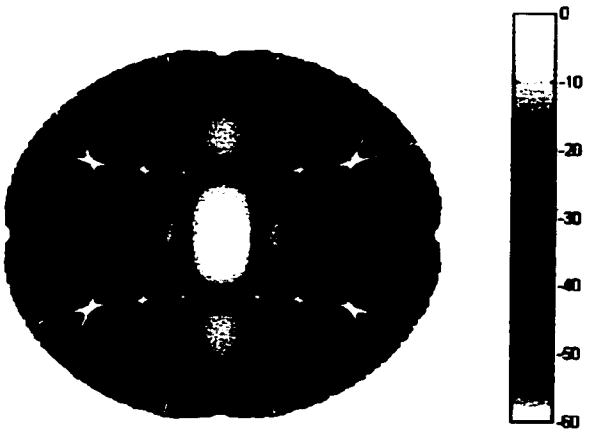

Figure 6.1: Array factor of 8×4 element planar array

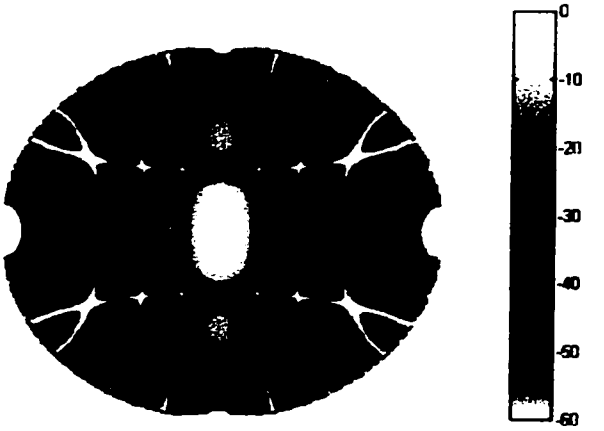

Figure 6.2: Array pattern of 8×4 element planar array without coupling

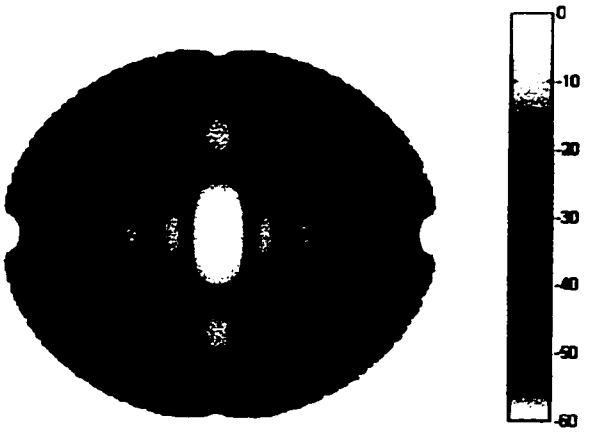

Figure 6.3: Array pattern of 8×4 element planar array with coupling

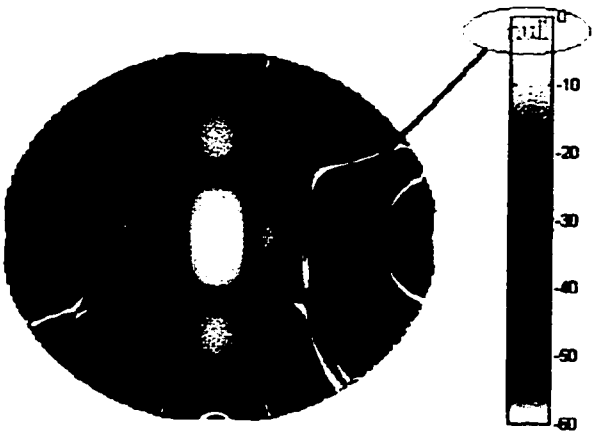

Figure 6.4: Single null steered array pattern of 8×4 element planar array without coupling. The null is at $\theta = 38^0$ and $\phi = 0^0$

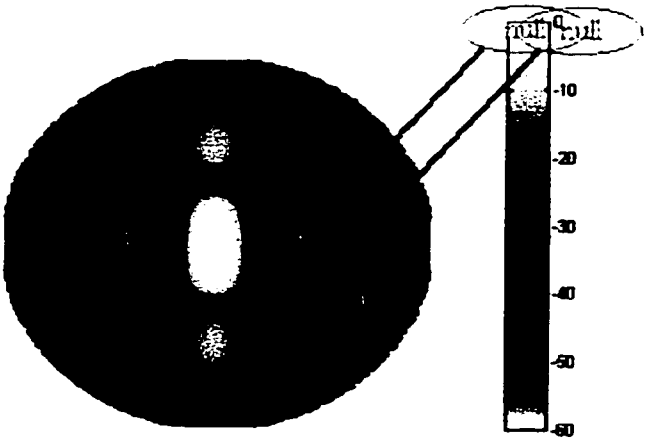

Figure 6.5: Double null steered array pattern of 8×4 element planar array without coupling. The nulls are at $\theta = 60^0$ and $\theta = 38^0$ where $\phi = 0^0$

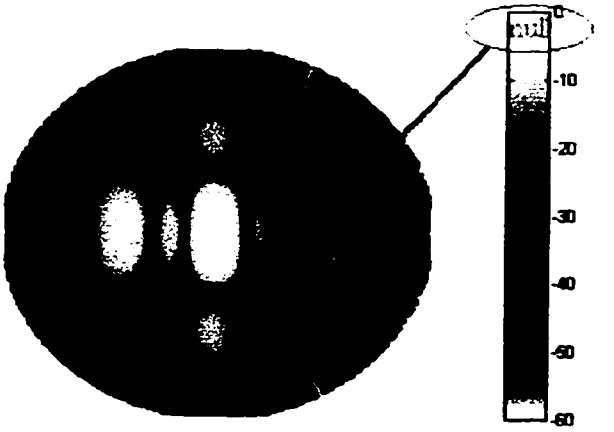

Figure 6.6: Single null steered array pattern of 8×4 element planar array with coupling. The null is at $\theta = 38^0$ and $\phi = 0^0$

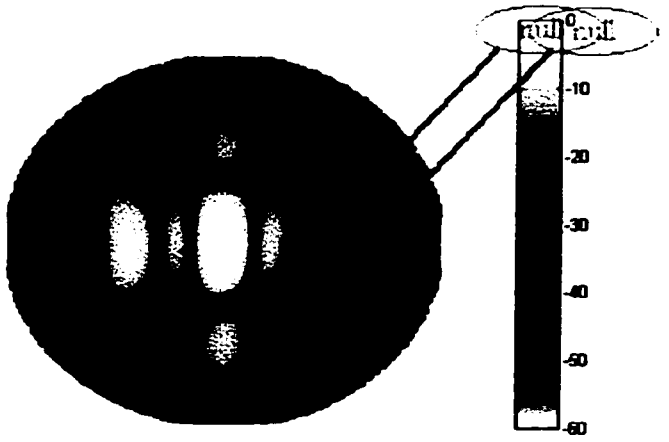

Figure 6.7: **Double null steered array pattern of 8×4 element planar array with coupling. The nulls are at $\theta = 60^0$ and $\theta = 38^0$ where $\phi = 0^0$**

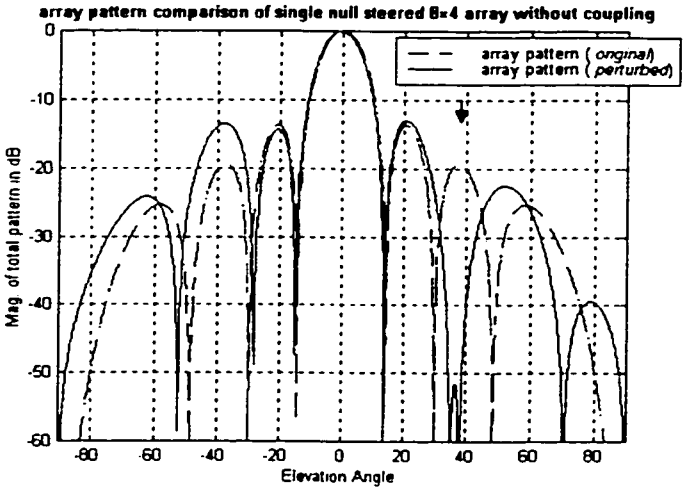

Figure 6.8(a): Comparison of array patterns of the array without coupling before and after single null steering. The null is at $\theta = 38^0$ and $\phi = 0^0$

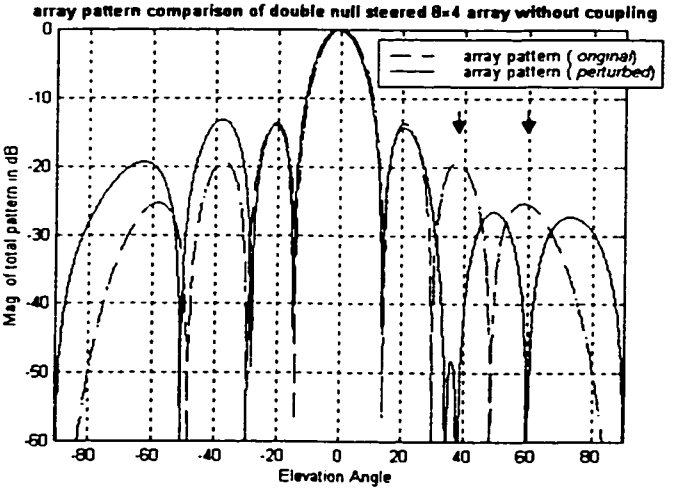

Figure 6.8(b): Comparison of array patterns of the array without coupling before and after double null steering. The nulls are at $\theta = 60^0$ and $\theta = 38^0$ where $\phi = 0^0$

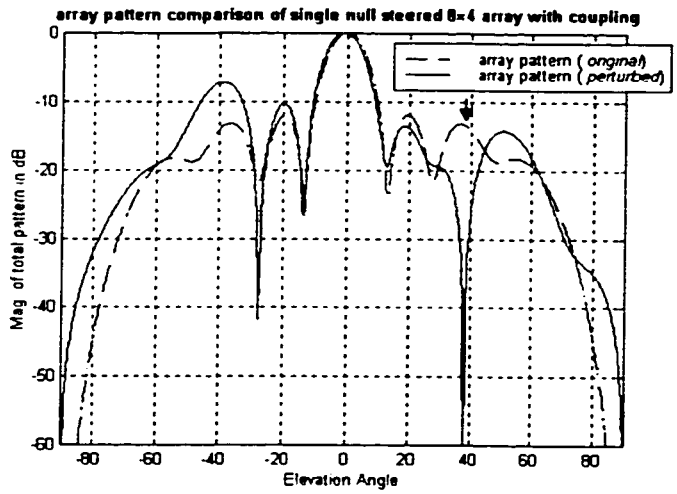

Figure 6.9(a): Comparison of array patterns of the array with coupling before and after single null steering. The null is at $\theta = 38^0$ and $\phi = 0^0$

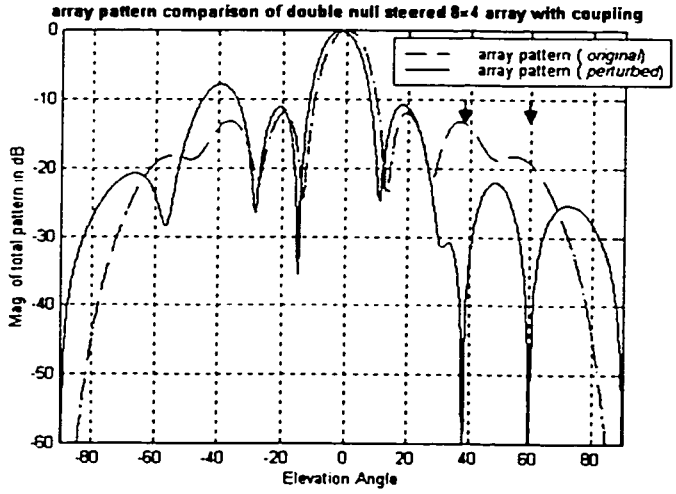

Figure 6.9(b): Comparison of array patterns of the array with coupling before and after double null steering. The null are at $\theta = 60^0$ and $\theta = 38^0$ where $\phi = 0^0$

6.2 The 12×8 Element Array

The 3D array factor of the 12×8-element array is shown in figure 6.10. Figures 6.11 and 6.12 displays the 3D array pattern for cases of no coupling and with coupling respectively. Figures 6.13 and 6.14 are the 3D patterns of a microstrip array without coupling after single and double null steering respectively. Similar plots for the case of coupling are given in figures 6.15 and 6.16. Figure 6.17 compares the array pattern of the array without coupling before and after null steering and figure 6.18 compares the array pattern of the array with coupling before and after null steering. The results are tabulated in table 6.2 below.

Null at (θ,ϕ) = (48,0)	P. T.	Pop.	Mute	Gen.	P_cr	BW (p)	SLL (p)	BW (o)	SLL (o)
Array factor	10	60	1%	261	0.5	8.55°	-12.2 dB	8.55°	-13.0 dB
Array pattern (no coupling)	10	60	1%	261	0.5	8.5°	-12.6 dB	8.5°	-13.4 dB
Array pattern (with coupling)	26	60	1%	886	0.5	8°	-11.5 dB	8.1°	-12.7 dB
Nulls at (θ,ϕ) = (48,0) and (38,0)	P. T.	Pop.	Mute	Gen.	P_cr	BW (p)	SLL (p)	BW (o)	SLL (o)
Array factor	18	60	1%	227	0.5	8.55°	-13.0 dB	8.55°	-13.0 dB
Array pattern (no coupling)	18	60	1%	227	0.5	8.5°	-13.35 dB	8.5°	-13.4 dB
Array pattern (with coupling)	39	60	1%	436	0.5	8.2°	-12.0 dB	8.1°	-12.7 dB

Table 6.2: comparison of the results of the 12×8 element array ($\phi = 0^0$)

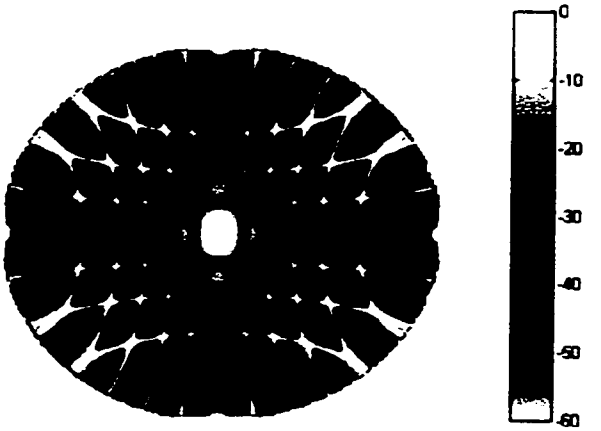

Figure 6.10: Array factor of 12×8 element planar array

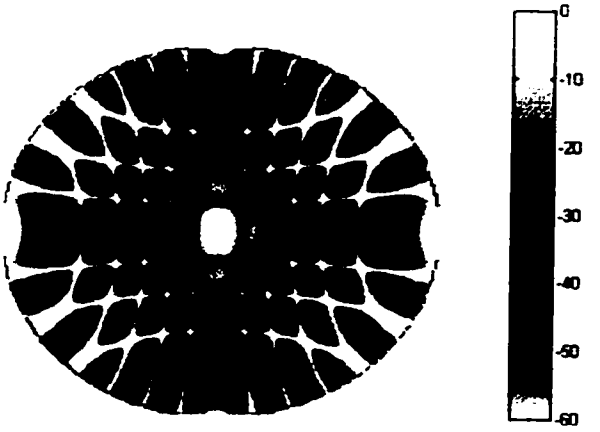

Figure 6.11: Array pattern of 12×8 element planar array without coupling

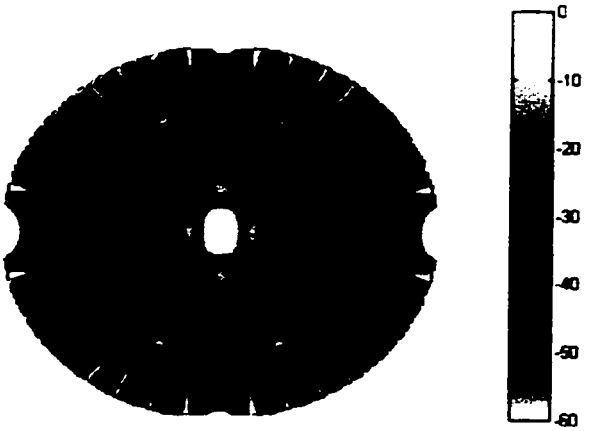

Figure 6.12: Array pattern of 12×8 element planar array with coupling

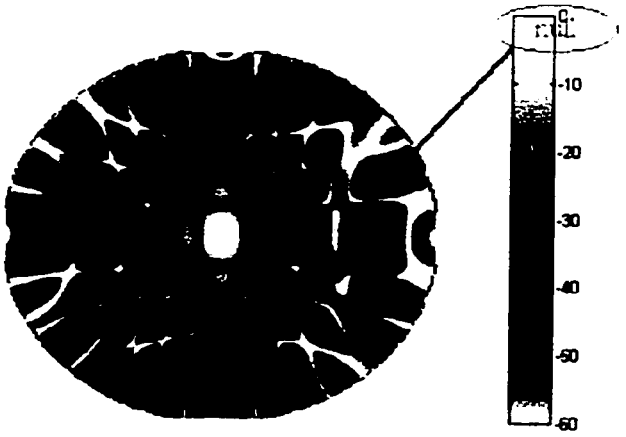

Figure 6.13: Single null steered array pattern of 12×8 element planar array without coupling. The null is at $\theta = 48^0$ and $\phi = 0^0$

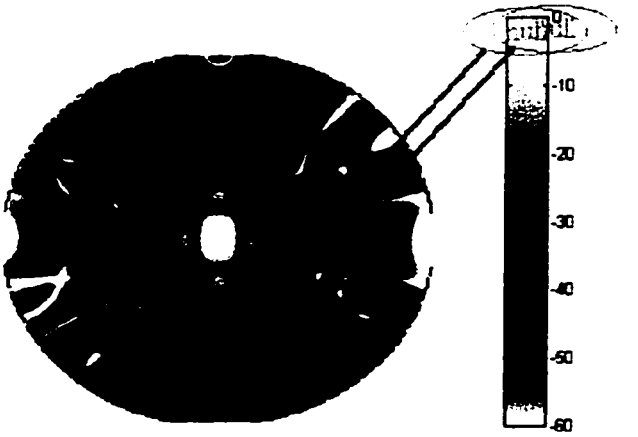

Figure 6.14: Double null steered array pattern of 12×8 element planar array without coupling. The nulls are at $\theta = 48^0$ and $\theta = 38^0$ where $\phi = 0^0$

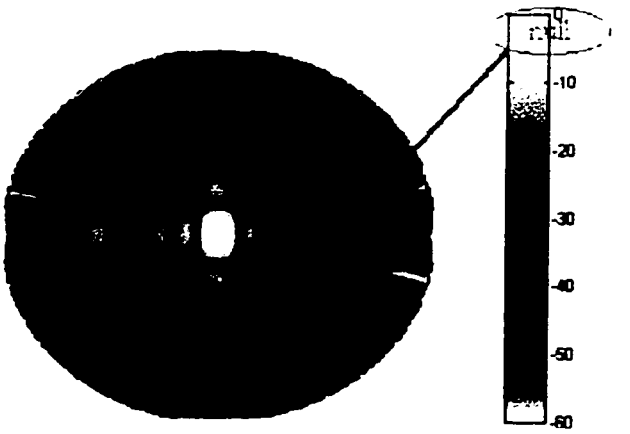

Figure 6.15: Single null steered array pattern of 12×8 element planar array with coupling. The null is at $\theta = 48^0$ and $\phi = 0^0$

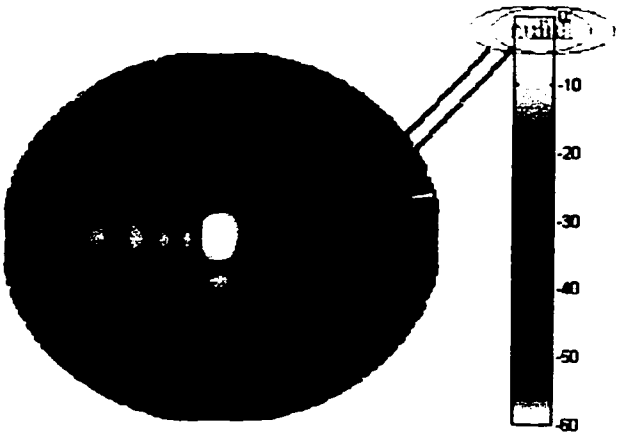

Figure 6.16: **Double null steered array pattern of 12×8 element planar array with coupling. The nulls are at $\theta = 48^0$ and $\theta = 38^0$ where $\phi = 0^0$**

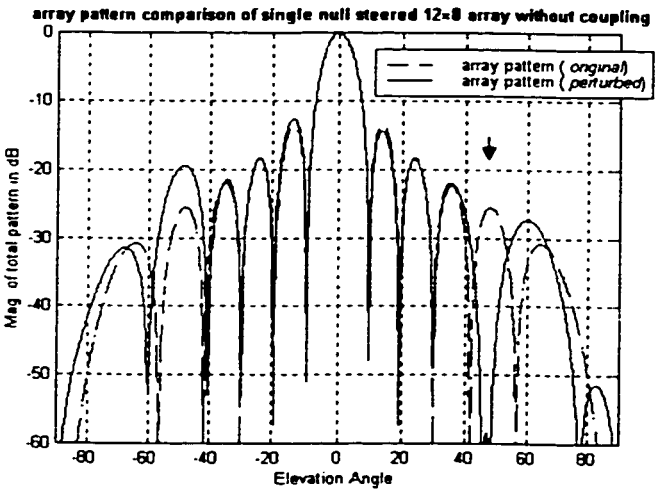

Figure 6.17(a): Comparison of array patterns of the array without coupling before and after single null steering. The null is at $\theta = 48^0$ and $\phi = 0^0$

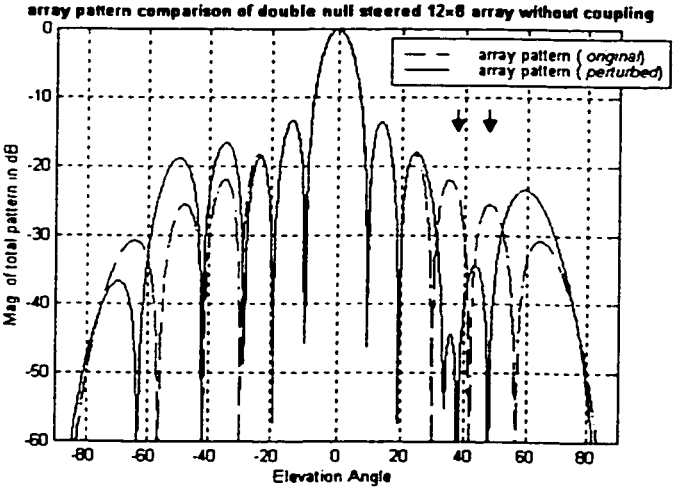

Figure 6.17(b): Comparison of array patterns of the array without coupling before and after double null steering. The nulls are at $\theta = 48^0$ and $\theta = 38^0$ where $\phi = 0^0$

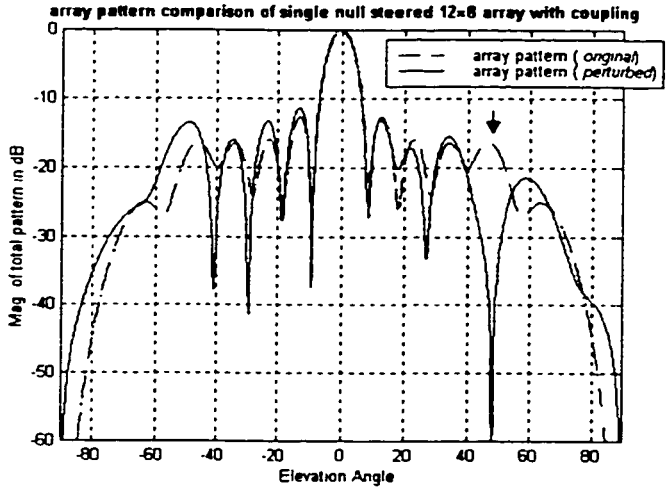

Figure 6.18(a): Comparison of array patterns of the array with coupling before and after single null steering. The null is at $\theta = 48^0$ and $\phi = 0^0$

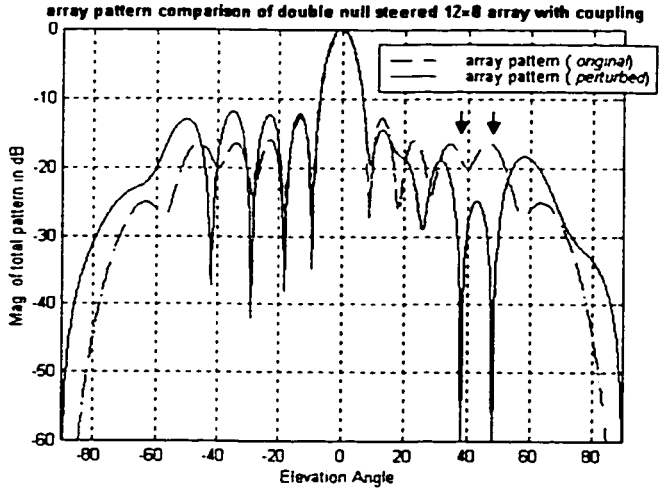

Figure 6.18(b): Comparison of array patterns of the array with coupling before and after double null steering. The null are at $\theta = 48^0$ and $\theta = 38^0$ where $\phi = 0^0$

6.3 The 12×12 Element Array

The 3D array factor of the 12×12 element array is shown in figure 6.19. Figures 6.20 and 6.21 displays the 3D array pattern for cases of no coupling and with coupling respectively. Figures 6.22 and 6.23 are the 3D patterns of a microstrip array without coupling after single and double null steering respectively. Similar plots for the case of coupling are given in figures 6.24 and 6.25. Figure 6.26 compares the array pattern of the array without coupling before and after null steering and figure 6.27 compares the array pattern of the array with coupling before and after null steering. The results are tabulated in table 6.3 below.

Null at (θ,ϕ) = (48,0)	P. T.	Pop.	Mute	Gen.	P_cr	BW (p)	SLL (p)	BW (o)	SLL (o)
Array factor	10	60	1%	607	0.5	8.55°	-12.0 dB	8.55°	-13.0 dB
Array pattern (no coupling)	10	60	1%	607	0.5	8.5°	-12.5 dB	8.5°	-13.4 dB
Array pattern (with coupling)	25	60	1%	6157	0.5	8.05°	-12.0 dB	8.1°	-12.7 dB
Nulls at (θ,ϕ) = (48,0) and (24,0)	P. T.	Pop.	Mute	Gen.	P_cr	BW (p)	SLL (p)	BW (o)	SLL (o)
Array factor	17	60	1%	2845	0.5	8.55°	-12.3 dB	8.55°	-13.0 dB
Array pattern (no coupling)	17	60	1%	2845	0.5	8.5°	-12.7 dB	8.5°	-13.4 dB
Array pattern (with coupling)	38	60	1%	449	0.5	8.15°	-10.6 dB	8.1°	-12.7 dB

Table 6.3: comparison of the results of the 12×12 element array ($\phi = 0^0$)

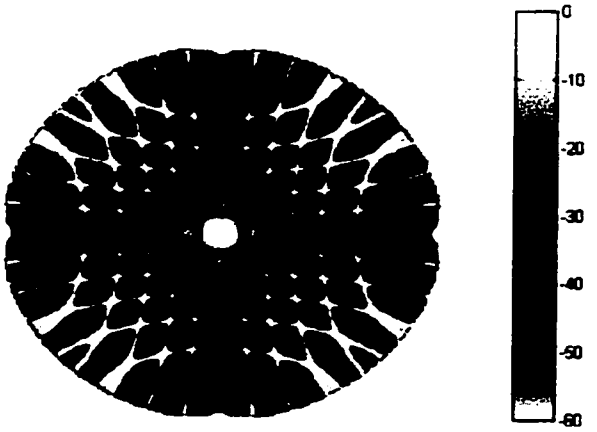

Figure 6.19: Array factor of 12×12 element planar array

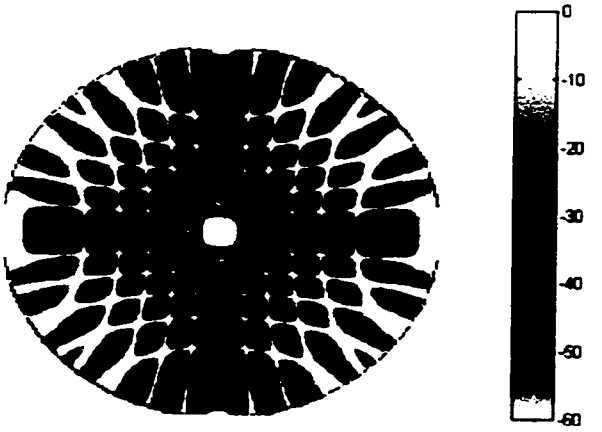

Figure 6.20: Array pattern of 12×12 element planar array without coupling

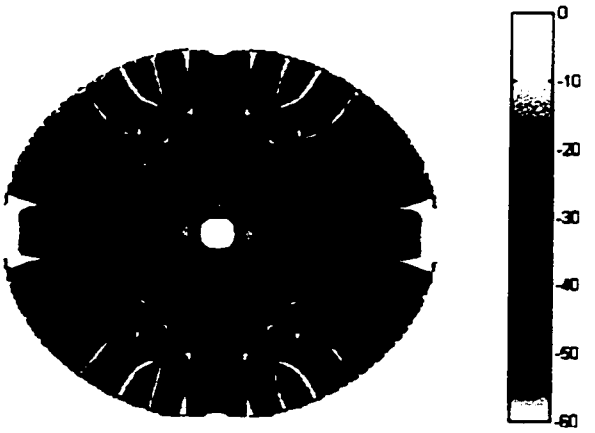

Figure 6.21: Array pattern of 12×12 element planar array with coupling

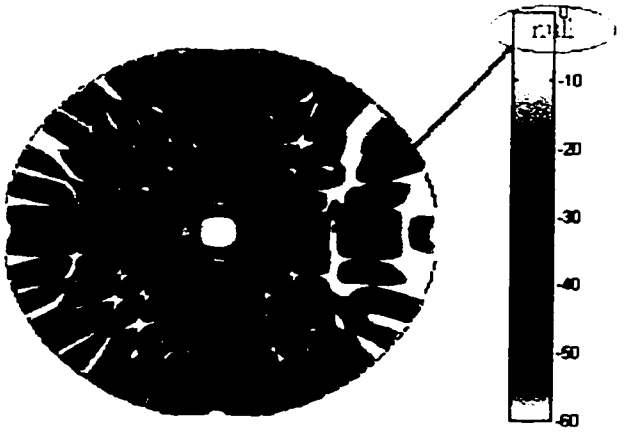

Figure 6.22: Single null steered array pattern of 12×12 element planar array without coupling. The null is at $\theta = 48^0$ and $\phi = 0^0$

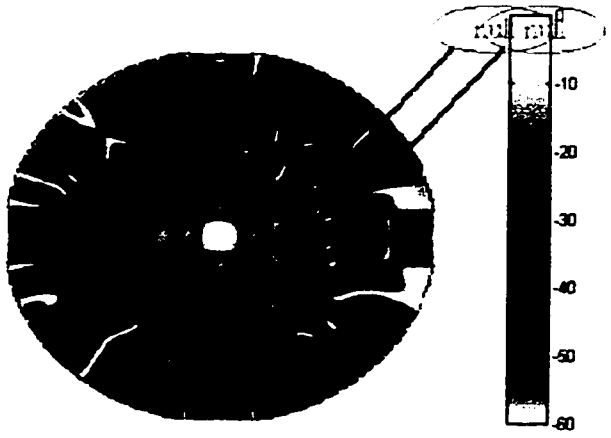

Figure 6.23: Double null steered array pattern of 12×12 element planar array without coupling. The nulls are at $\theta = 48^0$ and $\theta = 24^0$ where $\phi = 0^0$

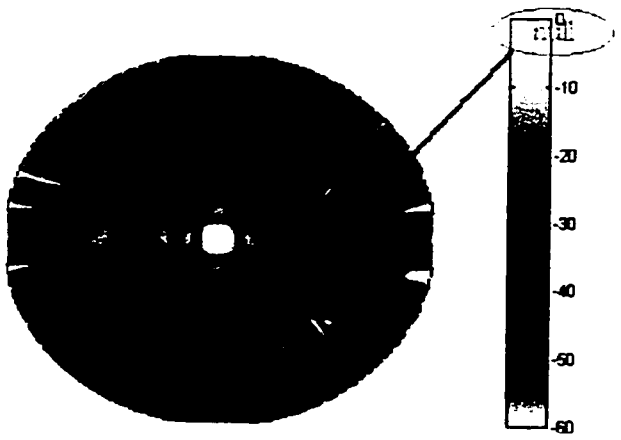

Figure 6.24: Single null steered array pattern of 12×12 element planar array with coupling. The null is at $\theta = 48^0$ and $\phi = 0^0$

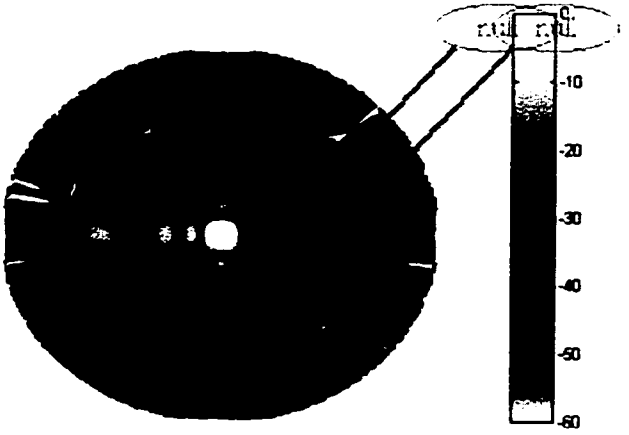

Figure 6.25: Double null steered array pattern of 12×12 element planar array with coupling. The nulls are at $\theta = 48^0$ and $\theta = 24^0$ where $\phi = 0^0$

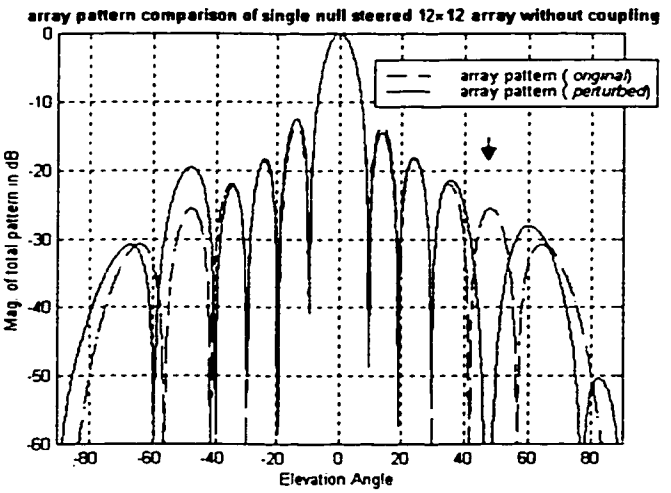

Figure 6.26(a): Comparison of array patterns of the array without coupling before and after single null steering. The null is at $\theta = 48^0$ and $\phi = 0^0$

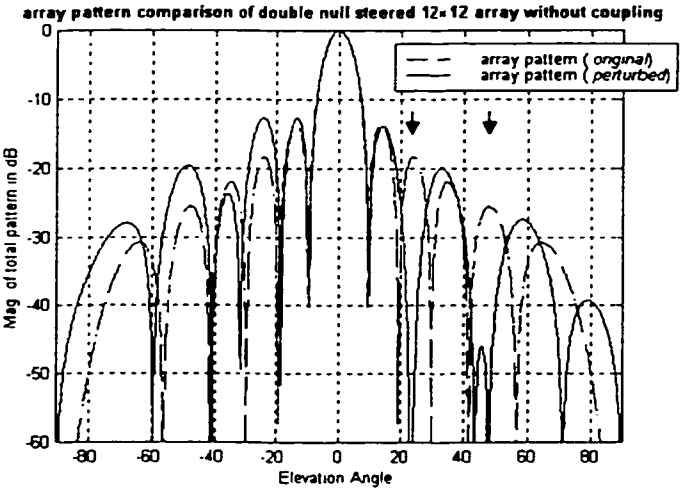

Figure 6.26(b): Comparison of array patterns of the array without coupling before and after double null steering. The nulls are at $\theta = 48^0$ and $\theta = 24^0$ where $\phi = 0^0$

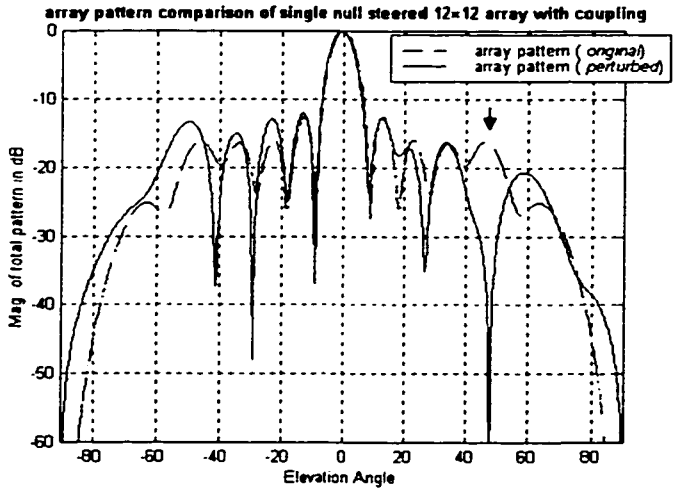

Figure 6.27(a): Comparison of array patterns of the array with coupling before and after single null steering. The null is at $\theta = 48^0$ and $\phi = 0^0$

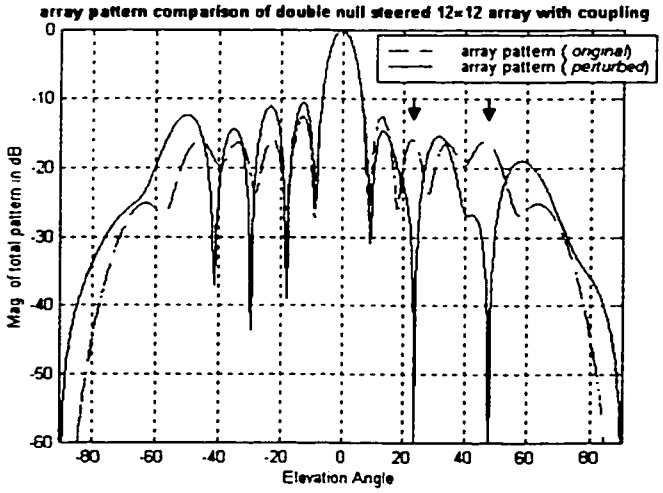

Figure 6.27(b): Comparison of array patterns of the array with coupling before and after double null steering. The null are at $\theta = 48^0$ and $\theta = 24^0$ where $\phi = 0^0$

CHAPTER 7

CONCLUSIONS AND SUGGESTIONS FOR FUTURE WORK

7.1 Conclusions

The following conclusions are drawn based on the work done.

- Mutual coupling effects are taken into consideration in a microstrip planar array while steering the nulls. Phase variation technique is used by means of genetic algorithm to achieve null steering. Greater phase tolerance was required to steer the nulls of the microstrip array when coupling between the elements is considered.

- Rectangular microstrip antenna is used to as the element of the array to make the array conformal and suitable for the mobile applications.
- The aim of the work was to study microstrip planar array radiation characteristics with mutual coupling considerations and steer its nulls to arbitrary directions using phase only technique by means of genetic algorithm. This has been successfully achieved and nulls of –60 dB depths were steered.
- For the 8×8 element microstrip array with inter element spacing (dx = dy = 0.5λ), the array patterns under the case of no coupling (neglecting the coupling effects) and with coupling (not neglecting the coupling effects) are compared to study the effect of coupling. The half power beam width of array with coupling reduced by 0.7^0 than compared with the half power beam width of array without coupling. Therefore the main beam became narrower after taking mutual coupling into consideration. The side lobe level of the array with coupling is greater than the side lobe level of the array without coupling by 1.65 dB. The same phenomenon was observed in arrays of different sizes, which were studied to investigate the effect of the number of elements on the array performance.
- Single and double nulls were steered using genetic algorithm. It proved to be a very effective tool to steer the nulls. It has been applied on planar arrays of different sizes to do null steering.
- To implement the algorithm by phase variation technique, phase shifters are used. For each array, there is a minimum phase tolerance required to obtain a null at a particular location, below which it may not be possible to achieve a null even for greater number of generations.

- It is relatively easy to steer a null at smaller phase tolerance for an array of large size as we have an increased number of control parameters.
- Placing a null close to the main beam requires greater phase tolerance than in the case of placing a null away from the main beam. Also greater phase tolerance was required to steer nulls after mutual coupling is taken into consideration than was required when mutual coupling was neglected. The tables 7.1 through 7.4 summarize the results obtained to form a null in a given location and the phase tolerance required to steer single and double nulls for different arrays.
- The effect of inter element spacing on mutual coupling of the array and therefore its array performance was studied by varying the inter element spacing from 0.2λ to 0.7λ. As the inter element spacing is increased, the array pattern with coupling became increasingly close to the array pattern without coupling but the number of side lobes are increased.
- This work has showed that successful null steering can be achieved in planar arrays in which mutual coupling effects are taken into consideration.

Array without coupling	Null location (θ)	Phase tolerance
8×4	38	14
8×8	38	14
12×8	48	10
12×12	48	10

Table 7.1: Single null results of the array without coupling

Array with coupling	Null location (θ)	Phase tolerance
8×4	38	28
8×8	38	28
12×8	48	26
12×12	48	25

Table 7.2: Single null results of the array with coupling

Array without coupling	Null locations (θ_1,θ_2)	Phase tolerance
8×4	60, 38	20
8×8	60, 38	20
12×8	48, 38	18
12×12	48, 24	17

Table 7.3: Double null results of the array without coupling

Array with coupling	Null locations (θ_1,θ_2)	Phase tolerance
8×4	60, 38	42
8×8	60, 38	42
12×8	48, 38	39
12×12	48, 24	38

Table 7.4: Double null results of the array with coupling

7.2 Suggestions for future work

Following suggestions are made for the continuation of this work.

- Microstrip planar arrays with mutual coupling effects were studied analytically. The results can be used to practically build microstrip arrays. Special attention should be given to the design of the feed network.
- There are many methods that can be used to feed microstrip antennas. The four most popular are the microstrip line, coaxial probe, aperture coupling and proximity coupling. More information about these can be obtained from [1]. Microstrip line and coaxial probe possess inherent asymmetries, which generate higher order modes that produce cross-polarized radiation. Aperture and proximity coupling overcome these problems and therefore are more efficient. These methods can be used to feed the designed array.
- Square, dipole (strip), and circular microstrip patch elements are most common because of attractive radiation characteristics and low cross-polarization. These can be used as the elements of the planar array for different applications. It will be useful to develop the mutual coupling expressions for these elements.
- For the microstrip, we assumed the current distribution along the length of the patch to be sinusoidal. More accurate distribution can be obtained using moments method. It would be interesting to compare the results and find the amount of deviation in the results due to this approximation.

- Simplified models for the microstrip antennas can be used to do the analysis for its radiation characteristics. The three models for the analysis of the microstrip are
    - Transmission line model
    - Cavity model
    - Multiport network model
- Different array configurations can be considered and studied analytically. Genetic algorithm can be applied to steer the nulls of these arrays. The results obtained from genetic algorithm can be compared with the results obtained from other search techniques like tabu search.

APPENDIX A

A.1 Relation Between the Cylindrical and Rectangular Coordinate Systems

The cylindrical coordinate axis orientation was taken as according to the requirement in the derivations in Chapter 3. The cylindrical coordinate system is shown in figure A.1 where the axis of the cylinder is along the x-axis. If 'ρ' is the radius of the cylinder the relation between x, y, z, ρ and θ is given by

$$x = x \tag{A.1}$$
$$y = \rho \sin\theta \tag{A.2}$$
$$z = \rho \cos\theta \tag{A.3}$$

Referring to figure A.2(a) and A.2(b), the relation between the unit vectors is given by equations A.4 through A.6. The vector 'A' is written in rectangular and cylindrical coordinates given by equations A.7 and A.8.

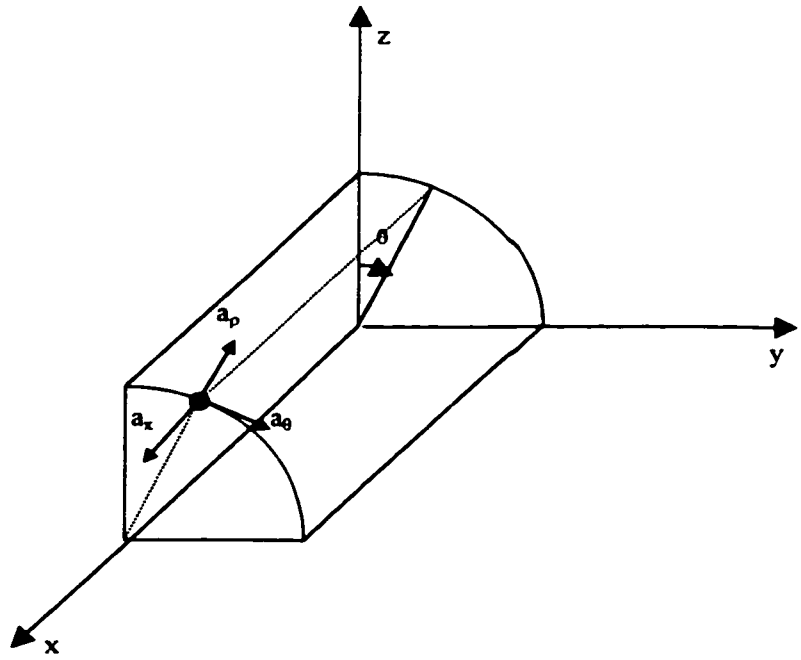

Figure A.1: Cylindrical Coordinate System

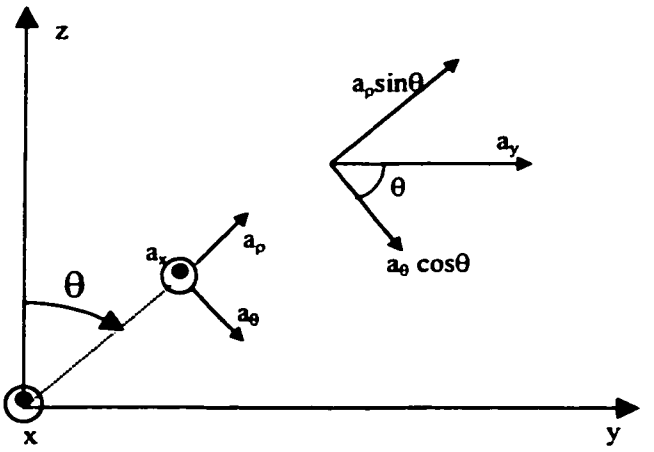

Figure A.2 (a): Geometry for the unit vector a_y

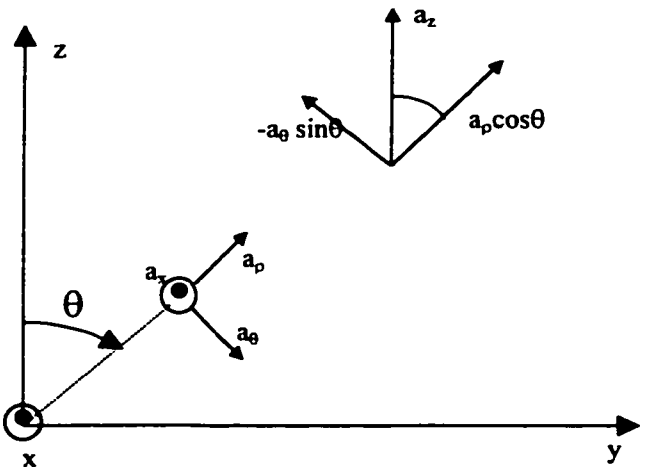

Figure A.2 (b): Geometry for the unit vector a_z

Thus by referring to the figures A.2(a) & (b), the relation between the unit vectors is given by

$$\bar{a}_x = \bar{a}_x \tag{A.4}$$

$$\bar{a}_y = \bar{a}_\rho \sin\theta + \bar{a}_\theta \cos\theta \tag{A.5}$$

$$\bar{a}_z = \bar{a}_\rho \cos\theta - \bar{a}_\theta \sin\theta \tag{A.6}$$

$$A = \bar{a}_x A_x + \bar{a}_y A_y + \bar{a}_z A_z \tag{A.7}$$

$$A = \bar{a}_x A_x + \bar{a}_\theta A_\theta + \bar{a}_\rho A_\rho \tag{A.8}$$

Using the relations A.4, A.5, A.6 in equation A.7, we can write

$$A = \bar{a}_x A_x + (\bar{a}_\rho \sin\theta + \bar{a}_\theta \cos\theta)A_y + (\bar{a}_\rho \cos\theta - \bar{a}_\theta \sin\theta)A_z$$

$$A = \bar{a}_x A_x + \bar{a}_\theta (A_y \cos\theta - A_z \sin\theta) + \bar{a}_\rho (A_y \sin\theta + A_z \cos\theta)$$

$$\Rightarrow$$

$$A_x = A_x$$

$$A_\theta = A_y \cos\theta - A_z \sin\theta$$

$$A_z = A_y \sin\theta + A_z \cos\theta$$

in matrix form representation

$$\begin{bmatrix} A_x \\ A_\theta \\ A_\rho \end{bmatrix} = \begin{bmatrix} 1 & 0 & 0 \\ 0 & \cos\theta & -\sin\theta \\ 0 & \sin\theta & \cos\theta \end{bmatrix} \begin{bmatrix} A_x \\ A_y \\ A_z \end{bmatrix} \tag{A.9}$$

The equation in matrix form given by equation A.9 can be used to convert a rectangular coordinate system in cylindrical coordinate system.

A.2 Curl Of a Vector 'A' in Cylindrical Coordinates

To find the curl of a vector, we follow the Ampere's law [44]. Ampere's law states that the magnetomotive force around a closed path is equal to the current enclosed by the path.

$$i.e.\ \oint A.ds = I \qquad amperes \tag{A.10}$$

Illustrating this point further, consider a conducting region in which there is a current density **J** (figure A.3). The coordinates of the point A be (x,θ,ρ). The magnetomotive force around the closed path ABCDA can be obtained by summing the magnetomotive forces (mmf's) along the four sides of the rectangle. If the average value of mmf over the path AB is A_θ and is A_ρ over the path AD, then the following relations hold

$$mmf\ from\ A\ to\ B = A_\theta \rho \Delta\theta \tag{A.11}$$

$$mmf\ from\ B\ to\ C = \left(A_\rho + \frac{\partial(A_\rho)}{\rho \partial\theta} \rho \Delta\theta \right) \Delta\rho \tag{A.12}$$

$$mmf\ from\ C\ to\ D = -\left(A_\theta + \frac{\partial(\rho A_\theta)}{\rho \partial\rho} \Delta\rho \right) \rho \Delta\theta \tag{A.13}$$

And,

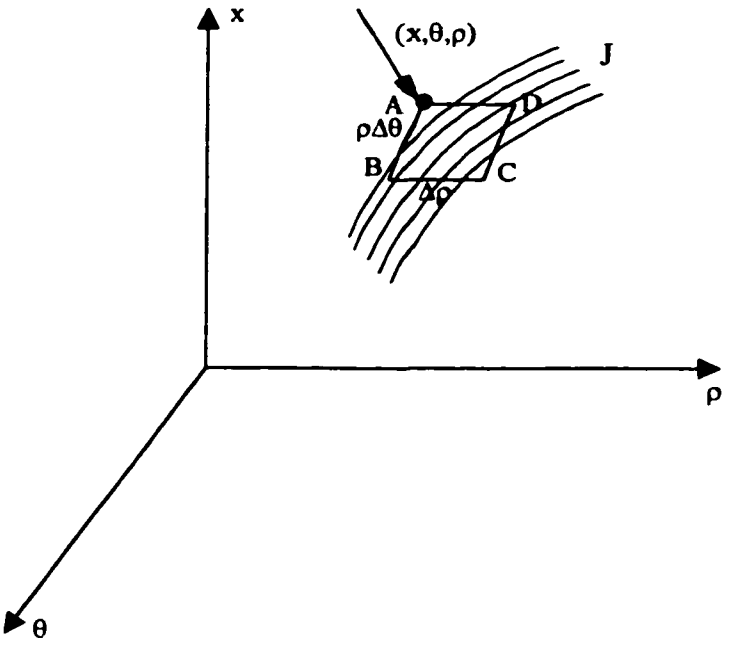

Figure A.3: ABCDA is a closed path which is rectangular with dimensions '$\rho\Delta\theta$' along AB and '$\Delta\rho$' along BC; J is the current density

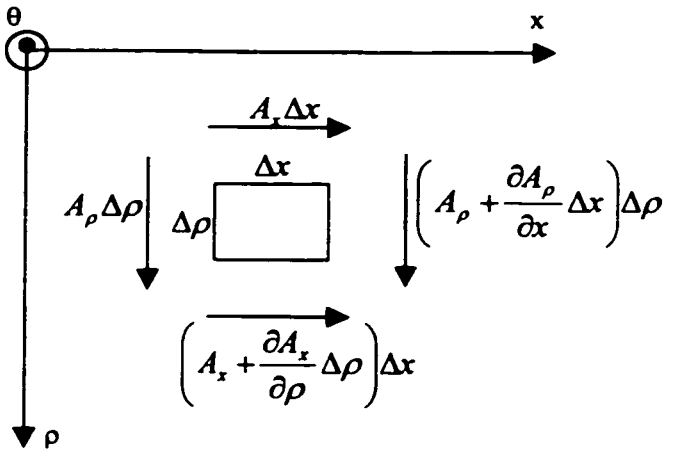

Figure A.4: 'θ' component of the curl of vector A

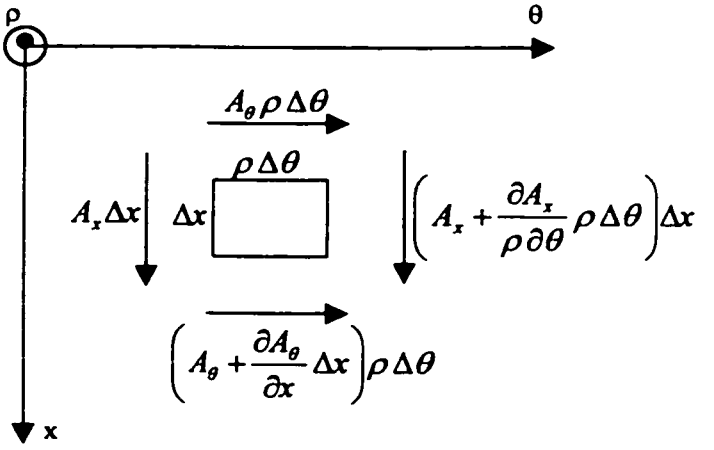

Figure A.5: 'ρ' component of the curl of the vector A

$$mmf\ from\ D\ to\ A = -A_\rho \Delta\rho \tag{A.14}$$

$$\therefore\ mmf\ around\ closed\ path = \frac{\partial A_\rho}{\rho\,\partial\theta}\rho\Delta\theta\Delta\rho - \frac{\partial(\rho A_\theta)}{\rho\,\partial\rho}\rho\Delta\theta\Delta\rho \tag{A.15}$$

$$total\ flux\ out\ of\ closed\ loop\ ABCDA\ is = J_x \rho\Delta\theta\Delta\rho$$

$$\therefore\ J_x = (\nabla \times A)_x = \frac{1}{\rho}\left(\frac{\partial A_\rho}{\partial\theta} - \frac{\partial(\rho A_\theta)}{\partial\rho}\right) \tag{A.16}$$

similarly from figures A.4 & A.5, we get

$$(\nabla \times A)_\theta = \left(\frac{\partial A_x}{\partial\rho} - \frac{\partial A_\rho}{\partial x}\right) \tag{A.17}$$

$$(\nabla \times A)_\rho = \left(\frac{\partial A_\theta}{\partial x} - \frac{\partial A_x}{\rho\,\partial\theta}\right) \tag{A.18}$$

APPENDIX B

Flow Chart of Genetic Algorithm

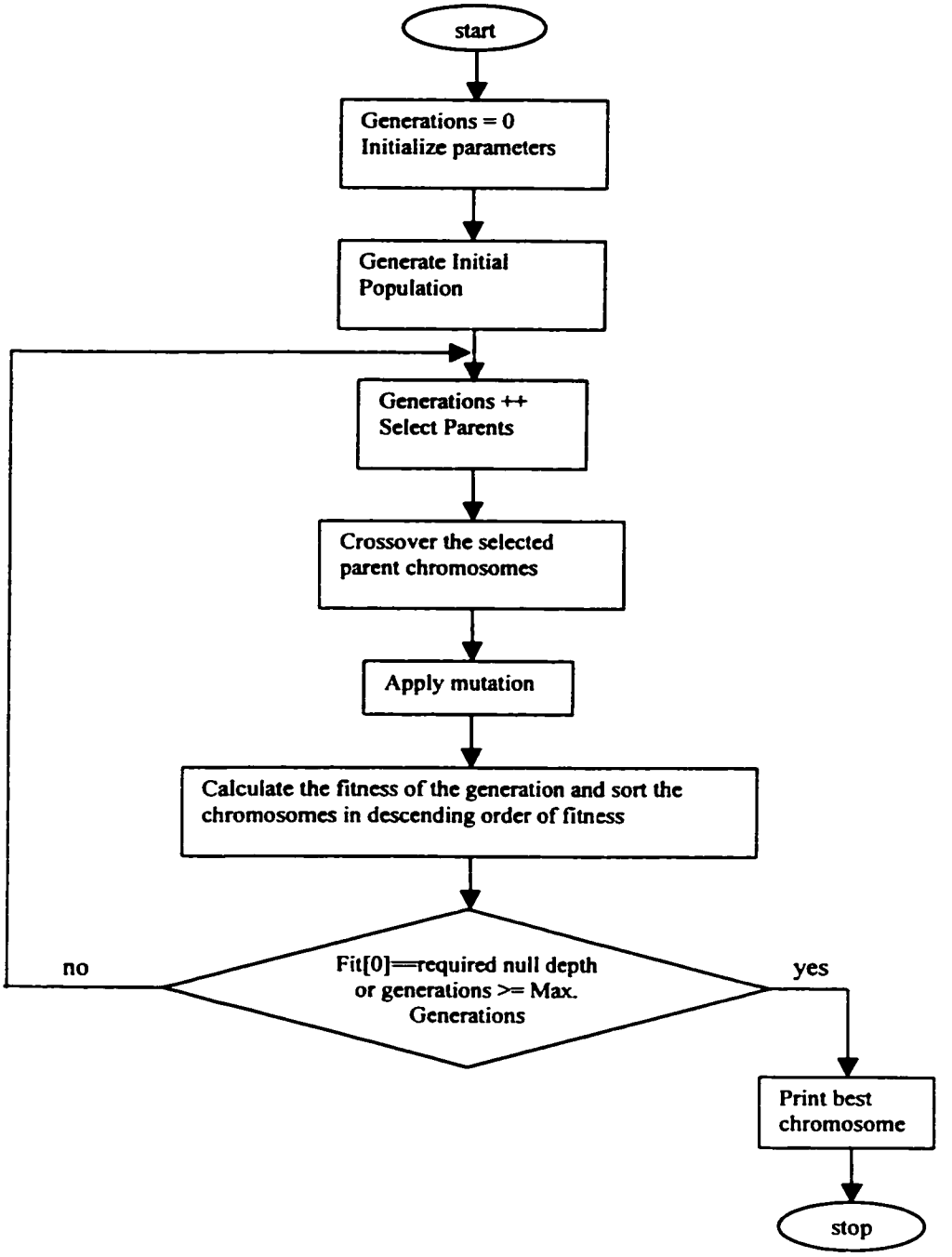

Figure B.1: Flow chart of the genetic algorithm

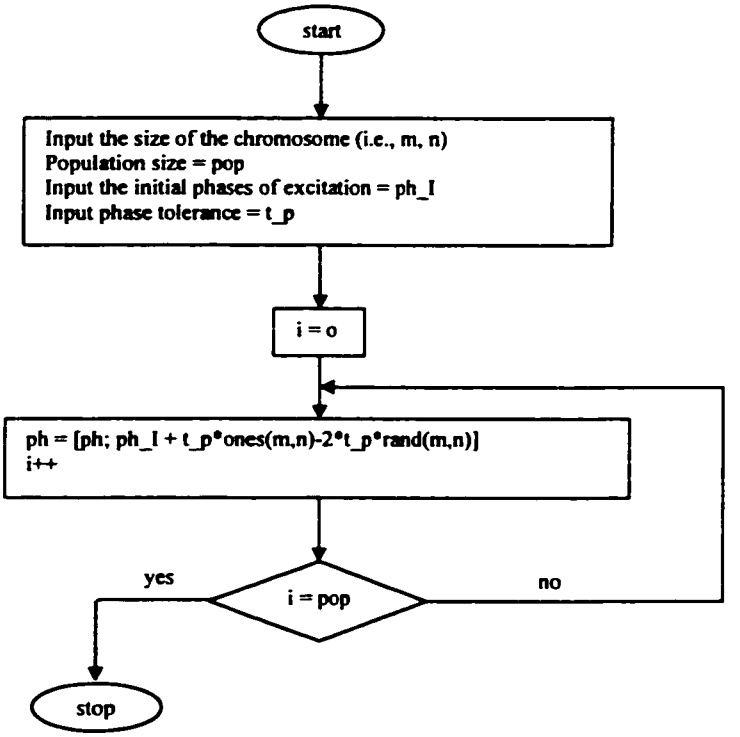

Figure B.2: Population initialization routine's flow chart

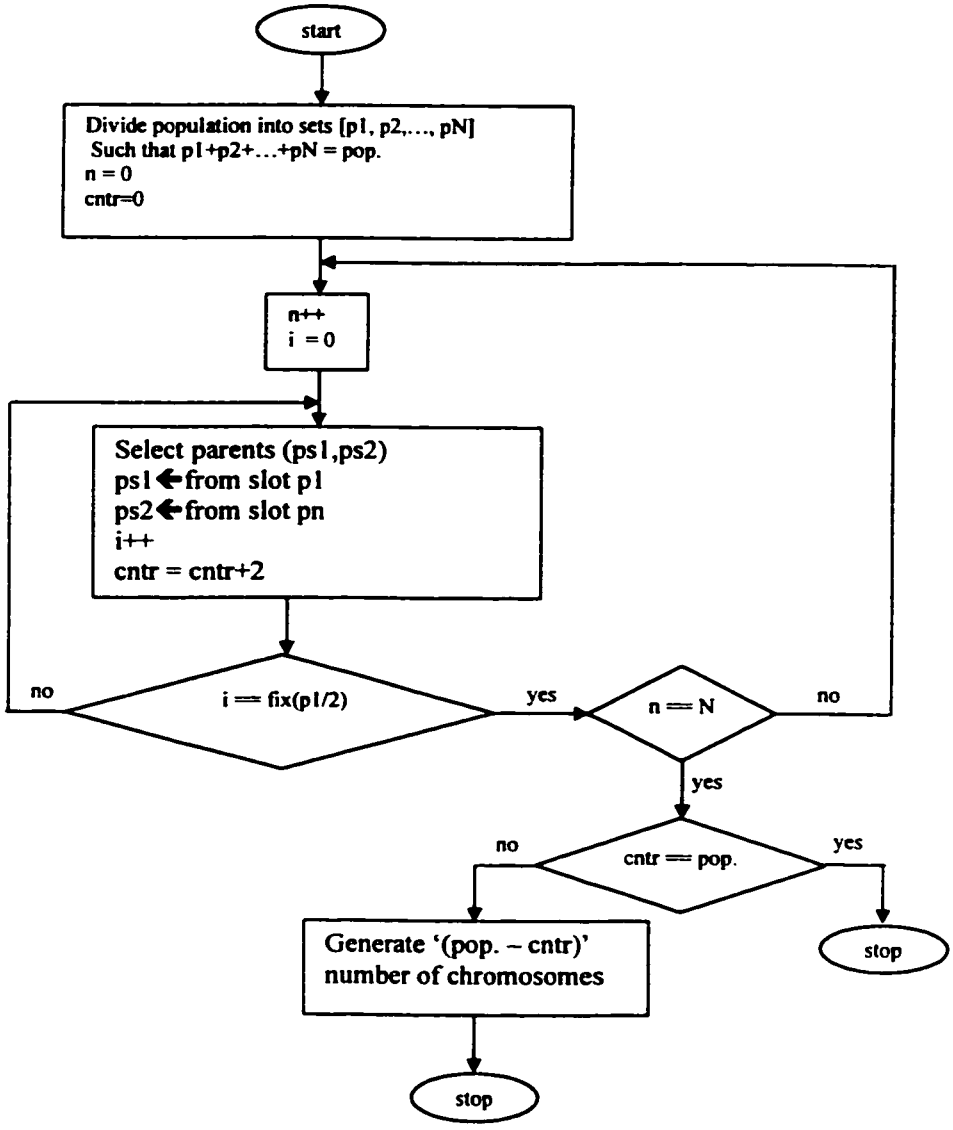

Figure B.3: Flow chart illustrating the selection routine based on the roulette wheel principle in which higher fitness chromosomes have better chance of mating

Bibliography

1. Constantine A. Balanis, "Antenna Theory Analysis and Design", *John Wiley and Sons, New York, 2nd edition*, 1997.
2. Mohammad Nuruzzaman, "Null Steering in Planar Antenna Arrays using Genetic Algorithms", *MS thesis*, KFUPM, SA, June 1998.
3. T. H. Ismail, "Null Steering in Phased and Adaptive Arrays by Controlling the Element Positions", *PHD Dissertation*, KFUPM, SA, August 1991.
4. M. J. Mismar and T. Ismail, "Null Steering using Minimax Approximation by Controlling Only the Current Amplitudes", *Int. J. Electronics*, pages 409-415, 1995.
5. W. P. Liao and F. L. Chu, "Null Steering in Planar Arrays by Controlling only Current Amplitudes using Genetic Algorithms", *Microwave and Optical Technology letters*, pages 97-103, 1997.
6. W. P. Liao and F. L. Chu, "Application of Genetic Algorithms to Phase-Only Null Steering of Linear Arrays", *Electromagnetics*, page(s): 171-183, 1997.

7. A. Tennant, M. M. Dawoud and A. P. Anderson, "Array Pattern Nulling by Element Position Perturbations Using a genetic Algorithm", *Electronic Letters*, pages 174-176, 3rd February 1994.

8. T. H. Ismail and M. M. Dawoud, "Null Steering in Phased Arrays by Controlling the Element Positions", *IEEE Transactions on Antenna and Propagation*, vol. 39, no. 11, page(s): 1561-1566, 1991.

9. Syed Tariq Magrabi, "Cancellation of Grating Lobes in Scanned Linear Antenna Arrays Using Genetic Algorithm", *MS Thesis*, KFUPM, Dhahran, SA, May 1998.

10. I. J. Bahl, P. Bhartia, " Microstrip Antennas", *Artech House, Inc., 610 Washington Street, second printing*, 1882.

11. R. C. Hansen, "Phased Array Antennas", *Wiley Series in Microwave and Optical Engineering,* John Wiley & Sons, Inc., 1998.

12. J. R. James, P. S. Hall, "Handbook of Microstrip Antennas", *IEE electromagnetic wave series 28*, 1989, Published by Peter Peregrinus Ltd., London, United Kingdom.

13. Y. T. Lo, S. W. Lee, "Antenna Handbook", van nostrand reinhold company, New York, 1988.

14. Mikhled Alfaouri, "Design Considerations for Low Sidelobe levels for Rectangular Microstrip Array Antennas", *radio science conference, proceedings of fifteenth national*, page(s): B2/1 – B2/9, 1998.

15. P. S. Hall, "Application of Sequential Feeding to Wide Bandwidth, Circularly Polarised Microstrip Patch arrays", *microwaves, antennas and propagation, IEE proceedings H*, volume: 136 5, page(s): 390-398.

16. Wojciech Sadowski, Custodio Peixeiro, "Microstrip Patch Antenna for a GSM 1800 Base Station", *microwaves and radar, mikon'98, 12th international conference on*, vol. 2, page(s): 409-413, 1998.

17. J. P. Daniel, M. Himdi, D. Thouroude, "Printed Antenna Arrays: Examples of Commercial Applications", *antennas and propagation for wireless communications, IEEE-APS conference on*, page(s): 105-108, 1998.

18. Shuguang Chen, Ryuichi, "Mutual Coupling Effects in Microstrip Patch Phased Array Antenna", *antennas and propagation society international symposium, IEEE, volume(2)*, page(s): 1028-1031.

19. Schelkunoff S. A., "A Mathematical Theory of Linear Arrays", *Bell System Technical Journal*, vol. 22, page(s): 80-107, 1943.

20. Vu T. B., "Method of Null Steering without using Phase Shifters", *IEE Proceedings part H*, 131:243-246, August 1984.

21. Davies D. E. N., "Independent angular steering of each zero of the directional pattern for a linear array", *IEEE transactions on antennas and propagation*, AP-15, page(s): 296-298, 1967.

22. M. Sabry Rizk, "Null Steering antennas for mobile communications", *PHD Thesis*, University of London, February 1977.

23. Davies D. E. N., "Circular Arrays", *Chapter 12 in the Handbook of Antenna Design*, A. W. Rudge, K. Milne, A. D. Olver and P. Knight eds. Peter Peregrinus, Stevenage, vol. II, 1983.

24. Davies D. E. N. and Rizk M. S. A. S., "A broadband experimental null-steering antenna system for mobile communications", *the radio and electronic engineer*, vol. 48, no. 10, page(s): 509-517, October 1978.

25. Davies D. E. N. and Rizk M. S. A. S., "A Small radius circular array with 360^0 null-steering capability", *IEE conference on antennas and propagation publ. 169*, page(s): 60-64, 1978.

26. Davies D. E. N. and Rizk M. S. A. S., "Electronic steering of multiple-nulls for circular arrays", *electronics letters*, vol. 13, no. 22, page(s): 669-670, 27^{th} October 1977.

27. "Introduction to Evolutionary Computing Techniques", *Electronic Technology Directions to the year 2000*, 1995. Page(s): 122-127.

28. John R. Koza, "Survey of Genetic Algorithms and Genetic Programming", *WESCON/95, Conference record, 'Microelectronics Communications Technology Producing Quality Products Mobile and Portable Power Emergency Technologies'*, page(s): 589-594, 1995.

29. Daniel S. Weile and Eric Michielssen, "Genetic Algorithm Optimization Applied to Electromagnetics: A review", *IEEE transactions on antennas and propagation*, vol. 45, no. 3, March 1997.

30. M. M. Dawoud, T. H. Ismail, "Experimental Verification of Null Steering by Element Position Perturbations", *IEEE transactions on antennas and propagation*, vol. 40, no. 11, November 1992.

31. R. J. Mitchell, B Chambers, A. P. Anderson, "Array Pattern Control in the Complex Plane Optimised by a Genetic Algorithm", *10^{th} international conference on antennas*

and propagation, IEE, conference publication no. 436, page(s): 1.330-1.333, 14-17 April 1997.

32. A. B. Alona Boag and R. Mittra, "Design of electrically loaded wire antennas using genetic algorithms", *IEEE transactions on antennas and propagation*, vol. 44, No. 5, pages 687-695, May 1996.
33. Randy L., Haupt, "Thinned Arrays Using Genetic Algorithms", *IEEE transactions on antennas and propagation*, vol. 42, pages 993-999, July 1994.
34. Leehter Yao, "Nonlinear Parameter Estimation via the Genetic Algorithm", IEEE transactions on signal processing, vol. 42, no. 4, April 1994.
35. Qing Li, Edward J. Rothwell, "Scattering Center Analysis of Radar Targets Using Fitting Scheme and Genetic Algorithm", *IEEE transactions on antenna and propagation*, vol. 44, no. 2, February 1996.
36. Ponniah Ilavarasan, Edward J. Rothwell, Kun-Mu Chen and Dennis P. Nyquist, "Natural Resonance Extraction from Multiple Data Sets Using a Genetic Algorithm", *IEEE transactions on antennas and propagation*, vol. 43, no. 8, August 1995.
37. W. A. Swart and J. C. Olivier, "Numerical Synthesis of Arbitrary Discrete Arrays", *IEEE transactions on antennas and propagation*, vol. 41, no. 11, page(s): 1541-1550, November 1993.
38. A. T. Villeneuve, "Taylor Patterns for Discrete Arrays", IEEE transactions on antenna and propagation, vol. AP-32, no. 10, page(s): 1089-1093, October 1984.
39. Petro O. Savenko and Volodymyr J. Anokhin, "Synthesis of Amplitude-Phase Distribution and Shape of a Planar Antenna Aperture for a given Power Pattern",

IEEE transactions on antennas and propagation, vol. 45, no. 4, page(s): 744-747, April 1997.

40. Boon Poh Ng, Meng Hwa, and Chichung Kot, "A Flexible Array Synthesis Method Using Quadratic Programming", *IEEE transactions on antennas and propagation*, vol. 41, no. 11, page(s): 1541-1550, November 1993.
41. F. Ares, R. S. Elliott, and E. Moreno, "Design of Planar Antenna Arrays to Obtain Efficient Footprint Patterns with an arbitrary Footprint Boundary", IEEE transactions on antennas and propagation, vol. 42, no. 11, page(s): 1509-1514, November 1994.
42. M. M. Dawoud, A. Tennant, A. P. Anderson, "Null Steering and Pattern Synthesis of Array Antennas by genetic algorithms", *conference proceedings on microwaves 94*, IEE, page(s): 112-116, 1994.
43. I. Ryzhik, "Tafeln Tables", *Band 1/ Volume 1, Verlag MIR, Moskau*, 1981.
44. Edward c. Jordan, Keith g. Balmain, "Electromagnetic Waves & Radiating Systems", *Prentice-Hall, second edition, New Delhi*, 1993.

Vita

- Meerja Khalim Amjad
- Born in Vijayawada, India on 2nd May 1975
- Received Bachelor's degree in Electronics and Communication Engineering from Osmania University, Hyderabad, India, July 1996
- Completed Master's degree in Electrical Engineering from King Fahd University of Petroleum and Minerals, Dhahran, Saudi Arabia, February 2000